FUNCTIONALIZED PEG-4MAL HYDROGELS FOR DELIVERY OF DENDRITIC CELLS IN TOLEROGENIC APPLICATIONS

A Dissertation
Presented to
The Academic Faculty

by

Nicholas Michael Beskid

In Partial Fulfillment
of the Requirements for the Degree
Doctor of Philosophy in BioEngineering
Georgia Institute of Technology

Georgia Institute of Technology
December 2020

FUNCTIONALIZED PEG-4MAL HYDROGELS FOR DELIVERY OF DENDRITIC CELLS IN TOLEROGENIC APPLICATIONS

Approved by:

Dr. Julia E. Babensee, Advisor
School of Biomedical Engineering
Georgia Institute of Technology

Dr. Edward Botchwey
School of Biomedical Engineering
Georgia Institute of Technology

Dr. Andres Garcia
School of Mechanical Engineering
Georgia Institute of Technology

Dr. Jacob Kohlmeier
School of Microbiology and Immunology
Emory University

Dr. Susan Thomas
School of Mechanical Engineering
Georgia Institute of Technology

Date Approved: [July 23, 2020]

ACKNOWLEDGEMENTS

I was determined and hopeful when I first started at Georgia Tech as a Master's student, but I never expected that my graduate journey would end here. Very early in my first semester, a spot for a doctoral student opened up in a research lab that was the exact intersection of my two favorite fields of study: immunology and biomaterials science. I knew I couldn't pass up the opportunity to pursue a Ph.D. at this university. The thought that this one decision would dramatically change my path for the next half-decade of my life is not something that I fully appreciated at the time.

I would first and foremost like to thank my doctoral advisor Dr. Julie Babensee for giving me this opportunity to conduct research in her lab. Dr. Babensee constantly pushed me to read the literature more critically, design experiments more thoroughly, conduct experiments more rigorously, interpret our results with more vigor and explain the data more clearly. Dr. Babensee was the driving force that motivated me to continually improve myself and my research. Around the midpoint of my second year, I thought back to six months prior and realized just how much more I accomplished in a day compared to then. This trend continued until the day of my defense. Working with Dr. Babensee truly helped shape my path and my worldview, and this experience is one that I will look fondly upon for the rest of my life.

I would next like to acknowledge the members of my thesis committee: Dr. Andrés García, Dr. Susan Thomas, Dr. Edward Botchwey, and Dr. Jacob Kohlmeier. The expertise provided by my committee was invaluable, and this thesis would not have been possible without each member. I also want to recognize my committee for going even further and

offering encouragement, advice, and community during my time at Georgia Tech. Next, I want to thank our collaborator, Dr. Brian Evavold, for working so closely with us on our therapy's design and testing on his animal disease model, even after moving from Emory University to the University of Utah. I'd also like to thank one of Dr. Evavold's researchers, Elizabeth Kolawole, for her patience and thoroughness in training me very early in my doctoral research.

I want to thank Dr. Babensee's previous student, Sangeetha Srinivasan, for helping me transition into Dr. Babensee's Lab, even after she had left Atlanta for her new job. I would also like to thank the IBB and EBB core technicians who continued to train me in areas that Sangeetha could not do virtually. Sommer Durham and Andrew Shaw deserve additional thanks for assisting me with equipment usage and experimental design at all hours of the day and night. Thank you as well to the PRL staff for the many hours they worked to keep the animal facilities in IBB running smoothly. My early training really was a joint effort by Sangeetha Srinivasan, research staff, and other doctoral students I grew close to over the years.

I want to extend further gratitude to Dr. Andrés García, who acted as an unofficial co-advisor throughout my project and welcomed me into his weekly lab meetings and student office space, which significantly changed the course of my education. This new community led to almost immediate access to a wealth of knowledge (that would have otherwise taken days or week to figure out on my own), opportunities to work as part of a team, to train others, and to brainstorm ideas. To the students of the García Lab (who are too many to mention): I am so glad that so many of us grew to be friends, and it has been a pleasure sharing this experience with all of you. I'd like to extend a special thanks to my

desk mate Michael Hunckler, whose second-shift schedule coincided with mine, for all of the stimulating discussions across science, politics, nature, and existentialism.

I offer my thanks to the undergraduate researchers that participated in our lab meetings and assisted my experiments: Brandon Nguyen, Anneliese Leach, Malek Moumne, Mia Giandinoto, Ethan Jordan, Priya Arya, and Ayan Dasgupta. I appreciate your hard work and all of your contributions to the research in Dr. Babensee's Lab. To the new student taking over my project, Fredrick Bulondo, it has been a pleasure getting to know you. Thank you for making the transition so easy considering the difficulties of passing on techniques virtually. I have no doubt you'll continue this work with the same rigor that Dr. Babensee has taught me.

I owe quite a bit of thanks to my academic advisor, Laura Paige, for what seems like monthly help on all things administrative, operational, and personal over the last five years. Thank you for seeing my potential and for bringing me the opportunity to become a doctoral student. During the strenuous and often daunting process of pursuing a doctorate, I always felt supported with you in my corner. I imagine that every other BioEngineering student at Georgia Tech shares this sentiment. It was a pleasure to work with you and you deserve more thanks than we could ever give. Next, I want to acknowledge Dr. Johnna Temenoff for going beyond her duties as part of the Graduate Leadership Program to help guide me at a crossroads in my graduate studies. Thank you for genuinely caring and for your thoughtful advice that helped bring me to where I am today.

I am grateful to our funding sources, the National Institute of Health, the Georgia ImmunoEngineering Consortium, and the Atlanta Clinical & Translational

Science Institute, for providing our lab the means to conduct the research in this thesis and for aiding in my educational and professional development. In particular, the T32 ImunnoEngineering program established a structured space to learn, network, and grow alongside other doctoral students conducting research in this rapidly developing field.

Finally, I want to recognize those closest to me for their unconditional support throughout this period. To my parents, Gail and Gary Beskid: thank you for instilling in me the importance of education from a very young age. Teaching me to love learning and to be a lifelong learner may have been the most formidable value that shaped me into the man I am today. I can't thank you enough for all you have done, every step of the way, and for always being there to listen. Thank you for fully supporting my pursuit of higher education. You helped give me the confidence that I needed to see this through. I am lucky to call you both my parents.

To my wife Tay: I know its cliché, but I truly and honestly could not have done this without you. I will never forget the moment I told you about the possibility for my two-year graduate program to extend to a "five-to-seven" year commitment to doctoral research, and you were immediately supportive. You were right by my side throughout this odyssey, experiencing all of my ups and downs just the same. I feel as though you went through this program with me. I appreciate you more than you know, and I will never forget the many, many ways you supported me during these last five years. I am beyond grateful to have you in my life.

If you want to go fast, go alone. If you want to go far, go together.

TABLE OF CONTENTS

LIST OF TABLES

LIST OF FIGURES

LIST OF SYMBOLS AND ABBREVIATIONS

AF488	AlexaFluor-488
aLN	artificial lymph node
AM	acetoxymethyl
ANOVA	analysis of variance
APC	antigen-presenting cell
BBB	blood-brain barrier
BSA	bovine serum albumin
CCK-8	cell counting kit-8
CCL	chemokine ligand
CCR10	CC-chemokine receptor-10
CCR5	CC-chemokine receptor-5
CCR6	CC-chemokine receptor-6
CCR7	CC-chemokine receptor-7
CCR9	CC-chemokine receptor-9
CD	cluster of differentiation
cDC	conventional dendritic cell
CFA	complete Freund’s adjuvant
CFSE	carboxyfluorescein succinimidyl ester
CLR	c-type lectin receptor
CNS	central nervous system
CTLA-4	cytotoxic T-lymphocyte-associated protein 4
DAMP	damage-associated molecular patterns
DC10	interleukin-10-treated dendritic cell
DCs	dendritic cells
DMEM	Dulbecco's Modified Eagle Medium
DTT	dithiothreitol
EAE	Experimental Autoimmune Encephalomyelitis
EC_{50}	half-maximal effective concentration
ECM	extracellular matrix
EDTA	ethylenediaminetetraacetic acid
EthD-1	ethidium homodimer-1
FACS	fluorescence-activated cell sorting
FBS	fetal bovine serum
FMO	fluorescence minus one
FoxP3	Forkhead Box P3

FRC	fibroblastic reticular cell
FSC	forward scatter
G'	storage modulus
G"	loss modulus
GATA3	GATA-binding protein 3
GFP	green fluorescent protein
GM-CSF	granulocyte-macrophage colony-stimulating factor
H&E	hematoxylin and eosin
HBSS	Hank's Buffered Salt Solution
HEPES	4-(2-hydroxyethyl)-1-piperazineethanesulfonic acid
HEV	high endothelial venules
HGF	hepatocyte growth factor
HLA-G	human leukocyte antigen G
HS-IL-10	interleukin-10 with free thiol
IACUC	Institutional Animal Care and Use Committee
iDC	immature dendritic cell
IDO	indoleamine 2,3-dioxygenase
IFN-γ	interferon-γ
IFNβ-1α	interferon β-1α
IL-10	interleukin-10
IL-10R	interleukin-10 receptor
IL-12	interleukin-12
IL-17	interleukin-17
IL-2	interleukin-2
IL-23p19	interleukin-23 subunit alpha
IL-4	interleukin-4
IL-6	interleukin-6
IVIS	*in vivo* imaging systems
LFB	Luxol fast blue
LN	lymph node
LPS	lipopolysaccharide
LTα	lymphotoxin-α
MBP	myelin basic protein
mDC	mature dendritic cell
MFI	mean fluorescence intensity
MHC	major histocompatibility complex
MMP	matrix metalloproteinase
MOG	myelin-oligodendrocyte glycoprotein

MP	microparticle
MS	Multiple Sclerosis
NLR	Nod-like receptor
NOD	non-obese diabetic
NP	nanoparticle
OVA	ovalbumin
PAMP	pathogen-associated molecular patterns
PBMCs	peripheral blood mononuclear cells
PBS	phosphate buffered saline
PD-1	programmed cell death protein 1
PD-L1	programmed-death ligand-1
pDC	plasmacytoid dendritic cell
PDMS	poly(dimethylsiloxane)
PEG	poly(ethylene glycol)
PEG-4MAL	maleimide-functionalized 4-arm poly(ethylene glycol)
PEG-IL10	PEG-4MAL-bound-IL-10
PEI	polyethyleneimine
pHEMA	poly(2-hydroxyethyl methacrylate)
PI	propidium iodide
PLGA	polylactic-co-glycolic acid
PLP	proteolipid protein
pMHC	peptide-major histocompatibility complex
PRL	Physiological Research Laboratory
PRR	pattern recognition receptor
PT	pertussis toxin
RBC	red blood cell
RDG	GRDGSPC peptide
RGD	GRGDSPC peptide
RIG-I	retinoic acid-inducible gene-I
RLR	RIG-I-like receptor
ROR-γt	Retinoic acid receptor–related orphan receptor γt
RR-MS	Relapsing-Remitting Multiple Sclerosis
SDS-PAGE	sodium dodecyl sulfate-polyacrylamide gel electrophoresis
SI	staining index
SLE	Systemic Lupus Erythematosus
SSC	side scatter
STIM-DC	stimulated dendritic cell
T1D	Type 1 Diabetes

T_C	cytotoxic T cell
TCEP	tris(2-carboxyethyl)phosphine
TCR	T cell receptor
TGF-β	transforming growth factor-β
T_H	T helper cell
T_H1	T helper type 1 cell
T_H17	T helper type 17 cell
TLO	tertiary lymphoid organoid
TLR	toll-like receptor
TNF-α	tumor necrosis factor-α
Tr1	type 1 regulatory T cell
Treg	regulatory T cell
VD3	1,25-dihydroxyvitamin D3
VPM	GCRDVPMSMRGGDRCG peptide
σ	standard deviation

SUMMARY

Seminal research in biomaterials and immunoengineering has enabled the development of advanced therapies to treat cancer, autoimmunity, and other immune-related pathologies. A vital mediator of the immune system that is often targeted by pharmaceutical and biological therapeutics is dendritic cells (DCs), which bridge the innate and adaptive immune system. DCs are a crucial initiator of adaptive immunity, which directs downstream immunological effector functions in specific tissues targeted with precision through antigen-based tissue targeting. More recently, DCs have successfully been utilized as cell therapies for transplantation, vaccines, tumor clearance, and autoimmunity. The discovery of the Biomaterial Adjuvant Effect by Dr. Julie Babensee incited a field of investigation into the use of biomaterials as stimulators of immunity and, more recently, delivery vehicles that also act as adjuvants. While much effort has been contributed to biomaterials for immunostimulatory applications such as vaccines and cancer, there has been far less focus on biomaterials that promote tolerance and regulatory mechanisms. To date, no biomaterials have been shown to inherently promote tolerogenic processes *in vivo*. The goal of biomaterial constructs for delivery of cell therapies against autoimmune disease has historically been to develop bioinert biomaterials that simply do not activate the immune system. Here we engineer a maleimide-functionalized 4-arm poly(ethylene glycol) (PEG-4MAL) hydrogel as a biomaterial for delivery of DCs in tolerogenic applications. The objective of this work will be explored in three parts: (1) to characterize DC-biomaterial interactions towards optimization of PEG-4MAL hydrogels to suit DCs, (2) to introduce regulatory properties into PEG-4MAL hydrogels through

functionalization with the tolerogenic cytokine interleukin-10 (IL-10), and (3) to assess the efficacy and mechanism of tolerance by PEG-4MAL delivered DCs in treating a mouse model of autoimmunity.

DCs are continually sampling their surroundings for danger signals and are easily activated by recognition of foreign epitopes, mechanical stress, pH changes, and metabolic disturbances. In developing a tolerogenic biomaterial, it was first necessary to characterize DC responses to the biophysical and biochemical properties of PEG-4MAL hydrogels. The PEG-4MAL polymer formulation was selected due to its high degree of modularity and its ability to be end-functionalized with various peptides. DCs were first encapsulated in PEG-4MAL hydrogels with varying polymer density to modulate the stiffness of their surroundings. DCs in softer hydrogels (~200 Pa) remained viable, immature, and exhibited normal morphology after 24 hours. However, encapsulation in stiffer hydrogels (400-800 Pa) resulted in widespread cell death and elongated morphologies. Next, DCs were encapsulated in PEG-4MAL hydrogels functionalized with various concentrations of adhesive peptides GRGDSPC (RGD) or its scrambled counterpart, GRDGSPC (RDG). DCs remained viable and immature with normal morphology at all concentrations tested (0.08-1.0 mM), contrary to previous studies which showed RGD-induced DC maturation on a 2D substrate. These differences can be attributed to the stark differences between 2D and 3D phenomena or the limited range of RGD concentrations tested here were simply too low to activate DCs. DCs were also encapsulated in PEG-4MAL hydrogels with various macromer sizes (10 kDa, 20 kDa, 40 kDa) to decouple hydrogel stiffness and mesh size. Similarly, DCs from these gels had viability and phenotypes consistent with immature DC controls. Lastly, PEG-4MAL hydrogels were synthesized with various crosslinking

peptides (GCRDVPMSMRGGDRCG, VPM; dithiothreitol DTT) to modulate their degradability. Encapsulated DC viability and phenotype were not adversely affected by crosslinker type after 24 hours. Importantly, stiffness should be a significant consideration in the development of biomaterial delivery systems and should be modulated to support the cells being delivered. Our results show that PEG-4MAL constructs are widely flexible in their design for tolerogenic applications such that properties such as mesh size, degradability, and adhesive ligand can be tuned for application-specific purposes. For this project, we selected 20 kDa macromers at 4.5% (wt/v), which results in hydrogels with a mesh size that allows DC migration and a stiffness that supports DC viability and an immature phenotype. The highly degradable crosslinker VPM was selected to further enable DC migration and structural remodeling after injection. Lastly, RGD (1.0 mM) was selected as the adhesive ligand to promote endogenous cell infiltration and vascularization.

This optimization of the biophysical and biochemical properties of PEG-4MAL hydrogels resulted in a biomaterial that successfully supports DC viability and an immature phenotype. However, another critical characteristic of PEG-4MAL is that its maleimide chemistry allows functionalization with peptides other than adhesive ligands. Towards developing a truly tolerogenic biomaterial, our second objective was to tether the tolerance-inducing cytokine IL-10 to the polymer backbone of PEG-4MAL. Maleimide functional groups have high specificity for free thiols, most commonly found on cysteine residues. IL-10 does not have any free cysteines in its native state, so our first step was to add free thiols to IL-10 using 2-iminothiolane (Traut's reagent). Traut's reagent targets primary amines that occur in lysine residues, of which IL-10 has 13. Evaluation of free thiols on IL-10 after 1-hour incubation with Traut's reagent at 30 molar excess resulted in, on

average, all 13 lysine residues being thiolated. Subsequent incubation with PEG-4MAL at a ratio of 1,000:1 (PEG-4MAL:IL-10) for 15-30 minutes resulted in successful mono-PEGylation of IL-10, as illustrated by a shift in molecular weight from 19.6 kDa to ~40 kDa visualized by sodium dodecyl sulfate-polyacrylamide gel electrophoresis (SDS-PAGE). We employed a liver mast cell line (MC/9 cells) that proliferates in response to IL-10 to test the bioactivity of PEGylated IL-10 (PEG-IL10). Bioactivity was tested by two methods, the first of which included proliferation measurements by cell counting kit-8 (CCK-8) 48 hours after treatment. At 4 and 24 hours after the addition of CCK-8, MC/9 cell proliferation was indistinguishable between IL-10 and PEG-IL10. As a more robust test of bioactivity, half-maximal effective concentration (EC_{50}) curves were constructed by treating MC/9 cells with titrated doses of IL-10 or PEG-IL10. Both treatments resulted in similar levels of proliferation of MC/9 cells at all concentrations, and their EC50 values were almost identical (~0.003 ng/well). IL-10 was shown to exhibit controlled release from PEG-IL10 hydrogels over 4-8 days. DCs in PEG-IL10 hydrogels also exhibited significantly higher viability and lower expression of maturation markers than DCs in PEG-4MAL hydrogels after 48 hours. Additionally, both IL-10 and encapsulation contribute to the protective effects of this system against high levels of inflammation, which is a sizable challenge against cell therapies in autoimmune patients. These PEG-IL10 hydrogels are capable of IL-10 treatment through three mechanisms: (1) through burst release of untethered IL-10 from hydrogels, (2) through controlled release of PEG-IL10 as hydrogels degrade, and (3) through direct presentation of tolerance-inducing epitopes to encapsulated cells.

The final objective of this project was to evaluate the efficacy and mechanism of action of hydrogel-delivered DCs in a mouse model of Multiple Sclerosis (MS). Mice with experimental autoimmune encephalomyelitis (EAE) exhibit many of the same characteristics as MS, such as antigen-specific autoimmune mechanisms, inflammation-induced lesions in the CNS, resultant loss of motor function, and symptoms that progress in severity. Previous studies have shown that the effectiveness of tolerogenic treatment is highly dependent on the location of DCs. A primary motivation for biomaterial delivery is to improve the efficacy of cell therapies through co-localization to the target site and post-injection support. Thus, hydrogel-encapsulated DCs, DCs alone, or empty hydrogels were injected prophylactically in the neck of mice near the cervical lymph nodes (LNs). Mice receiving DCs by either delivery method experienced a delay in the onset of symptoms, while only mice receiving hydrogel-delivered DCs had durable amelioration of symptoms by peak disease. This difference in symptom severity suggests that the improved retention of DCs at the injection site, post-injection support provided by PEG-4MAL hydrogels, or both contributed to a more robust treatment. Post-processing of mouse tissues highlighted a significant increase in the frequency of antigen-specific CD11b+ (CD, cluster of differentiation) cells in the central nervous system (CNS) for hydrogel-delivered DC groups, which have been previously identified as playing a fundamental role in immune tolerance through the production of tolerogenic cytokines and induction of regulatory T cells. Subsequent experiments utilizing congenic mice strains to differentiate between delivered and endogenous cells showed a marked level of endogenous cell infiltration into hydrogels 24 hours post-injection. In these same mice, maturation markers on endogenous DCs were also significantly decreased in both the hydrogel environment and the CNS,

suggesting that the downstream effects of the treatment reached the CNS in some way. These infiltration effects were recapitulated *in vitro*, with splenocytes infiltrating far deeper into DC-laden hydrogels than blank hydrogels, pointing to DCs as drivers of endogenous cell recruitment. A series of autologous co-culture experiments were conducted to further investigate the method of tolerance induction *in vitro*. DCs receiving various treatments were co-incubated with splenocytes for 72 hours and T cell phenotypes were assessed. Immature DCs (iDCs), tolerogenic DCs (DC10s), and DCs recovered from PEG-4MAL or PEG-IL10 hydrogels all produced significantly higher frequencies of regulatory T cells than activated DC controls or splenocytes alone. This increase in regulatory T cells was accompanied by an increase in the expression of programmed cell death protein 1 (PD-1) in T cells, signifying regulatory capabilities in CD4+ T cells and suppression of CD8+ T cells. Additionally, these regulatory effects were only achieved in co-cultures utilizing antigen, suggesting that the function of tolerance by these DCs is highly antigen-dependent. Taken together, the experiments in Chapter 6 demonstrate the ability of optimized PEG-4MAL hydrogel delivery scaffolds to improve the robustness of therapeutic DCs and provides evidence towards how these DCs ameliorate symptoms of EAE. Based on the data discussed herein, a newly proposed mechanism of tolerance can be derived: post-injection, hydrogel-encapsulated DCs recruit endogenous lymphocytes which infiltrate the biomaterial niche. DCs then modulate host T lymphocytes directly, host antigen-presenting cells (APCs) which subsequently modulate T cells, or both. Tolerized host immune cells then migrate to the CNS, where inflammation is regulated at the site of injury, impairing the progression of lesions and ameliorating symptoms of paralysis.

This experiment conducted herein takes advantage of the highly modulatory PEG-4MAL hydrogel system to develop tolerogenic, IL-10-conjugated hydrogels that enable targeted delivery of DCs and support DC viability, an immature phenotype, and tolerogenic function. This biomaterial construct protects encapsulated DCs from external inflammation while tolerizing adjacent cell populations through IL-10 release. The downstream regulatory effects that originate at the immunosuppressive biomaterial niche significantly ameliorate symptoms of EAE, confirming that this optimized biomaterial delivery system improves the efficacy of a tolerogenic DC therapy. Additionally, the DC-biomaterial interactions characterized herein accentuate the flexibility in tuning PEG-4MAL hydrogels for other tolerogenic applications.

CHAPTER 1. INTRODUCTION

Multiple Sclerosis is an autoimmune disease that causes neurodegeneration through damage to the myelin sheath structure, leaving the brain's axons susceptible to damage[1,2]. xThis neurodegeneration often results in impaired motor skills, and an estimated 75% of Multiple Sclerosis patients are unemployed after 15 years due to the hardships of the disease[3]. Few options exist for treatment of Multiple Sclerosis, and the pharmaceutical agents currently being employed function through systemic immunosuppression which is accompanied by an increased risk of developing other autoimmune diseases, susceptibility to opportunistic infection, and other complications[4,5]. Drugs aiming to prevent the onset or progression of Multiple Sclerosis have variable patient responsiveness and can only be monitored by long-term tracking of relapses[4]. Recent strategies to treat autoimmune disease without shutting down systemic immunity have focused on modulating immune cells in an antigen-specific manner[6]. Biomaterial delivery of immunomodulatory cells improves the effectiveness of these cellular therapeutics by promoting cell viability and functionality and by localizing cells to a disease-relevant site. We hypothesize that biomaterial delivery systems functionalized with immunosuppressive cytokine IL-10 will promote DC-mediated amelioration of autoimmunity.

The main objective of cellular therapies against autoimmune disease involves skewing the T cell compartment towards tolerance in an antigen-specific manner. Thus, the design of biomaterials to maintain cell viability and the ability to condition T cells towards tolerance is paramount for effective treatments. As IL-10 has been shown to induce a tolerizing phenotype in DCs[7,8], the proposed delivery system utilizes IL-10 covalently-

tethered to PEG-4MAL polymers in a bulk hydrogel carrying therapeutic DCs. This strategy aims to fully optimize the viability, function, and localization of delivered DCs by (1) uncovering structure-function relationships between PEG-4MAL scaffolds and encapsulated DCs, by (2) incorporating adhesive and immunological cues to promote the sustained function of therapeutic DCs post-injection, and by (3) validating the contribution of PEG-4MAL delivery and the mechanism of tolerance in a mouse model of MS.

1.1 Research Significance and Innovation

The innovation here lies mainly in applying cutting-edge immunological and neuropathological concepts for tolerance-induction and immunomodulation that can be induced and capitalized on using the multi-component modular, biomaterial approach. It is anticipated that the proposed strategy will be clinically translatable due to its personalized, scalable, immunomodulatory ability for multiple MS antigens, localized at a key anatomical location as a means of modulating the immune status. The unique concepts used here include the use of IL-10 for IL-10-secreting DC10s induction as these cells have a unique role in tolerance induction through human leukocyte antigen G (HLA-G) and type 1 regulatory T cells (Tr1)[9]. A significant advantage of DC10s is the ability to process and present other self-antigens in a regulatory context[10], whereas acellular, single antigen-based approaches are limited to one epitope[11,12]. The environment surrounding the cell-based delivery system and cervical LNs can influence the recruitment of immune cells and antigen from the CNS. It is expected that tolerogenic DCs will modulate autoimmune mechanisms by conditioning cognate T cells and other DCs recruited to the gel and the cervical LNs. Tolerized endogenous DCs and Tregs will exert their effects after migration

to the CNS, which is antigen-driven[13] and increased in individuals with MS[14]. Using notation for the human system, the mechanisms of this immunomodulation is expected to be multifunctional (1) through an IL-10 and HLA-G+-mediated inhibition of effector cells[15-17], (2) HLA-G1 trogocytosis to form both of CD8+ and CD4+ HLA-G+ regulators[18], and (3) IL-10 induced expression of HLA-G to form Tr1[19]. In the human application, tolerogenic DCs will be derived from peripheral blood mononuclear cells (PBMCs), which has been shown to produce stable and tolerance-inducing cells even when derived from patients with Systemic Lupus Erythematosus (SLE)[20] and MS[21].

Another innovation is delivering the biomaterial in the cervical (neck) region to localize immunomodulation at an anatomical site of unique pathophysiological significance for the CNS[22-24], and presumably for disease intervention. Thus, hydrogels containing DCs will be injected subcutaneously into the neck of mice, the region drained by the cervical LNs, which also drain the CNS[25,26]. In this way, the immunomodulatory function of these DCs and their secreted products are placed at the relevant tissue site for MS, where immune cells and antigens from the CNS would drain to the cervical LNs[27]. Scalability is achievable by this biomaterial delivery strategy to facilitate translation to large animal models and clinical applications. The base polymer of the hydrogel, PEG, is used in FDA-approved products, and the hydrogel degradation products have no local or systemic toxicity, minimal inflammation, and are rapidly cleared via the urine (96% clearance in 24 hours)[28]. Although injectable PEG-based hydrogels have not yet been pursued for FDA-approval, these biomaterials are safely used *in vivo* across a wide variety of applications in the literature[29-31]. In general, this tolerogenic biomaterial system serves as a model for developing cell-delivery scaffolds in immunosuppressive applications and

other complex immunological diseases where a multipronged approach is needed (e.g., islet transplantation for treatment of Type I diabetes, T1D). This biomaterial carrier's ability to target delivered cells and provide post-injection support at the implant site is expected to yield benefits analogous to use of injectable materials to support islet engraftment or for delivery of stem cells.

CHAPTER 2. SPECIFIC AIMS

2.1 Specific Aim 1

Characterize the relationships between the biophysical and biochemical properties of PEG-4MAL hydrogels and dendritic cell viability and an immature phenotype.

2.1.1 Significance and Approach

Aim 1 is focused on the relationship between the mechanical properties of biomaterials scaffolds and the viability and phenotype of encapsulated DCs. Much effort has been dedicated to studying materials that act as adjuvants to DCs (including past work from this lab). Still, little has been done to further develop biomaterial delivery systems for DCs functioning in the opposite context, immunosuppression. Biomaterial epitopes that mimic pathogen-associated molecular patterns (PAMPs) and damage-associated molecular patterns (DAMPs) have long been the focus of immune cell-biomaterial interactions. However, this research aims to characterize the relationship between biophysical and biochemical properties, both microscopic and macroscopic, and DC viability and phenotype. The stiffness, mesh size, degradability, and adhesive properties of PEG-4MAL hydrogels will be probed through varying the polymer density, macromer size, crosslinker type, and adhesive peptides. The results from Aim 1 are expected to elucidate the governing principles influencing DC viability and phenotype to provide a framework for the development of biomaterials tailored to DCs in tolerogenic applications. This work will serve as an optimization process for the delivery scaffold to be used in Aims 2 and 3, as well as an investigative approach to defining the effect of these bulk hydrogels with varying

biophysical and biochemical properties on DCs. We hypothesize that RGD-functionalized hydrogels with lower stiffnesses and moderate mesh sizes that are fast will best support encapsulated DC viability and an immature phenotype.

2.2 Specific Aim 2

Design and characterize controlled release hydrogel systems functionalized with IL-10 to further support viability and an immature phenotype in DCs, protect DCs from inflammation, and directly tolerize cells adjacent to the delivery site.

2.2.1 Significance and Approach

Materials that have no activating effects on immune cells have been discovered and were previously considered "bioinert," but the research proposed here aims to transform a polymer-based biomaterial into a material that is capable of directly inducing tolerance while also achieving targeted cell delivery. To date, there have been no biomaterial epitopes identified that inducing tolerogenic or regulatory signaling in DCs. The multifunctional biomaterial platform utilized herein allows direct attachment of biomolecules to the polymer structure, enabling both (1) presentation of immunomodulators to encapsulated cells and (2) controlled release of immunomodulators. For subsequent experiments in this thesis, the optimized hydrogel formulation for our proof-of-concept disease model will be utilized based on the findings from Aim 1. The goal for this aim is to engineer immunomodulatory PEG-4MAL scaffolds that support therapeutic DC viability and function through covalently tethering IL-10 to PEG-4MAL. This process will first involve the modification of IL-10 to add free thiol groups before developing the PEGylation process. The bioactivity of PEG-4MAL-bound-IL-10 (PEG-

IL10) will be thoroughly investigated and the effect of tethered IL-10 on DCs before and after release from hydrogels will be quantified. Additionally, proposed experiments will illustrate the protective effect of hydrogel encapsulation and IL-10 treatment against inflammation by incubating DC-laden hydrogels in media with a relatively high concentration of a moderate stimulus (tumor necrosis factor-α, TNF-α; and interferon-γ, IFN-γ) or a severe stimulus (lipopolysaccharide, LPS). The controlled release of tethered IL-10 from the optimized PEG-IL10 hydrogels will be modeled and tuned to meet the needs of our *in vivo* application. We hypothesize that IL-10 conjugation to PEG-4MAL will not significantly affect its bioactivity. We expect that these hydrogels will promote a tolerogenic phenotype in encapsulated DCs, protect encapsulated cells from inflammation, and directly tolerize nearby cells through the controlled release of IL-10.

2.3 Specific Aim 3

Assess the ability and primary mechanism of hydrogel-delivered dendritic cells to ameliorate symptoms in a mouse model of MS.

2.3.1 Significance and Approach

While identifying DC-biomaterial interactions to develop a suitable delivery system (Aim 1) and engineering an otherwise benign biomaterial to induce tolerance (Aim 2) represent significant contributions to scientific knowledge, Aim 3 focuses on confirming the benefits of biomaterial delivery *in vivo*, which is most important to advancing the clinical translation of DC therapies. Experiments in Aim 3 will first assess the ability of the proposed cell-biomaterial therapy to ameliorate autoimmune disease in a model of experimental autoimmune encephalomyelitis (EAE) compared to DCs delivered

subcutaneously. DC10s are known to be proficient at inducing T regulatory cells, but these experiments aim to illustrate the importance of targeted delivery and post-injection cell support provided by our immunosuppressive biomaterial niche. Processing immunological and disease-relevant tissues (such as the spleen, LNs, CNS, and the hydrogel site) of EAE mice will provide insights into the mechanism of tolerance that leads to amelioration of symptoms. By employing congenic strains of mice, delivered DCs can be tracked, and the phenotypes of delivered and endogenous cells can be distinguished. Migration and co-culture studies *in vitro* will be conducted to recapitulate the effects observed *in vivo* and further support the proposed mechanism. We hypothesize that, compared to DCs inoculated independently, hydrogel-delivered DCs will significantly ameliorate symptoms of EAE mice through the induction of T regulatory cells mediated by IL-10.

CHAPTER 3. LITERATURE REVIEW

3.1 The Role of Dendritic Cells in Immune Responses

3.1.1 Adaptive Immune Responses

Identification of DCs was credited to Ralph Steinman in 1973 when he discovered that these cells were required to produce a humoral immune response[32]. He named these cells based on their dendritic extensions, a process by which DCs create a greater cell surface area for enhanced antigen sampling. DCs are considered professional antigen-presenting cells (APCs), whose primary role is to phagocytose proximal antigen, internally process antigens, and present antigens on major histocompatibility complexes (MHCs) to condition other immune cells. DCs are responsible for recognizing self and foreign antigens and subsequent conditioning of T cells, B cells, and other immune cell types.

The three effector mechanisms of adaptive immunity[33,34], defined as being antigen-specific, are: (1) B cell differentiation into plasma cells, which secrete specific antibodies as the humoral response; (2) $CD4^+$ T helper (T_H) cells are conditioned by APCs and assist immunogenic functions through cytokine release and effector cell support; and (3) $CD8^+$ cytotoxic T (T_C) cells are conditioned by APCs and specifically attack antigen-presenting pathogens. Thus, DCs are necessary to instruct the downstream immune response for effective immunity in response to foreign antigens or homeostatic tolerance in response to self-antigens.

3.1.2 Development and Function of Dendritic Cells

DC development begins with hematopoietic progenitor cells in the bone marrow, which differentiate into plasmacytoid DC (pDC) or conventional DC (cDC) progenitors that circulate through the body[35,36]. Plasmacytoid and conventional DCs differ in their morphology, surface marker expression, function, and expression of PRRs[35]. The life cycle of DCs includes differentiation into immature DCs, infiltration into peripheral tissues, sampling the environment for antigen, phenotypic maturation in response to a pathogen, migration to proximal LNs, and conditioning effector cells until cell death. DCs have an extremely limited ability to proliferate, and it has been estimated that the lifespan of DCs is on the order of 2 weeks once reaching the fully differentiated iDC state[37].

Circulating DCs continue to develop and infiltrate peripheral tissues through the vasculature where naïve, or immature, DCs begin to sample antigen. In peripheral tissues, DCs are continually sampling their environment using pattern recognition receptors (PRRs) such as toll-like receptors (TLRs), Nod-like receptors (NLRs), c-type lectin receptors (CLRs), and retinoic acid-inducible gene-I (RIG-I)-like receptors (RLRs) to search for epitopes that warrant an immune response[38]. Upon ligation of PRRs, DCs envelope the foreign material through phagocytosis, receptor-mediated endocytosis, or micropinocytosis, and each affects the presentation of peptides by DCs differently[39,40]. Intracellular DC machinery then digests proteins and presents a representative peptide on MHC-I or MHC-II (depending on the context) to enable highly specific conditioning of lymphocytes with the same specificity[41]. After processing foreign antigen, DCs fundamentally change their function by downregulating molecules involved in antigen sampling (CC-chemokine receptor-5, CCR5, and CCR6) and upregulating cell surface

markers (CD80, CD86) and cytokines (TNF-α; interleukin-12, IL-12) involved in conditioning lymphocytes and CC-chemokine receptor-7 (CCR7), which drives their migration to LNs[14,42]. LN architecture enables fast and efficient sampling (driven by lymphocyte affinity to peptide-MHC, pMHC) of lymphocytes by DCs searching for immune cells specific to the presented antigen. Once a cognate lymphocyte is found, the process of conditioning involves three types of signaling: (1) T cell receptors (TCR) bind to pMHC on DCs to ensure DCs are modulating the appropriate lymphocyte, (2) differential expression of co-stimulatory (CD80, CD86) and co-inhibitory (programmed-death ligand-1, PD-L1) molecules signaling activation or regulation of lymphocyte functions, and (3) distinct secreted cytokines (IL-10, IL-12, TNF-α, interleukin-6, IL-6; transforming growth factor-β, TGF-β) that inform the type of effector function to be induced[43-45]. Additionally, there have been some examples DCs imprinting a target location for T cells to migrate to, although this does not always occur (or has not been identified). For instance, gut-homing lymphocytes primed by retinoic acid-induced upregulation of $\alpha_4\beta_7$ and CC-chemokine receptor-9 (CCR9)[46]. Similarly, DCs imprint skin trafficking on lymphocytes by vitamin D-mediated upregulation of CC-chemokine receptor-10 (CCR10) on T cells[47]. Recent studies have shown that lung resident DCs were capable of targeting lymphocytes to the lung tissue via CCR4[48,49].

DCs are the bridge between innate and adaptive immunity and the most proficient cells at conditioning antigen-specific immune responses. DCs are directly involved in vaccination and immunotherapies due to their plastic and robust nature. As cells indispensable to a competent immune system, DCs are an important target for both immunoactivation, as related to infectious disease prevention[45] and treatment of solid

tumors[50,51]; and immunosuppression, as related to transplantation acceptance[52] and autoimmunity[6,53,54].

3.2 Pathophysiology of Multiple Sclerosis

Treatment of MS in human patients is the eventual goal of the research conducted herein. Biomaterial optimization and design will be tailored to the context of MS treatment and will be validated in a murine model of MS (EAE). However, the strategies developed here can be modified to cater to any cell therapy delivered in an immunosuppressive context, such as in the treatment of autoimmune disease, transplantation, and allergy. Autoimmune diseases are disorders of the immune system which, due to genetic predisposition[55] or environmental factors[56-58], result in chronic inflammation or antigen-specific destruction within the body. The initiators of autoimmune disease are varied and widely debated, but common threads suggest that immune cells recognize self-antigens as foreign pathogens and activate immune response to host tissues[59]. Breakdowns in homeostatic tolerance mechanisms may also contribute to disease, by which developing autoreactive T cells escape negative selection in the thymus. In antigen-specific autoimmune diseases such as MS, DCs and other APCs have been implicated in the pathological changes that lead to autoimmune disease[59,60].

3.2.1 Multiple Sclerosis

MS is an autoimmune inflammatory disease characterized by axonal demyelination in the CNS and resultant neurological deficits[59,61]. Multiple sclerosis (MS) is the most common cause of chronic neurological disability and remains a considerable detriment to the health and financial well-being of the US population[61]. Within 15 years of diagnosis of

relapsing-onset MS, 75% of patients are unemployed[61]. It is estimated 3% of the US population is affected by an autoimmune disorder, including MS[2]. Neurodegeneration due to MS can lead to a loss of motor control, cognitive deficits, and eventual paralysis[59]. Currently, there is no cure for MS, and present treatment strategies aim to slow the progression of neurodegeneration in patients through inhibition of neuroinflammation. The autoimmune attack on the CNS in MS has been suggested to be a secondary pathogenic factor evoked by CNS injury[62]. Autoimmunity against myelin antigens, such as myelin basic protein, further exacerbates the autocatalytic process of neurodegeneration[59]. IFN-γ-producing T_H1 and interleukin-17 (IL-17)-producing T_H17 CD4+ helper T cells contribute to CNS autoimmunity[63]. T_H1 and T_H17 cells are proinflammatory and propagate autoimmune responses through uncontrolled activation of other T_H cells, myelin-specific CD8+ T cells, autoantibody-producing B cells, and cognate DCs[64]. This immunoactivation can be controlled by tolerance-inducing regulatory T cells (Tregs) and regulatory B cells, and a deficit of regulatory Forkhead Box P3+ (FoxP3+) T cells (CD4+ and CD8+) is associated with MS lesions[15,65]. Thus, the severity and progression of MS is dependent on the balance between the number and functional capacity of inflammatory auto-reactive T cells and Tregs[66]. Thus, many therapeutic strategies aim to either increase the number and functional capacity of Tregs or decrease the number and functional capacity of autoreactive T_H1, T_H17, and CD8+ T cells.

Leading treatment strategies include drugs such as beta interferons, glatiramer acetate, dimethyl fumarate, fingolimod, mitoxantrone, ocrelizumab, and natalizumab[5,61,67]. These drugs function through systemic immunosuppression by inhibiting immune cell proliferation, replacing endogenous immune components, and preventing immune cells

from crossing the blood-brain barrier (BBB)[5,68]. If successful, these treatments only act to slow disease progression and are accompanied by a myriad of side effects such as a higher risk of opportunistic infection, risk of autoimmunity, depression, and organ damage[4].

While the exact cause of MS is under debate[59], significant findings have highlighted both genetic[55] and environmental factors[2,57,58] as being correlated to the onset of MS. Candidate genes have been linked to both MS and other autoimmune diseases, suggesting that the onset of MS is indeed immune-mediated, likely through modulation of inflammatory cytokines[69,70]. Evidence of environmental factors contributing to autoimmunity primarily points toward molecular mimicry as the pathological mechanism, which is the concept that a foreign antigen processed by APCs may closely mimic an autoantigen[58]. Increased inflammation adjacent APC presentation of self-antigen and APC-induced activation towards molecular mimics results in an autoimmune state of autoreactive immune cells.

Once MS is established in an individual, T cells targeting epitopes on myelin basic protein (MBP), myelin-oligodendrocyte glycoprotein (MOG), or proteolipid protein (PLP) in the CNS destroy the myelin sheath leaving axons exposed[59]. Self-inflicted neurodegeneration causes signal propagation to be inefficient and eventually disrupted, which translates to a loss of motor control, other cognitive deficits, and eventual paralysis. Several disease subtypes of MS in humans exist, most commonly including relapsing-remitting MS (RR-MS), primary progressive MS, and secondary progressive MS[59]. The heterogeneity in disease subtype, diversity of target self-antigen, and variable patient responsiveness make MS difficult to treat effectively.

3.2.2 Mechanisms of Tolerance

In healthy individuals with a stable immune system, tolerance is achieved primarily through central tolerance and peripheral tolerance. Central tolerance is the process of negatively selecting autoreactive T cells and B cells in the bone marrow and thymus while they are in development[71]. Perturbations to these homeostatic tolerance mechanisms have been suggested to contribute to the development of autoimmune diseases.

In the thymus, T cells are first checked for their capability to bind to pMHC complexes before assessing their affinity to self-antigen[72]. T cells that bind self-peptides are signaled to apoptose, protecting the individual from the downstream auto-inflammation that would have otherwise occurred[34]. The purpose of peripheral tolerance is to inhibit any autoreactive lymphocytes that might escape central tolerance mechanisms. In peripheral tissues, self-reactive T cells are controlled in three ways: clonal deletion, conversion to T regs, or induction of anergy[73]. Clonal deletion is achieved by apoptosis of autoreactive T cells conditioned by healthy DCs that correctly identify self-peptides. This direct mechanism of killing T cells is analogous to the clonal deletion process in the thymus during central tolerance. DC-mediated conversion of autoimmune T cells into Tregs can also occur by secreting immunosuppressive cytokines (namely IL-10) and presenting co-inhibitory surface markers (or just a lack of co-stimulatory markers) in the context of self-pMHC complexes[74]. This process also induces tolerogenic phenotypes in other lymphocytes, such as macrophages and B cells. The final mechanism of peripheral tolerance is the induction of anergy, a state defined by T cell inaction in response to their cognate antigen. T cells are suppressed by DC presentation of the cognate antigen in the absence of co-stimulation (CD80, CD86) or the presence of co-inhibition (PD-L1)[75].

Anergic conditioning renders T cells ineffective which neutralizes its autoreactive immune response and moderates over-stimulated inflammation.

Tregs, whether induced or natural, play a vital role in the homeostasis of immunity in healthy individuals. Tregs maintain tolerance in CD4+ T helper cells, CD8+ cytotoxic T cells, B cells, and other lymphocytes, most notably through secretion of immunosuppressive cytokines, such as IL-10, adenosine, and TGF-β[76]. These cells are also able to regulate their educators, DCs, through a combination of immunosuppressive cytokines and presentation of cytotoxic T-lymphocyte-associated protein 4 (CTLA-4), which binds co-stimulatory molecules on DCs[77]. Regulatory T cells can tolerize cognate DCs through depletion of pMHC complexes from the surface of DCs in an antigen-specific manner by trogocytosing portions of the DC membrane[78]. Studies have shown that mature DCs tolerized by Tregs can become immunosuppressive by upregulating the production of indoleamine 2,3-dioxygenase (IDO), an immune checkpoint molecule that suppresses T effector cells and induces tolerized phenotypes in other lymphocytes[79]. Tregs also maintain functioning immunity by killing autoreactive T effector cells through Granzyme B-mediated apoptosis[80]. Increased levels of interleukin-2 (IL-2), a characteristic of T effector cell activation and proliferation, can be sensed by Tregs and leads to the initiation of these various immunosuppressive processes as a method to moderate inflammation[81].

3.2.3 Strategies for Intervention

Therapeutic modulation of the immune system to treat autoimmune disease is targeted mainly to the components of homeostatic tolerance discussed previously. Clinically active and progressive MS is treated with drugs such as interferon β-1α (IFNβ-1α), glatiramer acetate, teriflunomide, dimethyl fumarate, fingolimod, mitoxantrone,

alemtuzumab, and natalizumab[5,61,67]. These drugs generally suppress immune function by hindering immune cell proliferation, serving as an immune system decoy, and reducing immune cell migration through the BBB[68]. While these drugs slow MS progression, they only reduce the symptom severity and disease progression and are associated with increased risks of infection, depression, and organ damage[61]. Recent studies have shown effectiveness in ameliorating EAE with acellular, biomaterial-based tolerizing strategies, such as a dual-nanoparticle system that drains to LNs and modulates DCs *in vivo*[12]. However, acellular approaches are limited to the antigen being delivered and cannot adapt to antigen-spreading or unknown antigens. Therapeutic strategies based on DC-delivery also benefit from the ability to condition several types of immune cells directly and migrate based on chemotactic or antigen gradients *in vivo*.

Promoting tolerance towards MS-disease associated antigens is expected to ameliorate MS disease immune stimulation. Antigen-specific DC-based immunotherapies are being considered to replace the above noted broadly immunosuppressive drug therapies to reduce patient risks and maximize therapeutic outcomes[6]. Theoretically, antigen-specific therapeutic vaccination is designed to specifically restore tolerance to self-antigens. In this way, treatment specifically targets the autoimmune disease without systemic effects on the immune system. DC phenotype is central to determining the balance between immunity and tolerance, and an imbalance mirrors that of T cells and contributes to autoimmunity. This is demonstrated by DCs in the CNS that play dual roles of supporting the EAE disease process[82] or of inhibiting T cell responses leading to protection from EAE[83], presumably as directed by the DC phenotypic spectrum. As discussed previously, tolerogenic DCs can induce Tregs[84], which are responsible for inducing tolerance[85]. Tregs have the ability to

produce various anti-inflammatory molecules, such as immethridine, histamine H3-receptor agonist[86], or 14-dehydroergosterol[87], to affect endogenous DCs function.

The level of investigation into tolerogenic DC therapies has expanded since Getts et al. first demonstrated long-term T-cell tolerance using apoptotic splenocytes crosslinked to present encephalitogenic peptides[22,88]. Some protocols deliver tolerogenic DCs induced with immunomodulatory molecules such as 1,25-dihydroxyvitamin D3 (VD3)[89-91] and IL-10[92], while more recent strategies have employed hepatocyte growth factor (HGF)[93,94], BD750 (a JAK3/STAT5 inhibitor)[95], GSK-J4 (a selective inhibitor of JMJD3 and UTX)[96], triterpenoid CDDO-DFPA (RTA-408)[97], Tofacitinib (a Janus kinase inhibitor)[98], LPS[99], and apoptotic cells[100,101]. Interestingly, the mechanism by which apoptotic cell-treated DCs induce tolerance appears to mirror DCs treated with IL-10 and TGF-β, which function by blocking T_H17 cell activity[101] and inhibiting CD4+ effector memory T cell development[100]. Specifically, apoptotic cell-treated DCs induce Tregs by secreting TGF-β, inhibiting T cell proliferation by upregulating PD-L1, and by downregulating retinoic acid receptor–related orphan receptor γt (ROR-γt), IL-21, and IL-22 in CD4+ T cells[101]. Other strategies have genetically engineered tolerogenic DCs to overexpress various immune mediators, such as CD40 and interleukin-23p19 (IL-23p19)[102], and CCR5[103]. Recent studies administer tolerogenic DCs through intravenous, intradermal, intraperitoneal, intranodal, and subcutaneous delivery, resulting in a systemic distribution of therapeutic DCs[104,105]. However, systemic delivery may not be optimal as intracerebral (but not systemic) delivery of stimulatory or inhibitory tolerogenic DCs mediated EAE disease severity or amelioration, respectively, suggesting that the anatomical site for DC delivery is important for neurological functionality[106]. Furthermore, the primary antigen target may

not be known, or it may shift during disease progression, known as epitope spreading, making antigen responsiveness of adoptively transferred tolerogenic DCs a desirable benefit of this approach – a phenomenon known as "infectious tolerance"[107]. Another consistent trend across studies with tolerogenic DCs is that large numbers of cells and often multiple doses of tolerogenic DCs are necessary for significant amelioration of EAE[99,108,109]. Multiple doses are likely necessary due to the low yield of tolerogenic DCs that remain viable, tolerogenic, and reach the target site (cervical LNs). While multiple high doses of tolerogenic DCs may ameliorate autoimmunity in mice, this strategy presents a challenge to translation, where cost and cell number are major barriers to therapy development. The tolerogenic DCs utilized herein will take advantage of the natural immunosuppression provided by IL-10, which produces DCs that have superior tolerogenic function versus other treatments[7].

Tolerance-inducing therapeutics are currently under clinical investigation. To date, three open-label, single-center phase I clinical trials evaluating the safety and tolerability of myelin-derived peptide-pulsed tolerogenic DCs administered intradermally, intranodally, or intravenously are ongoing or have recently concluded (clinicaltrails.gov identifiers NCT02618902, NCT0290353, and NCT02283671)[110]. Nonetheless, numerous questions remain including dose, route, and frequency of administration before the widespread use of these vaccination strategies[111]. Of these, the route of delivery for tolerance inducing strategies is particularly important since the site of deposition of the administered product will influence the immune response induced. For induction of tolerance, tolerogenic DCs would need to exert their effects on autoreactive T cells found in relevant lymph nodes. Another cited issue is that delivered tolerogenic DCs may need

to shuttle to draining lymph nodes or may need to exert their immunomodulatory effect upon migration across the BBB. Steady-state migration of DC out of the CNS to cervical LNs is noted to be essential for the maintenance of immune tolerance to brain-derived antigens[112]. Results from NCT02283671 show that delivering tolerogenic DCs was safe but had limited efficacy based on secondary measurements[109]. In another DC therapy utilizing immunoactivated DCs to promote immune responses in solid tumors, migration towards lymph nodes was much lower after subcutaneous injection than after intradermal injection, whereas the migration of intravenously injected cells has so far not been monitored in humans[113,114]. Nevertheless, *in vivo* studies in patients with cancer have shown that, after intradermal injection, only 2–4% of the DCs migrate to draining lymph nodes[105]. Poor targeting of DCs has been supported in several murine studies, with one study showing DC accumulation in the liver and spleen after intravenous delivery[104] of tolerogenic DCs in a model of EAE. One potential problem with wide biodistribution of tolerogenic DCs is the hindrance of functional immunity in off-target organs. The physiological process for DC migration to LNs involves sampling antigen, maturing, and activating various migratory mechanisms. In the context of tolerogenic DCs, activation is counterproductive to the tolerizing function of the cell therapy, and alternative delivery methods need to be investigated. Improved delivery of tolerogenic DCs will contribute to better potency and lower costs which will be imperative after translation to autologous therapies, where cell number will be a limiting factor. Local delivery of tolerogenic DCs via biomaterial systems can overcome issues such as potency, risk of disease propagation, cost of therapy, and therapeutic efficacy.

3.3 Dendritic Cell Responses to Biomaterial Systems

3.3.1 Biomaterial Adjuvant Effect and Receptor Signaling

Biomaterials are an essential consideration to achieve the optimal effectiveness of immunotherapies, as shown by the elucidation of immune cell-biomaterial interactions by the work of Julie Babensee et al[115-117]. The discovery of differential responses in DC activation and downstream T cell stimulation to various biomaterials inspired many of today's biomaterial immunomodulation strategies. DCs adjust their immune function accordingly, based on direct recognition of PAMPs on biomaterials through PRRs[118,119], which can result in favorable immunoactivation (such as in vaccination) or unfavorable immunoactivation (such as in transplantation). Work in this field has shown differential DCs responses to glycoconjugates[119] and highlighted materials such as polyethyleneimine (PEI) and polylactic-co-glycolic acid (PLGA) as significant adjuvants for DCs[120]. Oppositely, discoveries of biomaterials with non-activating epitopes, including hyaluronic acid and agarose-based scaffolds, resulted in immature and stable responses from DCs. Thus, biomaterial selection criteria and scaffold design parameters are heavily application-dependent and must be considered carefully.

Beyond the recognition of specific adjuvanting epitopes, the use of biomaterials to deliver payloads within nanoparticles (NPs) and microparticles (MPs) illuminated another set of biomaterial properties that influence DC activity. Parameters such as particle size, shape, and charge have been shown to significantly impact DC maturation[121]. Some examples from recent studies have engineered biomaterial NPs and MPs to target endogenous DCs and direct antigen processing outcomes[51,122]. Biomaterial adjuvants such as PEI have been used as delivery vehicles for antigen and chemokines to instruct antigen-

specific activation of DCs *in situ*[123,124]. Biomaterial encapsulation of tissues such as islet clusters delayed host rejection in a model of autoimmune diabetes mellitus[29,125]. DC-stimulating biomaterials have been utilized as cell delivery systems in the case of DC vaccination against solid tumor antigens[50,126].

However, there are far fewer studies investigating tolerance-inducing biomaterials for the maintenance of homeostatic immunity. To our knowledge, there are no biomaterials with molecular patterns that potentiate tolerogenic signaling with the exception of polysaccharide A – an endotoxin response to LPS, which is generally outweighed by a parallel inflammatory response[127]. However, the modular PEG-4MAL biomaterial system has been shown to be non-activating towards immune cells and can be engineered to promote tolerance through other functionalities.

3.3.2 Effect of Mechanical Characteristics on Encapsulated Cells

The process of encapsulating DCs in three-dimensional biomaterial scaffolds expands the range of properties that can modulate encapsulated DCs. The effects of the biophysical and biochemical properties of the environment on DCs have not been characterized as well as the effects of biomaterial epitopes. Cellular differentiation, morphology, viability, and function have been shown to be mediated by cell-extracellular matrix (ECM) interactions such as cellular attachment and spreading[128,129].

Mechanosignaling due to matrices with differential stiffnesses direct mesenchymal stem cells (MSCs)[130], pancreatic progenitors[129], and neural stem cells[128] to commit to different developmental pathways. Integrin-mediated signaling resulting from cell-cell and cell-ECM interactions has been implicated in cell morphology, differentiation, survival, and other cell processes[128,131-135]. A previous study demonstrated an adhesive peptide

mimicking the bioactive epitope of fibronectin, RGD, differentially increased DC maturation with increasing RGD concentration[133]. It is unclear whether downstream signaling of DC receptor ligation by RGD or the ability for DCs to recognize the substrate stiffness due to RGD is responsible for maturation. Cellular signaling from cell-ECM interactions is often different between two- and three-dimensional matrices, and it is widely accepted that three-dimensional synthetic polymer matrices can be engineered to provide a more biomimetic cellular environment[136].

Additionally, mechanical stimulation of DCs leads to increased expression of co-stimulatory molecule CD86 and cell death[137]. These effects have been observed in our lab; when training new students to handle DC cultures correctly, physical disturbances to the culture plates often results in DCs with activated phenotypes similar to our mature controls. Poly(2-hydroxyethyl methacrylate) (pHEMA) and poly(dimethylsiloxane) (PDMS) hydrogel scaffolds with varying pore sizes have been shown to differentially modulate DC viability, expression of co-stimulatory markers (CD86, CD80), and secretion of inflammatory cytokines (TNF-α, IL-6)[138]. This handful of studies suggests that the scope of biomaterial properties that modulate DCs is more extensive than what has currently been studied.

3.4 Biomaterial Systems for Cell Delivery

3.4.1 Controlled Release of Biomolecules

Efforts towards engineering biomaterial systems with controlled release of biomolecules can be organized into two major categories: entrapment of biomolecules within biomaterials and tethering biomolecules to biomaterials. Strategies of biomolecule

entrapment include PLGA NPs with therapeutic payloads and polymer-dense hydrogel scaffolds loaded with drugs control release of payloads by designing a system that significantly impedes diffusion. Alternatively, tethering strategies include therapeutics bound to PEG chains to increase circulation time and hydrogel scaffolds that can be tethered with virtually any biomolecule to achieve sustained release as the scaffold degrades.

There are currently more than 200 approved biomolecules used to treat various diseases and there are over 1,500 in clinical trials. Biomolecules such as monoclonal antibodies, growth factors, hormones, and cytokines are most commonly used to kill specific cells or inactivate unwanted proteins but they can also be applied to influence cell differentiation, activation, migration, and other cellular processes. Many strategies have been developed to extend or improve the delivery of drugs, thereby increasing their effectiveness. Biomaterials have a major role in the design of controlled release systems for the delivery of biomolecules, most commonly through encapsulation of pharmaceutical and biological compounds. Nanoparticles, microparticles, hydrogels, and their biological analogs (liposomes, micelles, etc.) deliver payloads in a highly tunable fashion by modulating particle size, shape, hydrophobicity, degradability, charge, and other factors[139-141]. Site targeting can be accomplished through the functionalization of particles with tissue-specific peptides[142,143]. Diffusion of biological compounds from polymeric hydrogel systems can be further engineered by modulating hydrogel volume, drug concentration, and, most importantly, mesh size[144-146].

Controlled release through biomaterial functionalization is most simply achieved by conjugating polymer chains (i.e., PEGylation) to biomolecules to extend their half-life of

circulation by reducing renal clearance[147]. Biomaterial functionalization with chemokines, cytokines, or other biologics can direct cells to mediate cellular activities such as migration, proliferation, survival, and differentiation. This conjugation of biomolecules to biomaterial systems enables robust control over the rate and location of release in response to various stimuli. Microgels and hydrogel scaffolds degrade and release product differentially by exposure to water[148], proteases[149,150], ultraviolet light[151], change in pH[152], or combinatorial gates[153] depending on the hydrogel crosslinker. Engineering stimuli-sensitive crosslinkers allows for robust spatiotemporal control over biomolecule release.

The modular function of biomaterials to present biomolecules and control their release is an important consideration for immunomodulatory strategies. PEG-4MAL hydrogel systems are empowered by such approaches, enabling both immunomodulator presentation to encapsulated DCs and protease-responsive controlled release of immunomodulators.

3.4.2 Biomaterial Hydrogels as Cell Delivery Scaffolds

Hydrogel systems are increasingly being used as cell delivery scaffolds in cell therapy[126], transplantation[29,30], and regenerative medicine[154,155] applications. Hydrogels significantly improve the effectiveness of cell therapies through localized delivery of cells to disease-relevant sites. In transplantation, hydrogel delivery of transplanted cells or tissues prevents endogenous DC recognition of foreign antigens presented on transplanted tissues by functioning as barriers[29]. Hydrogel systems are especially utilized in a regenerative capacity, where the polymer matrix can serve as a temporary ECM to be remodeled by infiltrating cells in a tissue-specific manner while also presenting cues that support cell growth and vascularization[156].

Cellular differentiation, morphology, viability, and function have been shown to be mediated by cell-ECM interactions such as cellular attachment and spreading[128,129]. Cellular signaling from cell-ECM interactions is often different between two- and three-dimensional matrices, and it is widely accepted that three-dimensional synthetic polymer matrices can be engineered to provide a more biomimetic cellular environment[136]. Mechanosignaling due to matrices with differential stiffnesses direct mesenchymal stem cells (MSCs)[130], pancreatic progenitors[129], and neural stem cells[128] to commit to different developmental pathways. Cellular attachment due to various adhesive ligands in synthetic hydrogels control the fate of immune cell function and differentiation[157].

Mechanical properties of biomaterial scaffolds for cell delivery is an essential consideration for the viability and function of encapsulated cells. The highly modular PEG-4MAL platform benefits from both localized delivery of cell therapies and directing cellular responses through tunable mechanical and adhesive properties[131,158,159].

Biomaterials have widely been used to target various cell therapies to the respective sites of disease, including MSCs for chondral defects[160], macrophages for wound healing[161], and islet clusters for Type 1 Diabetes[29]. Biomaterial delivery enables post-injection control of tolerogenic DC fate, whereas tolerogenic DCs administered alone are at risk of off-target effects such as non-antigen-specific immunosuppression (due to cytokine release) and becoming immunogenic in the highly inflammatory environment of autoimmune patients, propagating disease instead of ameliorating it[162,163]. Highly customizable polymer hydrogel systems can be utilized to facilitate effective delivery of tolerogenic DCs to the cervical LNs (where CNS-resident DCs and antigens drain to, the primary site for conditioning autoreactive T cells)[112]. Using biomaterials to co-localize

DCs to the site of activity can improve the efficacy of DC therapies by shortening the distance of migration to the target site, positioning in proximity to recruit endogenous effector cells, or ensuring DCs enter the lymphatics upstream of the most disease-relevant LNs (cervical LNs for MS). A significant prerequisite for biomaterial selection in this context is that the material must be non-immunogenic, such that the tolerogenic DCs to be delivered are not adjuvanted by the material in any way during delivery. Agarose, alginate, and other non-adjuvanting materials were considered, but another non-adjuvanting material, polyethylene glycol (PEG), was chosen due to its branched macromer precursor of which each arm is terminated with a maleimide group (PEG-4MAL), allowing for the incorporation of bioligands such as adhesive peptides, degradable or non-degradable peptide crosslinkers, and growth factors[29,156]. Crosslinking of these macromers occurs through a Michael-type addition reaction, which is cytocompatible to enable cell encapsulation within the hydrogel[159]. This biomaterial system provides an injectable, *in situ* crosslinkable, degradable PEG hydrogel for localized delivery of tolerogenic DCs. Preparation of PEG-4MAL hydrogels is also very technically simple, and functional components of the system can be swapped out with ease. Collectively, the additional capabilities, modularity, and ease of use render PEG-4MAL hydrogels superior to other non-adjuvanting biomaterials and is thus our biomaterial of choice. The PEG-4MAL hydrogel system has been modulated for use with a variety of cells, including Islets of Langerhans[29,164], cardiac progenitors[165], and skeletal muscle satellite cells[166]. The multifactorial properties of this biomaterial system allow it to be tailored to the delivered cells through the selection of adhesive peptide, incorporation of growth factors, and degradability through crosslinker sequences[167]. These biomaterials locally deliver cells

amidst a cell-stabilizing mechanical environment that promotes cell survival signaling through adhesive ligand presentation and protects from inflammatory mediators[168].

This hydrogel system can also be tailored for on-demand biomolecule release through proteins being covalently bound to PEG-4MAL via free cysteines or through physically entrapment in the hydrogel polymer mesh[169]. Hydrogel physical properties such as mesh size, modulus, gelation rate, and degradation rate are controllable by varying formulation variables such as polymer density, PEG-4MAL precursor molecular weight, crosslinker used (non-degradable or fast or slow degrading), and an additive used to control reaction rate[170]. Immunosuppressive proteins (such as IL-10) can be covalently tethered within the polymer network and controlled-released to combat inflammation at the site of delivery. Release rates can be tuned by modifying the ratio of degradable and non-degradable crosslinkers, and the released biomolecules are fully bioactive[149]. Biomolecules non-covalently entrapped within hydrogels can be released by simple diffusion or in response to degradative enzymes for those with incorporated degradable crosslinkers. In total, this system is in many ways analogous to "niches" of *in vivo* activation nodes for DCs, where instead of activating endogenous DCs, delivered tolerogenic DCs tolerize other endogenous immune cells.

CHAPTER 4. BIOPHYSICAL AND BIOCHEMICAL DESIGN OF PEG-4MAL HYDROGELS TO SUPPORT DENDRITIC CELL VIABILITY AND AN IMMATURE PHENOTYPE

4.1 Overview

Many studies have shown a direct relationship between cell function and signaling induced by the biophysical and biochemical properties of the surrounding matrix[131,138,157,171]. Due to the plasticity of DCs, the end state of DCs delivered as part of a cell therapy is likely mediated by mechanosignaling resulting from encapsulation in PEG-4MAL hydrogels. Scaffold stiffness in immunological tissues has also been correlated with malignant cancers[172] and differential T cell function[173], further demonstrating the importance of these biomaterial design parameters.

Therefore, the objective of this aim is to examine the relationship between biophysical and biochemical properties of PEG-4MAL hydrogels and encapsulated DCs derived from murine bone marrow. Our goals are to (1) characterize the PEG-4MAL biomaterial platform, and (2) relate the biophysical and biochemical properties of PEG-4MAL hydrogel matrices to murine DC viability and maturation. The working hypothesis for this aim is that physiologically-relevant tissue stiffnesses will support DC viability and an immature phenotype, while RGD promotes DC attachment and survival signaling without causing DC maturation. The rationale for this hypothesis is that DCs will respond similarly to a similar environment as is recognized *in vivo*, which is supported by studies with other cell types and matrix stiffnesses[130-132,157,174]. Although the presentation of RGD has been shown to activate DCs when seeded on a 2D scaffold[133], there can be disconnects

in the magnitude of cellular responses between ligands presented in 2D and 3D[136,158], and the effect of RGD presented in a 3D scaffold on bone marrow-derived dendritic cells (BMDCs) has yet to be investigated. Completion of this aim is expected to define the effects of PEG-4MAL hydrogels characteristics on the phenotype of encapsulated DCs and to select the optimal parameters for DC delivery in the context of EAE treatment.

4.2 Materials and Methods

4.2.1 Animals

All live animal procedures were conducted under the approval of the Institutional Animal Care and Use Committee (IACUC) of the Georgia Institute of Technology. Mice were housed, maintained, and bred in the Physiological Research Laboratory (PRL) Animal Facility of the Georgia Institute of Technology. Animals were 8-to-12-week-old male C57BL/6J mice (Jackson Laboratories, Inc.).

4.2.2 Differentiation of Dendritic Cells

Bone marrow was harvested from 8-week-old male C57BL/6J mice, red blood cells (RBCs) were lysed, and the remaining cells were washed twice in phosphate-buffered saline (PBS) with 10% fetal bovine serum (FBS). Cells were then cultured ($1.5x10^6$ cells/mL) in Dulbecco's Modified Eagle Medium (DMEM) with 10% FBS supplemented with 20 ng/mL granulocyte-macrophage colony-stimulating factor (GM-CSF) and interleukin-4 (IL-4), refreshed every three days, for six days. On Day 6, non-adherent cells were removed, and fully differentiated adherent iDCs were released from plates using CellStripper (Corning) for 15 minutes at 37°C/5% CO_2. DCs were then treated with 50

ng/mL IL-10 (DC10), 50 ng/mL TNF-α and 10 ng/mL IFN-γ (stimulated DCs, STIM-DC), 1 μg/mL LPS (mature DCs, mDC) or no treatment (immature DC, iDC) and cultured (10^6 cells/mL) in 24-well plates for 24 hours at 37°C/5% CO_2.

4.2.3 PEG-4MAL Hydrogel Synthesis

PEG-4MAL macromer (20 kDa; Laysan Bio) was dissolved in PBS containing 10 mM 4-(2-hydroxyethyl)-1-piperazineethanesulfonic acid (HEPES) (pH 7.4). GRGDSPC (RGD) cell adhesive peptide (>95% purity; GenScript) was dissolved in 1x PBS containing 10 mM HEPES and added to the PEG-4MAL to produce a solution of RGD-functionalized PEG-4MAL. After 10 minutes of incubation, the protease-degradable crosslinking peptide GCRDVPMSMRGGDRCG (VPM; GenScript) was added and hydrogels were polymerized at 37°C/5% CO_2 for 5 min. For hydrogels encapsulating DCs, cells were added to the mixture of PEG-4MAL and RGD prior to the addition of crosslinker.

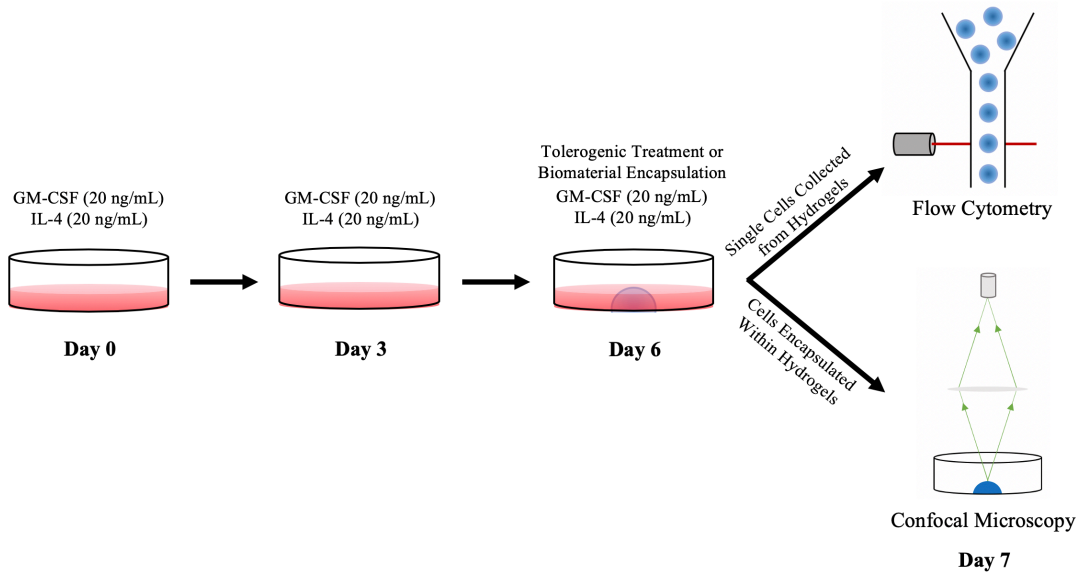

Figure 4.1. Schematic of BMDC culture, DC treatments schedule, and analysis techniques.

4.2.4 Characterization of Hydrogels

PEG-4MAL hydrogels were prepared as described in 4.2.3. Following this procedure, 10 µL hydrogels were cast in cylinder-shaped, Sigmacote-treated (Sigma-Aldrich) silicone molds. Once fully crosslinked, hydrogels were removed and swelled overnight in 1x PBS (pH 7.4) at 4°C. Hydrogels were then removed and examined using a rheometer (MCR-302, Anton Paar; CP10-2). Samples were maintained at 37°C while a frequency sweep (100 to 0.1 rad/s) was performed at a constant strain of 1%. Storage modulus (G') and loss modulus (G'') were determined by averaging values acquired within the linear range. PEG-4MAL hydrogels are viscoelastic materials that are primarily treated as linearly elastic based on higher G' values and lower G'' values (loss factor ~0.05 for most samples).

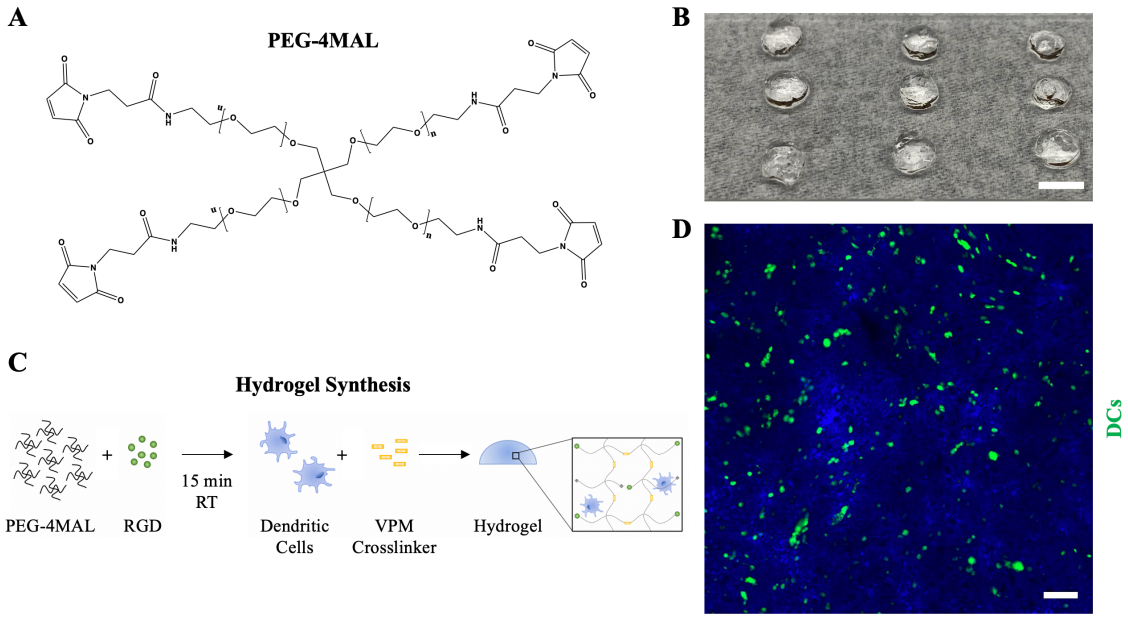

Figure 4.2. PEG-4MAL hydrogel overview and synthesis schematic. Schematic of a) PEG-4MAL chemical structure, b) macroscopic image of PEG-4MAL hydrogels (scale bar = 1 cm), c) process of hydrogel synthesis, and d) distribution of DCs in PEG-4MAL hydrogels (scale bar = 50 µm).

4.2.5 DCs Encapsulation in Hydrogels

PEG-4MAL hydrogels were prepared as previously described, with specified modifications to incorporate cells. After 10 minutes of incubating PEG-4MAL and RGD, DCs in 1x PBS containing 10 mM HEPES were added to the hydrogel solution at a concentration of 10^6 cells per 50 µL hydrogel. Immediately following the addition of DCs, the protease-degradable crosslinking peptide GCRDVPMSMRGGDRCG (VPM; GenScript) was added and hydrogels were polymerized at 37°C/5% CO_2 for 5 min. DC-laden hydrogels were incubated in the same DMEM-based media with cytokines, as specified previously.

4.2.6 Hydrogel Digestion

Media was removed and 1 mL collagenase II (2 mg/mL; Gibco) was added to each well of PEG-4MAL hydrogels encapsulating DCs. Hydrogels were incubated at 37°C/5% CO_2 for 15 minutes. Contents of wells were then pipetting directly into media with 25% FBS to quench collagenase II activity. Cells were collected by centrifugation at 300 xg and prepared for flow cytometry.

4.2.7 Flow Cytometry

DCs were washed with 1x PBS and then reconstituted in 100 µL of fluorescence-activated cell sorting (FACS) Buffer (Hank's Buffered Salt Solution, HBSS; 1% bovine serum albumin, BSA; 1 mM ethylenediaminetetraacetic acid, EDTA). TruStain FcX (anti-mouse CD16/32; BioLegend) was added, and cells were incubated on ice for 10 minutes. DCs were then stained with FITC-IA^b (AF6-120.1; BD), APC-CD86 (GL-1; BioLegend), BV785-CD11c (N418; BioLegend), and PE-PDL1 (MIH7; BioLegend) for 30 minutes on ice, protected from light. DCs were washed twice with FACS Buffer and analyzed on a flow cytometer (FACSAria III; BD). Propidium Iodide (PI) was added 5 minutes before analysis to assess viability. Gating strategies are illustrated in Figure A.5.

4.2.8 Confocal Microscopy

Cell viability was visualized by staining with calcein acetoxymethyl (AM) and ethidium homodimer-1 (EthD-1) and imaging on a confocal microscope (Nikon Eclipse Ti-E C2+). Media was removed and PEG-4MAL hydrogels encapsulating DCs were washed twice with 1x PBS by gentle pipetting. Samples were then stained with 1 µM

calcein AM and 1 μM EthD-1 in media without FBS for 20 minutes. Intact hydrogels were then washed two more times and media without FBS was added for imaging.

4.2.9 Cytokine Multiplexing

Supernatants were collected from samples at the end of culture and stored at -80°C until use. Samples were thawed to room temperature and treated according to the manufacturer's protocol for Bio-Plex Pro Mouse Cytokine 23-plex Assay (Bio-Rad). Samples were then analyzed on a Luminex MAGPIX. A linear range of cytokine concentrations was determined to optimal sample dilution according to cytokines of interest. Cytokines tested are categorized below in Table 4.1 based on their effects being inflammatory, pleiotropic, tolerogenic, or unrelated to DCs.

Table 4.1. Multiplexed Cytokines of Interest

Cytokines Assayed			
Inflammatory	Pleiotropic	Tolerogenic	Unrelated to DCs
IL-1α	IL-4	IL-10	IL-2
IL-1β	IL-13		IL-5
IL-3	G-CSF		IL-9
IL-6			IL-17A
IL-12p40			IFN-γ
IL-12p70			Eotaxin
TNF-α			
CCL2			
CCL3			
CCL4			
CCL5			
CXCL1			
GM-CSF			

*CCL = Chemokine ligand

4.2.10 Statistical Analysis

Experimental values are reported as mean and standard deviation for all samples. Statistical analysis was determined using one or two-way analysis of variance (ANOVA) coupled with Sidak's posthoc pairwise tests using GraphPad (Prism Inc.). All datasets were normally distributed. If datasets failed the Brown-Forsythe test (due to significant differences in variances between treatment groups), Welch's correction was applied to account for these differences and Dunnett's posthoc pairwise test was used. DC10 groups served as the control for comparison tests. p-values <0.05 were considered statistically significant. Error bars represent the standard deviation.

4.3 Results

4.3.1 Treated Dendritic Cells have Distinct Phenotypes and Secretory Profiles Mainly Distinguished by Cell Surface Markers CD86 & MHC-II and Cytokines IL-10, TNF-α, & CCL5

After 24 hours of treatment, DCs receiving various treatments exhibit distinct cell surface marker and secretory profiles. While viability was consistent across treatments, both TNF-α/IFN-γ-treated DCs and mDCs had significantly increased expression of both CD86 and MHC-II, with mDCs having the highest expression of both (Figure 4.3). Both adherent and non-adherent fractions of mDCs secreted significantly higher levels of TNF-α and CCL5, well known inflammatory cytokines (Figure 4.4). Interestingly, these mDCs also had increased secretion of anti-inflammatory IL-10 (Figure 4.4).

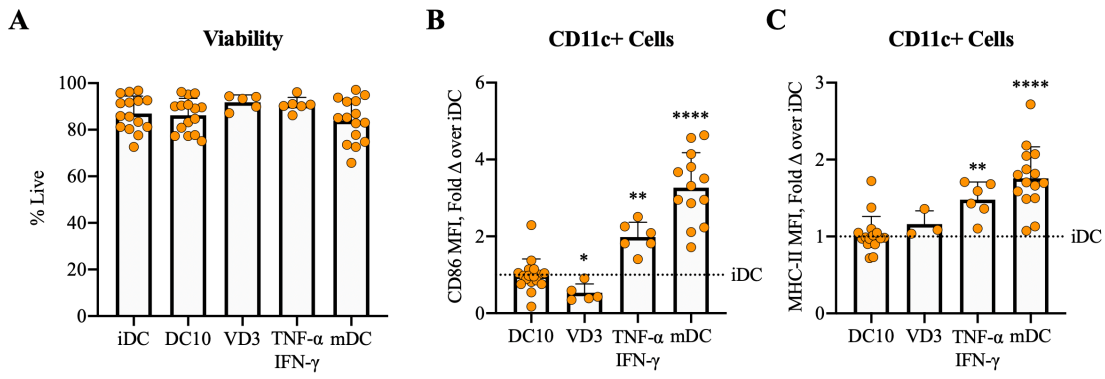

Figure 4.3. Viability and phenotype of CD11c+ DC controls. a) Live cells, b) CD86 expression, and c) MHC-II expression of DCs receiving various treatments were analyzed via flow cytometry after 24 hours. Live cells are defined by propidium iodide (PI) negative cells. ****p<0.0001, **p<0.01 and *p<0.05 via one-way ANOVA with Welch's correction and Dunnett's comparison test.

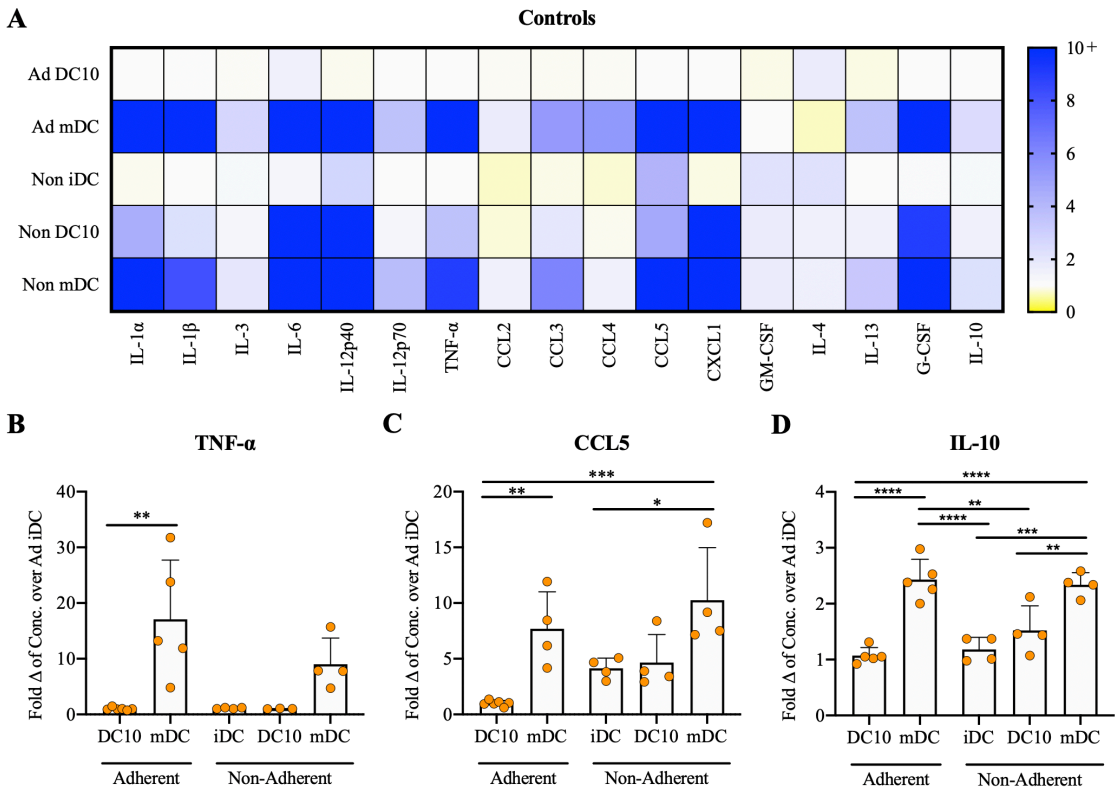

Figure 4.4. Cell secretory profiles of CD11c+ iDCs, DC10s, and mDCs analyzed by Luminex cytokine multiplexing. a) Heatmap of relevant cytokines assayed and comparison of fold change values for b) TNF-α, c) CCL5, and d) IL-10 compared to adherent iDC (Ad iDC). **p=0.0045 via Kruskal-Wallis test and Dunn's comparison test for b). ****p<0.0001, ***p<0.001, **p<0.01, and *p<0.05 via one-way ANOVA and Tukey's comparison test for c) and d).

4.3.2 Hydrogel Stiffness Increases and Mesh Size Decreases as Polymer Density Increases

An expected increase in hydrogel stiffness is represented by significantly higher values of G' and G'' with increasing polymer weight percentage (Figure 4.5). Mesh sizes of hydrogels were calculated using storage modulus based on Rubber Elasticity Theory[175,176]. Figure 4.5 illustrates a significant decrease in hydrogel mesh size with increasing polymer weight percentage, as the hydrogel polymer network becomes denser.

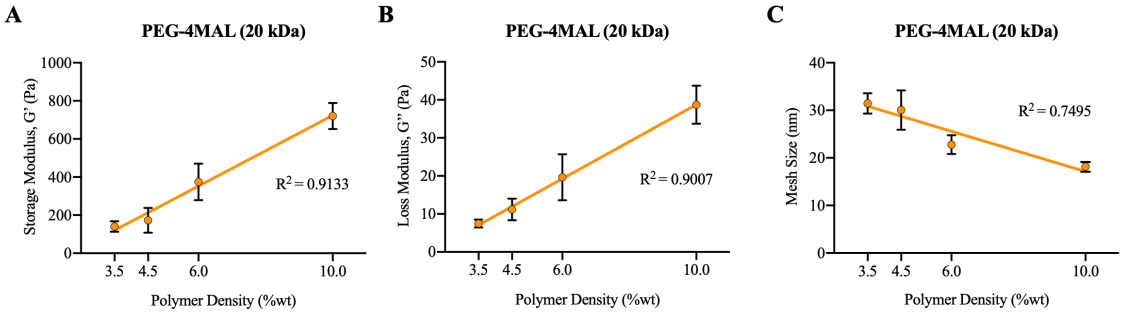

Figure 4.5. Hydrogel characterization of PEG-4MAL hydrogels using a cone-and-plate rheometer. a) Storage modulus (G') and b) loss modulus (G'') of PEG-4MAL hydrogels with varying polymer weight percentages. c) Mesh sizes of hydrogels with varying polymer weight percentages, calculated by Rubber Elastic Theory.

4.3.3 Viability of Encapsulated Dendritic Cells is Significantly Lower at Higher Hydrogel Stiffnesses

Softer hydrogels (3.5-4.5 wt%) supported DC viability, while stiffer hydrogels (6.0-10.0 wt%) resulted in widespread cell death of encapsulated cells (Figure 4.6). DCs that survived encapsulation in stiff hydrogels had elongated morphology, whereas DCs in soft gels exhibited typical round DC morphology (Figure 4.6). The number of live cells recovered after gel digestion was higher in softer hydrogels (3.5-4.5 wt%) (Figure 4.6). $CD11c^+$ DC expression of a common co-stimulatory molecule, CD86, was similar to immature DC controls after 24 hours of encapsulation in soft hydrogels (Figure 4.6). These results suggest that microenvironments with a storage modulus of ~150-250 Pa support BMDC viability and an immature phenotype.

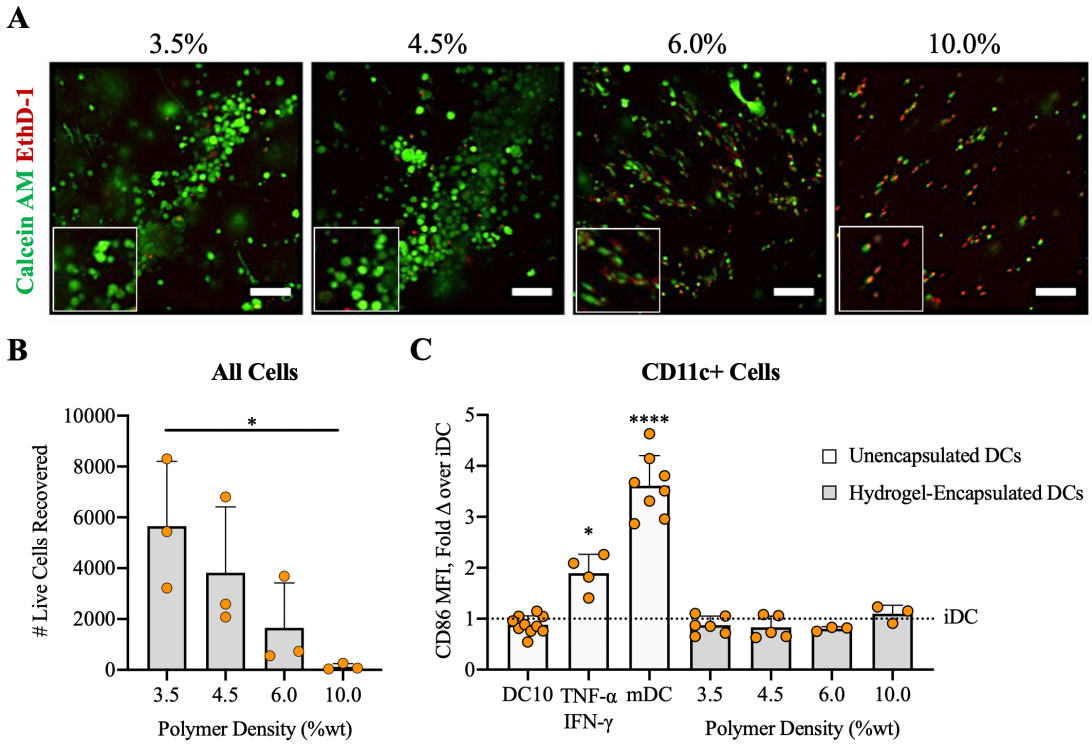

Figure 4.6. Viability and phenotype of CD11c+ DCs after 24 hours' encapsulation in PEG-4MAL hydrogels with various polymer weight percentages. a) Calcein AM (green) and Ethidium homodimer-1 (red) assessed by confocal microscopy (scale bar = 100 µm). b) Live cells recovered after collagenase II digestion and c) CD86 expression in DCs assessed by flow cytometry. White bars denote unencapsulated DCs in 24-well plates and gray bars denote hydrogel-encapsulated DCs. Live cells are defined by propidium iodide (PI) negative cells. *p<0.05 via one-way ANOVA and Tukey's comparison test for b). ****p<0.0001 and *p<0.05 via one-way ANOVA with Welch's correction and Dunnett's comparison test for c).

4.3.4 Adhesive Peptide RGD Does Not Significantly Alter Encapsulated Dendritic Cell Viability or Maturity

The viability of DCs encapsulated in all conditions was similar to controls (Figure 4.7). $CD11c^+$ DCs encapsulated in hydrogels with all concentrations of RGD and RDG had CD86 expression similar to immature controls (Figure 4.7). This data suggests that either RGD presented on 3D matrices does not cause maturation in DCs, which contradicts

previous studies performed in 2D[133], or that RGD concentrations utilized herein are too low to cause DC maturation.

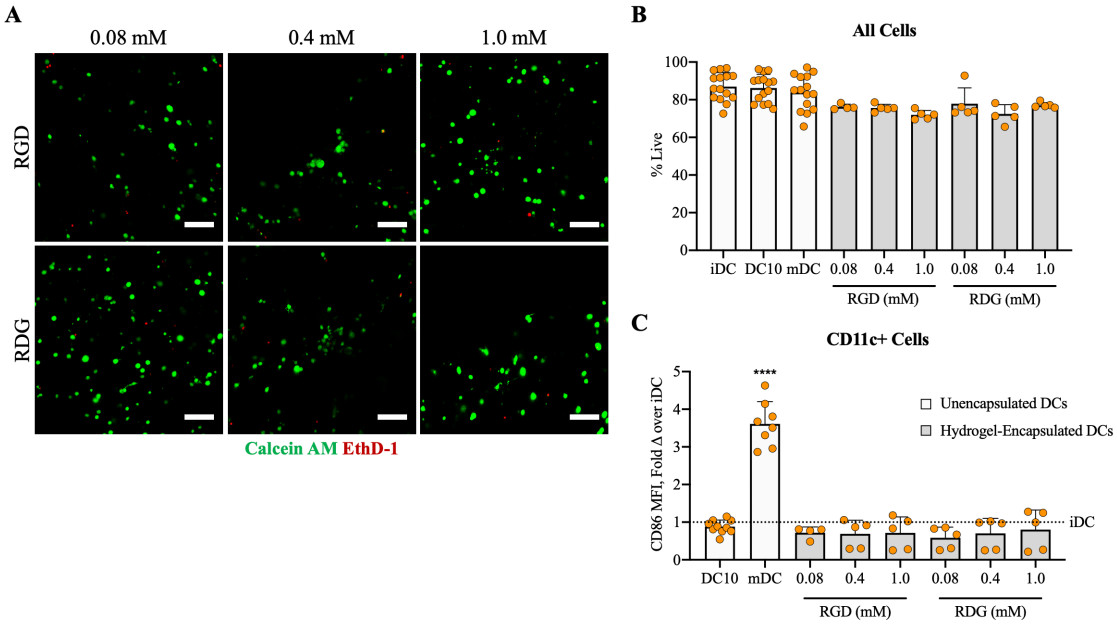

Figure 4.7. Viability and phenotype of CD11c+ DCs after 24 hours' encapsulation in PEG-4MAL hydrogels with various adhesive ligand concentrations. a) Calcein AM (green) and Ethidium homodimer-1 (red) assessed by confocal microscopy (scale bar = 100 µm). b) Live cells and c) CD86 expression assessed by flow cytometry. White bars denote unencapsulated DCs in 24-well plates and gray bars denote hydrogel-encapsulated DCs. Live cells are defined by propidium iodide (PI) negative cells. ****p<0.0001 via one-way ANOVA and Dunnett's comparison test.

4.3.5 PEG-4MAL Macromer Size Does Not Significantly Alter Encapsulated Dendritic Cell Viability or Maturity While Hydrogel Stiffness Remains Constant

Live cells recovered after gel digestion was higher in 10 kDa hydrogel samples than 20 kDa and 40 kDa hydrogel samples, while the viability of cells was similar between hydrogels of all macromer sizes (Figure 4.8). CD86 expression among encapsulated $CD11c^+$ DCs was similar to immature DC controls (Figure 4.8). This data suggests that DC

viability and phenotype is not significantly impacted by macromer size, but that smaller mesh sizes may contribute to better recovery of DCs from hydrogels.

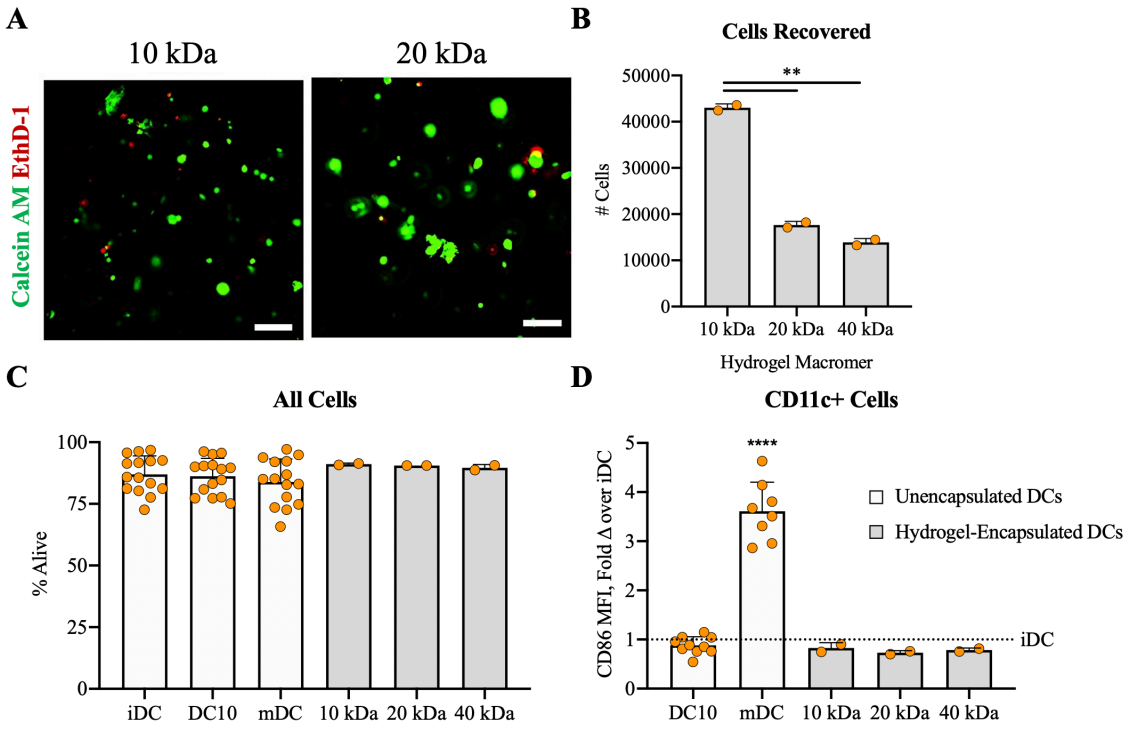

Figure 4.8. Viability and phenotype of CD11c+ DCs after 24 hours' encapsulation in PEG-4MAL hydrogels with various macromer sizes. a) Calcein AM (green) and Ethidium homodimer-1 (red) assessed by confocal microscopy (scale bar = 100 µm). b) Cells recovered after collagenase II digestion, c) live cells, and d) CD86 expression in DCs assessed by flow cytometry. White bars denote unencapsulated DCs in 24-well plates and gray bars denote hydrogel-encapsulated DCs. Live cells are defined by propidium iodide (PI) negative cells. **p<0.01 and ****p<0.0001 via one-way ANOVA with Welch's correction and Dunnett's comparison test.

4.3.6 Degradability Kinetics Dictated by Peptide Crosslinkers Does Not Significantly Alter Encapsulated Dendritic Cell Viability or Maturity

PEG-4MAL hydrogels were synthesized using a percentage of the crosslinker DTT (e.g. 25% DTT) with VPM constituting the remaining crosslinker (e.g. 75% VPM). The viability of cells collected from 0% DTT, 25% DTT, and 50% DTT-crosslinked PEG-

4MAL hydrogels was similar to immature DC controls (Figure 4.9). CD86 expression among encapsulated $CD11c^+$ DCs was similar to immature DC controls (Figure 4.9). This data suggests that hydrogel degradability kinetics do not significantly affect DC viability and phenotype, allowing for flexibility in crosslinker choices when designing PEG-4MAL hydrogels for *in vivo* applications.

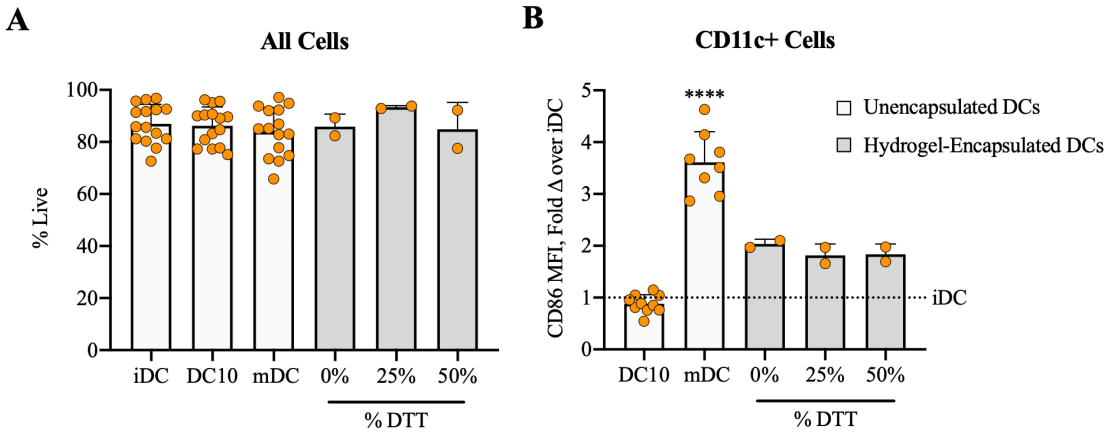

Figure 4.9. Viability and phenotype of CD11c+ DCs after 24 hours' encapsulation in PEG-4MAL hydrogels with ratios of degradable (VPM) and non-degradable (DTT) crosslinkers. a) Live cells, and b) CD86 expression in DCs assessed by flow cytometry. White bars denote unencapsulated DCs in 24-well plates and gray bars denote hydrogel-encapsulated DCs. Live cells are defined by propidium iodide (PI) negative cells. ****p<0.0001 via one-way ANOVA with Welch's correction and Dunnett's comparison test.

4.4 Discussion

4.4.1 Characterization of DC Controls

Reproducible controls needed to be validated to set a benchmark for DC viability, tolerogenicity, and maturity for later comparison. This characterization included analysis of cell phenotype (CD11c, MHC-II, CD86) and analysis of secreted biomolecules (23-plex, Table 4.1) by cytokine multiplexing. While DCs have been utilized by many different

academic research labs for many different applications, the differentiation and treatment protocols are just as varied. Thus, control phenotypes were established based on IL-10 treatment (DC10s), vitamin-D_3 treatment (VD3), stimulation with TNF-α and IFN-γ (TNF-α/IFN-γ), LPS (mDCs), or no treatment (iDCs). The DCs in this thesis were differentiated using a well-established culture protocol adapted from Pulendran et al[177,178]. VD3-treated DCs were included as a tolerogenic control that functions primarily through PD-L1 presentation, while DC10s have been shown to induce tolerance through both PD-L1 presentation and secretion of IL-10[7].

There were no significant differences in cell viability between treatment groups, although some mDC replicates had poor viability. An increase in cell number followed by a sharp decline was also observed following LPS treatment. Mature DCs and, to a lesser extent, TNF-α/IFN-γ DCs exhibited high levels of expression of CD86, a co-stimulatory molecule involved in activation of cognate T cells; and MHC-II, a protein that present antigenic peptides to cognate T cells. These results contrast DC10 and VD3 groups, which had similar phenotypes to iDCs. While the expression of MHC-II on iDC, DC10, and VD3 groups is less than that of TNF-α/IFN-γ DCs and mDCs, an increase in MHC-II on immature controls was observed from Day 6 to Day 8 of culture during characterization of controls (Figure A.6). This basal expression of MHC-II is sufficient for presentation of peptides to lymphocytes, as illustrated later in Chapter 6.

We observed an expected increase in the secretion of TNF-α for mDCs, while DC10 groups were similar to iDCs. mDCs also exhibited increased secretion of CCL5. Another key cytokine is IL-10, which had increased secretion in DC10 groups and even greater increased secretion in mDC groups. This IL-10 secretion has been shown to be a

compensatory mechanism to dampen the activation in response to LPS[179], which is a very rough stimulus generally not experienced *in vivo*, especially at this concentration (1 μg/mL). Additionally, some groups have utilized LPS treatment to induce a type of tolerogenic DCs[180].

Non-adherent DCs across all treatments showed secreted higher levels of CCL5 than their adherent DC counterparts, which is one of many distinct differences between the adherent and non-adherent fractions of DCs after six days of differentiation. Other major differences include the expression of CD86 and DC stability as measured by the recovery of DCs from hydrogels (Figure A.2).

The metrics discussed in the section will be used to classify the phenotypes of DCs after biomaterial treatments, using iDCs, DC10s, and mDCs as benchmarks for the immature, tolerogenic, and mature DC states, respectively.

4.4.2 Characterization of PEG-4MAL Hydrogels

Towards designing a biomaterial delivery system tuned specifically for DC delivery, it was first necessary to identify the relationships between PEG-4MAL polymer characteristics and the biophysical properties of the hydrogels. This characterization is well established and based on cone-and-plate rheological data. Although expected biophysical values such as storage modulus can be found in the literature, it is crucial to establish reproducible hydrogels that respond properly such that properties such as stiffness can be effectively manipulated to suit DCs. Factors of hydrogels that may contribute to irregularities include reagent purity, molarity, pH, hydrolyzation of maleimide functional groups, and handling technique.

Hydrogel stiffness (represented by storage modulus) and loss modulus increased linearly with increased polymer density, validating that additional PEG-4MAL was indeed crosslinked into the hydrogel structure. Mesh sizes were calculated by Rubber Elastic Theory[175] according to the formula below.

$$\xi = \left(\frac{G'A}{RT}\right)^{-1/3}$$

where G' is the storage modulus in Pa,

A is the Avogadro's constant (mol^{-1})

R is the gas constant ($cm^3\ Pa\ K^{-1}\ mol^{-1}$)

and T is the temperature (K)

Hydrogel mesh size is inversely related to PEG-4MAL polymer density, decreasing due to increased polymer concentration and entanglements. Mesh sizes are reported in nanometers, which theoretically represents the distance between two junctions of polymers[175]. Hydrogel mesh size can be tuned by altering PEG-4MAL macromer size while keeping hydrogel stiffness constant, which enables the optimization of both stiffness and mesh size to support DCs.

4.4.3 Effect of Polymer Density on PEG-4MAL Hydrogel-Encapsulated DCs

To develop a biomaterial delivery platform for DCs against autoimmune disease, it is vital that DCs remain viable and immature throughout delivery. Many studies have shown that the stiffness of biological and synthetic ECMs can influence viability, differentiation, phenotype, and function of encapsulated cells[128,131,157]. Thus, our first goal was to determine the optimal range of hydrogel stiffnesses that supported DC viability and an immature phenotype. The stiffness of the physiological equivalent, a lymph node,

cannot be accurately measured by standard rheological methods because the tissue is not fluidic[157]. The storage modulus of LNs measured by other methods have been reported as values from 1.5 kPa[181] to 150 kPa[182], but studies by Singh et al. cleverly compared these values to rheological values of their synthetic scaffolds and identified a storage modulus of ~2000 Pa for lymphoma malignant LNs[157]. Considering healthy LNs had stiffnesses less than half the values of malignant LNs, we expect the optimal hydrogel stiffness for DCs to be around 500-1000 Pa as measured using a cone-and-plate rheometer.

After 6 days of differentiation, DCs were encapsulated in PEG-4MAL hydrogels with varying stiffnesses, altered by PEG-4MAL polymer density. After 24 hours of encapsulation, DC viability, morphology, and distribution in hydrogels were evaluated by confocal microscopy. We observed that DCs within softer hydrogels (~150-250 Pa) with larger mesh sizes (~30 nm) were viable and had round morphologies that are characteristic of immature DCs. Oppositely, DCs within stiffer hydrogels (~400-750 Pa) exhibited widespread cell death and elongated morphologies. Cells within the hydrogel environment were well distributed across hydrogels of all tested stiffnesses, suggesting homogenous crosslinking during hydrogel synthesis despite challenges such as reagent purity, molarity, and pH, hydrolyzation of maleimide functional groups, and handling technique.

DCs were recovered from hydrogels after collagenase II digestion and their maturity was evaluated based on cell surface marker expression analyzed by flow cytometry. Collagenase II treatment at the specified concentration and duration did not significantly affect the expression of extracellular markers of interest on DCs (Figure A.1). The number of DCs recovered from soft hydrogels (3.5 wt%) was significantly higher than DCs recovered from stiff hydrogels (10.0 wt%). Interestingly, the maturity of recovered

DCs based on CD86 expression was not varied amongst the different PEG-4MAL hydrogel stiffnesses. The cell death observed in stiff hydrogels (6.0, 10.0 wt%) is likely due to the smaller mesh size of these dense hydrogels, resulting in inhibited diffusion of survival compounds. Hydrogels have been specifically designed to prevent the diffusion of coagulation molecules onto medical device surfaces[183] and remains a challenge for islet encapsulation strategies that aim to isolate encapsulated cells from host immunity[184]. Mechanical stress imposed on cells physically stretched by stiff hydrogels may be a secondary factor contributing to cell death. Thus, softer hydrogels are more favorable due to higher cell recovery and viability. Both 3.5 wt% and 4.5 wt% hydrogels similarly supported DCs, although 4.5 wt% hydrogels are much easier to handle that 3.5 wt% hydrogels. Thus, 4.5 wt% was selected as the optimal polymer density moving forward.

Notably, the stiffness of 4.5 wt% (~200 Pa) is much different than the stiffness of lymph nodes (500-1000 Pa)[157]. A possible explanation is that DCs derived from bone marrow using GM-CSF and IL-4 do not conform to established DC subtypes found *in vivo* and may respond to ECM stiffness differently. BMDCs may also share characteristics with pDCs or peripheral cDCs, which are circulatory or resident within various tissues other than LNs.

4.4.4 Effect of Adhesive Peptide, Macromer size, and Hydrogel Degradability on PEG-4MAL Hydrogel-Encapsulated DCs

The structure of the PEG-4MAL polymer allows manipulation through several parameters: polymer density (previously evaluated), macromer size, adhesive peptide, and crosslinker type. We next aimed to evaluate the effect of these parameters on encapsulated DC viability and phenotype.

Integrin-mediated signaling resulting from cell-cell and cell-ECM interactions has been implicated in cell morphology, differentiation, survival, and other cell processes[128,131,133-135]. The effect of RGD, a ubiquitous adhesive peptide sequence, on DC viability and phenotype was explored by utilizing confocal microscopy and flow cytometry techniques. To verify that any potential effect was due to RGD, a scrambled peptide GRDGSPC (RDG) with limited affinity to RGD-associated integrins ($\alpha_V\beta_3$, $\alpha_5\beta_1$, $\alpha IIb\beta_3$) was included as a control[185]. To maintain a constant stiffness, scrambled peptide should be included such that the total adhesive peptide concentration is the same for all samples. However, the concentration of adhesive peptide compared to the number of crosslinks in each hydrogel is small enough that we expect negligible differences in hydrogel stiffnesses.

DC morphology and viability appeared to remain constant across different concentrations of RGD or RDG based on confocal images. Cells recovered from hydrogels with various peptide concentrations exhibited similar viability and CD86 expression to iDC controls. Previous studies have shown that DCs seeded on 2D RGD-functionalized substrates are activated differentially with RGD concentration[133], which contrasts our results. RGD presentation by the 3D hydrogel systems engineered herein may not activate DCs due to the functional differences between 2D- and 3D substrates[136], but other possible explanations include: (1) RGD concentrations studied are simply too low to induce DC maturation, or (2) activation-related cell signaling in DCs is not actualized due to a lack of cell adhesion.

4.5 wt% hydrogels were synthesized with various PEG-4MAL macromer sizes to evaluate the effect on encapsulated DCs. While morphology and viability of DCs in 10 kDa and 20 kDa hydrogels were similar, significantly more DCs were recovered from 10

kDa hydrogels. Based on flow cytometry, viability and phenotype of recovered cells were consistent across all hydrogel formulations. Both polymer density and macromer size correlate to hydrogel stiffness, so modulation of macromer size and polymer density to achieve a constant hydrogel stiffness enables decoupling of these variables and isolation of the microarchitecture of polymer mesh networks. However, the experiment herein tested hydrogels with various macromer sizes and a constant polymer density, resulting in changes to both mesh size and stiffness. Thus, the effects of macromer size discussed here cannot be attributed solely to mesh size and this experiment needs to be repeated to isolate the effects of PEG-4MAL hydrogel mesh size on DC viability and phenotype.

Lastly, the effect of hydrogel degradability on encapsulated DCs was evaluated by synthesizing hydrogels with various ratios of degradable (VPM) to non-degradable (DTT) crosslinkers. Previous studies have demonstrated the benefit of degradable matrices on the cellular processes of encapsulated and infiltrating cells[131,158,186], and DCs have been shown to secrete matrix metalloproteinase (MMP)-1, MMP-2, MMP-3, and MMP-9[187]. Crosslinker composition did not significantly affect DC viability or phenotype based on analysis by flow cytometry.

4.4.5 PEG-4MAL Hydrogel Parameter Selection for in vivo Applications

Importantly, it is necessary to consider the *in vivo* application of these biomaterial-delivered DCs in selecting criteria for the optimal formulation. While DC viability and an immature phenotype are the most important considerations, variables that do not directly affect viability and phenotype enable the flexible design of our system based on *in vivo* functionality. Our proposed design aims to maximize the migration of cells in and out of hydrogels, ECM remodeling, and vascularization.

While recovery from 10 kDa hydrogels was significantly higher than 20 kDa and 40 kDa hydrogels, the constricted mesh size of 10 kDa hydrogels would impede both the migration of encapsulated DCs out of the hydrogel and infiltration of endogenous cells into the biomaterial. Based on considerations for the expected mechanism of immunomodulation *in vivo*, 20 kDa macromer size was selected as the optimal criteria.

The presence of RGD in synthetics matrices has been shown to promote ECM remodeling and vascularization *in vivo*[29,188]. Remodeling the ECM would favor our proposed design, such that DCs could effectively migrate to relevant tissues and restructure their surroundings as necessary. Thus, RGD incorporation was selected at a concentration of 1.0 mM for our optimized hydrogel system.

The VPM crosslinking peptide is effectively cleaved by MMP-2 and MMP-9[189] at physiological pH (7.4) at a relatively fast rate of 24,000 ± 1000 and 51,000 ± 3000 k_{cat}/K_M ($M^{-1}s^{-1}$), respectively[190]. Since DCs can secrete both MMP-2 and MMP-9, VPM-crosslinked hydrogels should be easily degradable by encapsulated DCs. Fast-degrading hydrogels will enable the migration of cells necessary for DCs to modulate endogenous immune cells. Thus, VPM was selected as the crosslinker moving forward.

A table with the optimized PEG-4MAL formulation is shown below in Table 4.2.

Table 4.2. PEG-4MAL Parameters Optimized for DCs

Category	Parameter	Significance
Polymer	PEG-4MAL	Biophysical and biochemical modularity, injectable, *in situ* crosslinking
Polymer Macromer Size	20 kDa	Porous enough to enable migration of DCs
Polymer Density	4.50%	~200 Pa stiffness supports DCs
Adhesive Ligand	RGD	Recognized by DCs, promotes infiltration and vascularization *in vivo*
Adhesive Ligand Conc.	1.0 mM	Ample concentration for DC attachment and infiltration/vascularization effects without affecting hydrogel architecture
Crosslinker	VPM	Fast-degrading to enable DC migration and immune cell infiltration

It is important to note that these criteria were selected specifically for the treatment of EAE in mice to improve the efficacy of DC therapies. However, the flexibility of parameters demonstrated here allows adjustments to be made to the biomaterial formulation to fit other applications not explored here. For example, non-degradable crosslinkers and shorter macromer sizes would benefit a system where the encapsulated cells were meant to be contained. Another example would be utilizing a different adhesive ligand to alter the composition of infiltrating cells or limit DC attachment to the hydrogel structure.

CHAPTER 5. FUNCTIONALIZATION OF PEG-4MAL HYDROGELS WITH IL-10 TO PROTECT AGAINST INFLAMMATION AND PROMOTE TOLEROGENICITY IN DENDRITIC CELLS

5.1 Overview

Anti-inflammatory immunological peptides such as IL-10 have been shown to induce tolerance in DCs[191-194] and promote DCs to induce Treg cells. A major challenge to current DC therapies is that the viability and tolerogenic state of DCs may be compromised *in vivo* due to systemic inflammation during autoimmunity[59], injection-related inflammation, and cross-conditioning by host autoreactive DCs and T cells[195]. Thus, the objective of this aim is to promote viability and tolerogenicity of delivered DCs by conjugating IL-10 to PEG-4MAL hydrogels, resulting in both (1) persistent presentation of IL-10 to encapsulated DCs and (2) immunosuppressive conditioning of endogenous immune cells through controlled release of IL-10. The immunosuppressive cytokine IL-10 was selected because IL-10-treated DCs have been shown to be proficient at inducing Tregs and inhibiting CD8+ T cell proliferation[7]. The hypothesis of this aim was that the thiolation of IL-10 and subsequent conjugation to PEG-4MAL will not affect its bioactivity and that PEG-IL10 hydrogels will act on encapsulated cells through the direct presentation of IL-10 and protease-mediated release of IL-10. Several other groups have achieved single-chain PEGylation of IL-10 to extend the circulation time of IL-10 treatment[196,197]. PEGylation of IL-10 by acylation and reductive amination were shown to decrease bioactivity by 35-fold and 3-fold[198], respectively, so thiolation of IL-10 will be pursued as an alternative method of

functionalization. PEG-IL10 has been previously incorporated into hydrogels to treat inflammation[199], but the bioactivity of PEG-IL10 produced by thiolation has not previously been characterized as part of a three-dimensional scaffold.

It is expected that PEG-IL10 hydrogels will strengthen the tolerogenic state of delivered DCs during delivery and post-injection. The rationale for this hypothesis is that IL-10 does not need to be internalized by DCs to initiate IL-10-receptor (IL-10R)-induced tolerogenic signaling[200-203]. Presentation of IL-10 to encapsulated DCs throughout delivery is expected to be similar to multiple doses of IL-10, which have been shown to reinforce tolerogenicity in otherwise highly plastic DCs. Conjugated-biomolecule release from VPM-crosslinked hydrogels has been studied extensively in several biomaterial platforms and occurs in an MMP-2- and MMP-9-sensitive manner[189]. Completion of this aim is expected to yield a degradable PEG-4MAL hydrogel with covalently-tethered IL-10 that retains its bioactivity and its tolerizing effect on DCs either by interacting with hydrogel-bound IL-10 or by IL-10 released from the hydrogel.

5.2 Materials and Methods

5.2.1 Animals

All live animal procedures were conducted under the approval of the Institutional Animal Care and Use Committee (IACUC) of the Georgia Institute of Technology. Mice were housed, maintained, and bred in the Physiological Research Laboratory (PRL) Animal Facility of the Georgia Institute of Technology. Animals were 8-to-12-week-old male C57BL/6J mice (Jackson Laboratories, Inc.).

5.2.2 Thiolation of IL-10

Recombinant murine IL-10 (Peprotech, Inc) was thiolated with 30 molar excess of Traut's reagent (Sigma Aldrich) in 1x PBS with 5 mM EDTA (Gibco) at pH 8.0 for 1 hour. Protein samples were then washed twice by diluting with 1x PBS (pH 8.0) and passing through a 10 kDa cellulose filter (Amicon Ultra; Millipore) at 14,000 xg. To quantify the extent of thiolation, samples were stained for free thiols using a Measure-iT Thiol Quantification Kit (ThermoFisher). The fluorescence intensity (Ex/Em: 494/517nm) of IL-10 modified with a free thiol (HS-IL-10), native IL-10, blank wells, and reduced glutathione standards were quantified on a spectrophotometer (Synergy H4; BioTek).

5.2.3 Conjugation to PEG-4MAL

Conjugation of S- IL-10 to PEG-4MAL was achieved by reacting both components at 1000:1 (PEG-4MAL:HS-IL-10) in 1x PBS (pH 7.0) for 30 minutes. To visualize the PEGylated IL-10, reacted protein was immediately loaded onto polyacrylamide gels (4-12% Bis-Tris; Invitrogen) and placed into a Novex Mini-Cell (Invitrogen) which was run in non-denaturing conditions. Migrated proteins were stained with SyproRuby (Invitrogen) and imaged on a Molecular Imager Gel Doc XR System (BioRad).

5.2.4 MC/9 Cell Bioactivity Assay

MC/9 cells (ATCC) were expanded in DMEM with 10% FBS, refreshing media every 2-3 days. To assess the bioactivity of PEG-IL10 compared to native IL-10, MC/9 cells were collected during log phase of cell growth and plated in DMEM with 3% FBS at 25,000 cells/well in a 96-well plate. Cells were treated with 5 ng/well co-stimulatory IL-4 (Peprotech) and either 2.5 ng/well IL-10 (Peprotech) or PEG-IL10. After 48 hours of

incubation, either cell counting kit-8 (CCK-8) (absorbance 240nm; Sigma Aldrich) or AlamarBlue (Ex/Em: 530/590nm; ThermoFisher) was added to each well. The proliferation of MC/9 cells in response to treatment was measured on a spectrophotometer (Synergy H4; BioTek) based on cellular metabolic byproducts. The experiment was repeated with titrated treatments to construct half-maximal effective concentration (EC_{50}) curves for native and PEGylated IL-10.

5.2.5 IL-10 Release Study

Recombinant murine IL-10 (Peprotech) was first tagged with AlexaFluor-488 (AF488) according to the manufacturer's protocol. AF488-IL-10 was then thiolated and PEGylated, as previously described. PEG-IL10 hydrogels were synthesized and swelled in 1x PBS (pH 7.4). Hydrogels with IL-10 tethered or IL-10 entrapped were synthesized and plated in PBS or collagenase II (1 mg/mL). Supernatants were collected intermittently and stored at -80^{o}C until use. Once all hydrogels had fully degraded, supernatants were collected and AF488 fluorescence (Ex495/Em519) was measured on a spectrophotometer (Synergy H4; BioTek).

5.2.6 Resistance to Re-Stimulation

iDCs were encapsulated in PEG-4MAL or PEG-IL10 hydrogels, as previously described. After incubation for 24 hours, either a stimulus treatment (150 ng/mL TNF-α and 30 ng/mL IFN-γ, 3x STIM) or LPS (2 μg/mL, 2x LPS). iDCs and DC10s with and without stimulus treatment served as controls. After an additional 48 hours, hydrogels were digested and analyzed via flow cytometry, as previously described.

5.2.7 Flow Cytometry

DCs were washed with 1x PBS and then reconstituted in 100 µL of FACS Buffer (Hank's Buffered Salt Solution, HBSS; 1% bovine serum albumin, BSA; 1 mM Ethylenediaminetetraacetic acid, EDTA). TruStain FcX (anti-mouse CD16/32; BioLegend) was added, and cells were incubated on ice for 10 minutes. DCs were then stained with FITC-IA^b (AF6-120.1; BD), APC-CD86 (GL-1; BioLegend), BV785-CD11c (N418; BioLegend), and PE-PDL1 (MIH7; BioLegend) for 30 minutes on ice, protected from light. DCs were washed twice with FACS Buffer and analyzed on a flow cytometer (FACSAria III; BD). Propidium Iodide (PI) was added 5 minutes before analysis to assess viability. Gating strategies are illustrated in Figure A.5.

5.2.8 Confocal Microscopy

Cell viability was visualized by staining with calcein AM and ethidium homodimer-1 (EthD-1) and imaging on a confocal microscope (Nikon Eclipse Ti-E C2+). Media was removed and PEG-4MAL hydrogels encapsulating DCs were washed twice with 1x PBS by gentle pipetting. Samples were then stained with 1 µM calcein AM and 1 µM EthD-1 in media without FBS for 20 minutes. Intact hydrogels were then washed two more times and media without FBS was added for imaging.

5.2.9 Statistical Analysis

Experimental values are reported as mean and standard deviation for all samples. Statistical analysis was determined using one or two-way ANOVA coupled with Sidak's posthoc pairwise tests using GraphPad (Prism Inc.). All datasets were normally distributed. If datasets failed the Brown-Forsythe test (due to significant differences in variances

between treatment groups), Welch's correction was applied to account for these differences and Dunnett's posthoc pairwise test was used. PEG-4MAL groups served as the control for comparison tests. p-values <0.05 were considered statistically significant. Error bars represent the standard deviation.

5.3 Results

5.3.1 IL-10 is Successfully Thiolated

The chemical process of thiolation is illustrated in Figure 5.1. Based on the standard curve (Figure 5.2), the mean concentration of free thiols on HS-IL-10 samples was 3.68 μM versus negligible values for untreated IL-10 (Figure 5.2). This magnitude of thiolation suggests that, on average, ~13 lysine residues were thiolated on each IL-10 protein, representing numerous free thiols present to be linked to a maleimide group on PEG-4MAL.

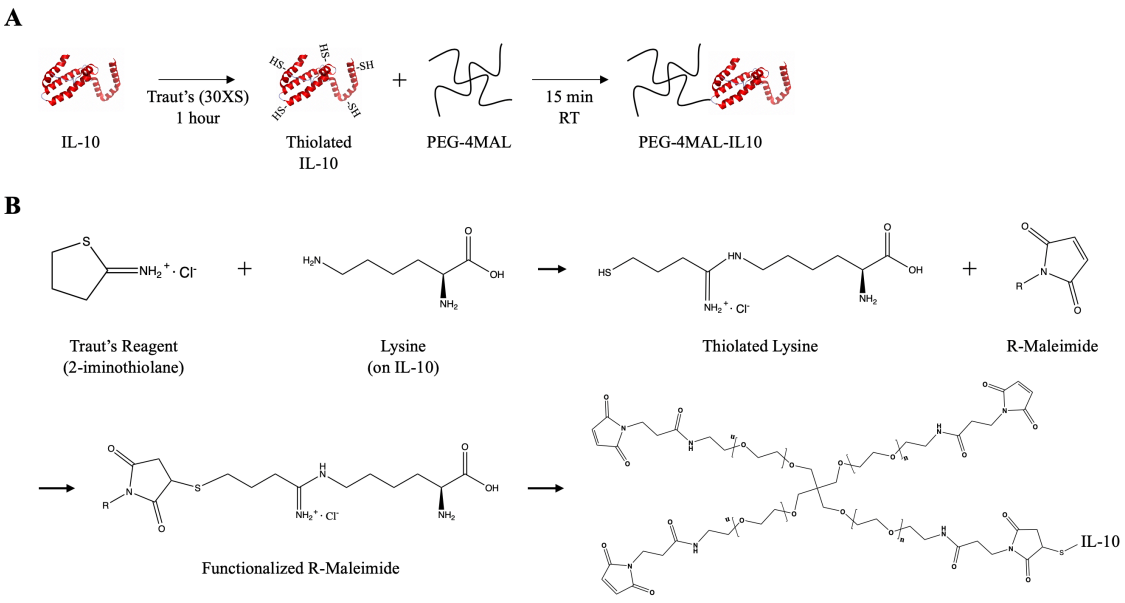

Figure 5.1. Schematic of functionalizing IL-10 onto the backbones of PEG-4MAL macromers. a) Visualization of tethering IL-10 to PEG-4MAL and b) chemical structures and process of thiolation and PEGylation.

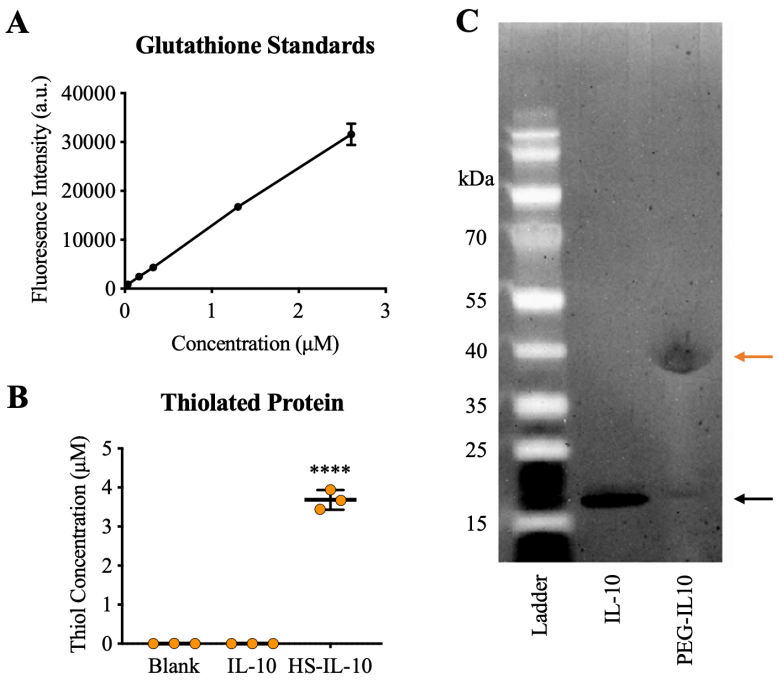

Figure 5.2. Quantification of thiolation of IL-10 using Traut's reagent and SDS-PAGE results of IL-10 PEGylation. a) Standard curve produced using glutathione. b) Concentration of free thiols on modified IL-10 proteins. c) Validation of tethering thiolated IL-10 to PEG-4MAL, as shown by unmodified IL-10 at 20 kDa (black arrow) and PEGylated IL-10 at 40 kDa (orange arrow). ****p<0.0001 via one-way ANOVA and Dunnett's comparison test.

5.3.2 Thiolated IL-10 is Effectively Conjugated to a Single PEG-4MAL

Successful conjugation was tested by reacting both components at 1000:1 (PEG-4MAL:HS-IL-10). An increase in molecular weight from ~19 kDa (IL-10; Lane 2; black arrow) to ~39 kDa (PEG-IL10; Lane 3; orange arrow) illustrates successful PEGylation of HS-IL-10 (Figure 5.2).

5.3.3 PEGylated IL-10 Retains its Bioactivity

While IL-10 is classified as a class II anti-inflammatory cytokine, liver mast cells exhibit pleiotropic behavior and have been shown to proliferate in response to IL-10[204]. Bioactivity of PEG-IL10 was measured by the proliferation of MC/9 cells, a murine liver

mast cell line commonly used in IL-10 bioactivity assays[205,206]. Absorbance was similar for native and PEGylated IL-10 at both 4 and 24 hours after the addition of the proliferation reagent (Figure 5.3). To further validate the activity of PEG-IL10, proliferation reagents were added in titrated amounts to construct EC_{50} curves for native and PEGylated IL-10. EC_{50} values for PEG-IL10 and native IL-10 were nearly identical at ~0.003 ng/well (Figure 5.3). These results suggest that PEG-IL10 bioactivity is similar to IL-10 in its native state.

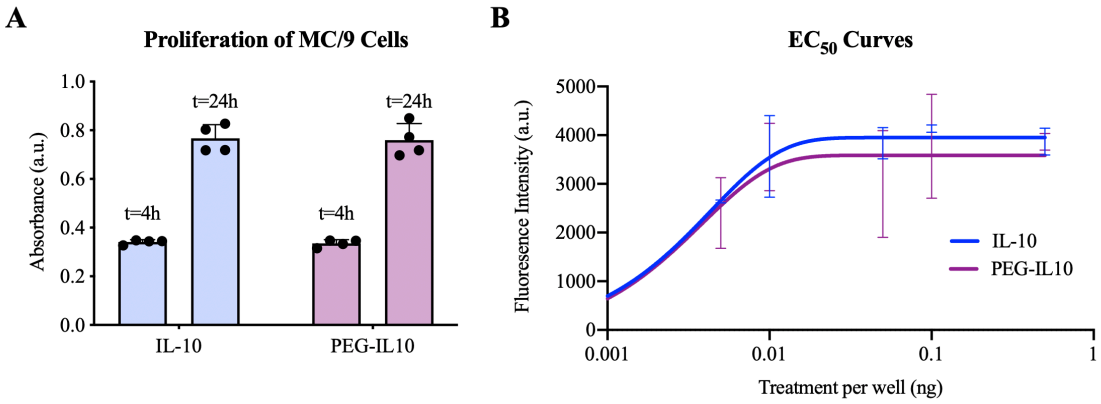

Figure 5.3. Bioactivity of PEG-IL10 based on the proliferation of MC/9 cells after 72 hours of incubation with treatments. a) MC/9 cell proliferation measured by CCK-8 metabolic assay. b) Half-maximal effective concentration (EC_{50}) curves produced by titration of treatments.

5.3.4 PEG-IL10 Hydrogels Exhibit Controlled Release of Tethered IL-10 in Response to Hydrogel Degradation

Hydrogels with IL-10 or HS-IL-10 in collagenase I had indistinguishable release profiles over 96 hours, with nearly 90% of protein released after just 5 hours (Figure 5.4). Hydrogels with IL-10 in PBS also exhibited rapid release of protein within the first 5 hours (~40 ng), whereas HS-IL-10 that was tethered to PEG-4MAL released only ~30 ng after 5 hours (Figure 5.4). For hydrogels in PBS with HS-IL-10, another ~10 ng of IL-10 was gradually released between 5-96 hours. Collagenase I was added to PBS hydrogels at 96

hours to release IL-10 still bound to hydrogels, after which another 6-8 ng of IL-10 was released (Figure 5.4). The initial burst release of HS-IL-10 from hydrogels in PBS is likely due to only a fraction of the HS-IL-10 being biochemically incorporated in PEG-4MAL hydrogels.

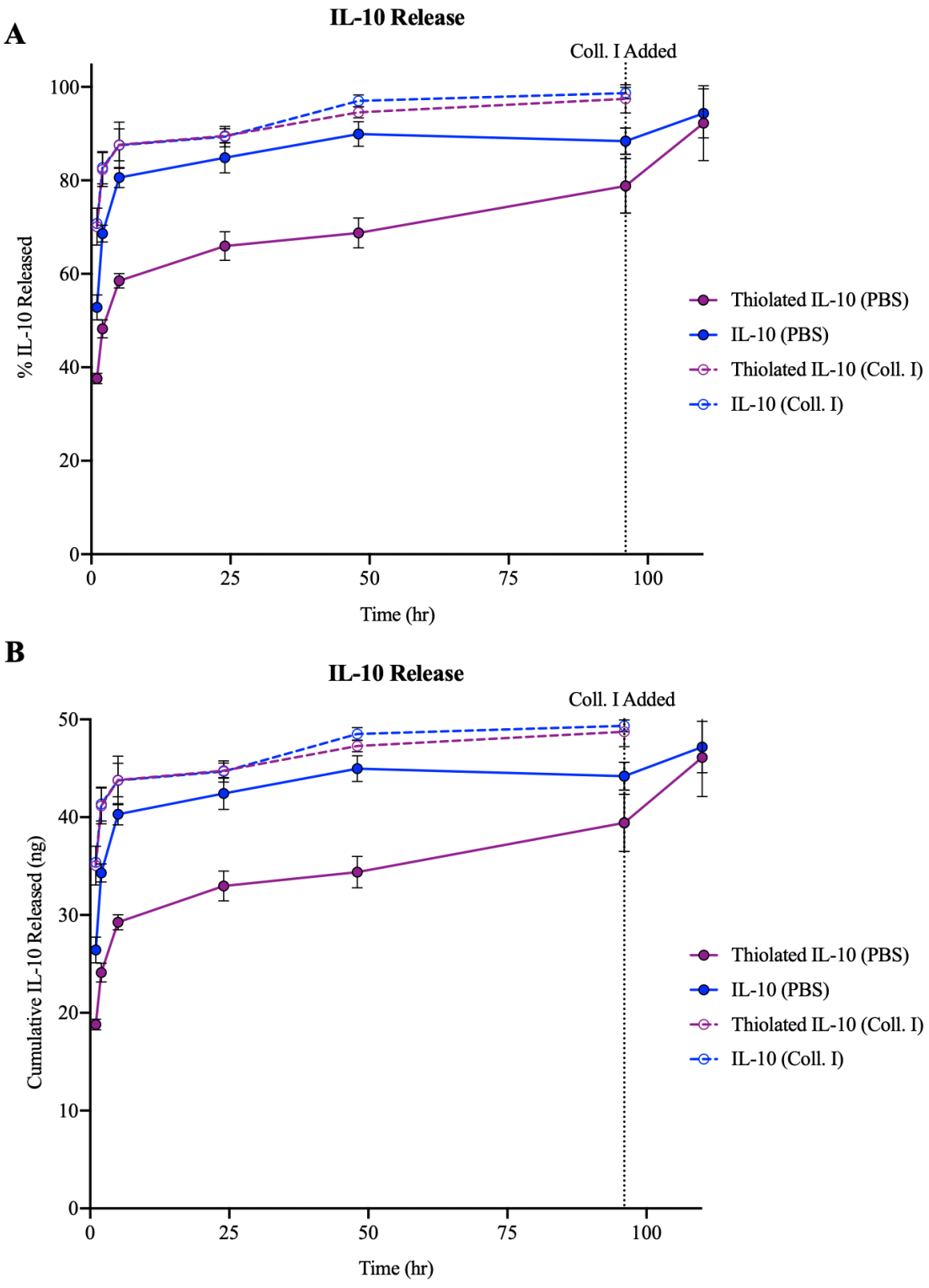

Figure 5.4. Controlled release curve of IL-10 from PEG-IL10 hydrogels in a) percentage and b) concentration of IL-10 released. Fluorescence intensity of AF488-tagged IL-10 in hydrogel supernatants was assessed over time.

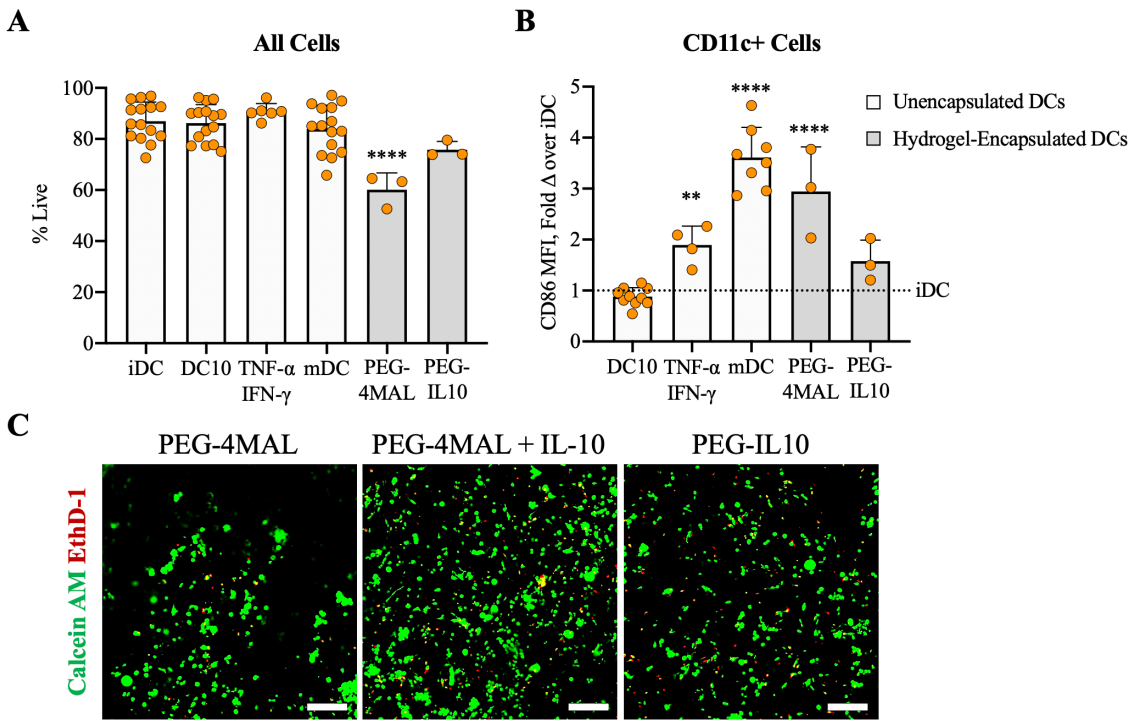

Figure 5.5. Viability and phenotype of CD11c+ DCs after 48 hours' encapsulation in PEG-4MAL or PEG-IL10 hydrogels. a) Live cells and b) CD86 expression assessed by flow cytometry. c) Calcein AM (green) and Ethidium homodimer-1 (red) assessed by confocal microscopy (scale bar = 100 µm). White bars denote unencapsulated DCs in 24-well plates and gray bars denote hydrogel-encapsulated DCs. Live cells are defined by propidium iodide (PI) negative cells. ****p<0.0001 and **p<0.01 via one-way ANOVA and Dunnett's comparison test.

5.3.5 PEG-IL10 Hydrogels Maintain Dendritic Cell Viability and an Immature Phenotype Longer than PEG-4MAL Hydrogels

CD11c+ DCs recovered from PEG-IL10 hydrogels exhibited significantly higher levels of viability (Figure 5.5) as compared to DCs from PEG-4MAL hydrogels after 48 hours. After 48 hours, DCs in PEG-4MAL hydrogels were activated to similar levels as mDCs, whereas DCs from PEG-IL10 hydrogels remained immature based on the expression of CD86 (Figure 5.5). The increased viability of DCs was independent of

whether IL-10 was entrapped in hydrogels or covalently tethered to the polymer backbone, as shown by the similar viability based on confocal images (Figure 5.5).

5.3.6 Both Hydrogel Encapsulation and IL-10 Treatment Contribute to Dendritic Cell Resistance to Inflammatory Cytokines

DCs received control treatments or biomaterial treatments for 24 hours before being re-stimulated with LPS to assess their resistance to maturation. Viability was similar across all treatments (Figure 5.6). 48 hours after re-stimulation, LPS-stimulated DC10s exhibited CD86 expression similar to mDCs, but not as high as LPS-stimulated iDCs (Figure 5.6). LPS-stimulated DCs encapsulated in PEG-4MAL hydrogels matured slightly to levels of CD86 similar to TNF-α/IFN-γ-treated DCs (Figure 5.6). However, LPS-stimulated DCs encapsulated in PEG-IL10 hydrogels had CD86 expression that was not significantly different from un-stimulated controls and remained immature (Figure 5.6). This data suggests that both IL-10 treatment and PEG-4MAL encapsulation contribute the DCs ability to resist maturation in response to LPS.

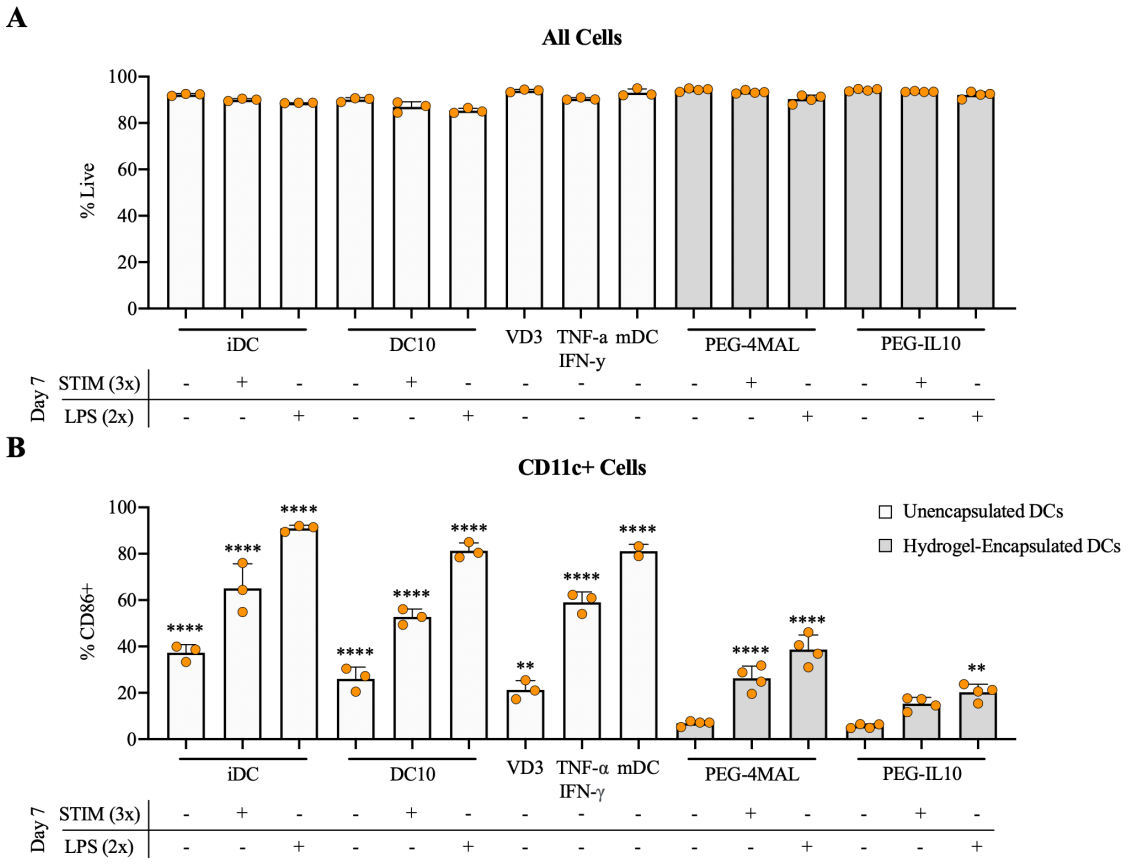

Figure 5.6. Resistance to re-stimulation of CD11c+ DCs receiving various treatments or after encapsulation in PEG-4MAL or PEG-IL10 hydrogels. 24 hours after treatments, DCs were stimulated with either TNF-a (150 ng/mL) and IFN-y (30 ng/mL) (STIM) or LPS (2 µg/mL). a) Live cells and b) CD86 expression assessed by flow cytometry 48 hours after re-stimulation. White bars denote unencapsulated DCs in 24-well plates and gray bars denote hydrogel-encapsulated DCs. Live cells are defined by propidium iodide (PI) negative cells. ****p<0.0001 and **p<0.01 via one-way ANOVA and Dunnett's comparison test.

5.4 Discussion

5.4.1 IL-10 Thiolated Using Traut's Reagent is Covalently Tethered to PEG-4MAL Macromers

Maleimide functional groups on PEG-4MAL polymers allow a wide array of proteins and peptides to be covalently linked to the polymer backbone through free thiols found in free cysteine residues. However, native IL-10 does not have any free cysteines and must be thiolated before being linked to PEG-4MAL.

Traut's reagent (2-iminothiolane) was used to add free thiols to IL-10 by reacting with primary amines on lysine residues on IL-10. Multiple concentrations of Traut's reagent were tested, but 30 molar excess was necessary for effective thiolation. The number of free thiols per IL-10 was found to be ~13, which is more than sufficient to enable covalent tethering to PEG-4MAL. One concern with this extent of thiolation is that IL-10 might then be able to bind multiple maleimide groups and thus act as a crosslinker.

A series of experiments were conducted to determine the best conditions for covalently tethering IL-10 to PEG-4MAL, including the ratio of PEG-4MAL to IL-10, incubation time, thiolation chemistry, IL-10 species, and SDS-PAGE parameters (Figure A.7). Thiolated IL-10 (HS-IL-10) was mixed with PEG-4MAL at a ratio of 1000:1 and incubated for 15 minutes before assessing the molecular weight using SDS-PAGE. Although PEG-4MAL and other polymer have been known to traffic through SDS-PAGE gels differently than a 20 kDa protein might, visual inspection clearly shows a change from IL-10 at 20 kDa to PEG-IL10 at 40 kDa, representing PEGylation of IL-10. At the tested conditions, a faint band can be observed at ~20 kDa for PEG-IL10 samples, suggesting that not all IL-10 was PEGylated. Mechanistically, this would result in immediate diffusion of

the unbound IL-10 to treat DCs and nearby endogenous cells, while incorporated IL-10 would be slowly released as the hydrogel degrades.

Using PEG-IL10, hydrogels were successfully synthesized and appeared macroscopically identical to PEG-4MAL hydrogels. Incorporation of IL-10 into PEG-4MAL hydrogels did not significantly affect the stiffness, as shown be rheological studies (Figure A.8).

5.4.2 PEG-IL10 Retains its Bioactivity

Even though IL-10 does not need to be internalized to promote tolerogenic signalling[200-203], a potential concern of IL-10 thiolation is that the bioactivity of IL-10 might be diminished due to the severe extent of thiolation. To test the bioactivity of PEG-IL10, we utilized a murine mast cell line that proliferates in response to IL-10, MC/9 cells. These cells were treated with either native IL-10 or PEG-IL10 and incubated for two days before adding CCK-8. Both 4 hours and 24 hours later, IL-10 and PEG-IL10 treated MC/9 cells exhibited similar levels of proliferation, suggesting the bioactivity of PEG-IL10 had not been affected.

To further evaluate the bioactivity, we constructed EC_{50} curves, which are commonly used to evaluate the effectiveness of a drug, antibody, or biologic. MC/9 cells were treated with titrated doses of IL-10 or PEG-IL10 and their proliferation was quantified by using Alamar Blue. EC_{50} values for native IL-10 and PEG-IL10 were nearly identical at ~0.003 ng/well, providing further evidence that the bioactivity of PEG-IL10 had not been diminished. These results suggest that IL-10 modification by thiolation is a superior method of PEGylation than acylation or reductive amination, both of which dramatically reduce its bioactivity[198].

Upon investigation of the crystal structures for IL-10 and its receptor, there is minimal overlap between IL-10/IL-10R binding sites and lysine residues on IL-10 (Figure A.9). Since the lysine residues on IL-10 are not directly involved in ligation of IL-10R, these residues tend to be more internal and hindered by more protruding receptor-binding residues. Thus, it is likely that these lysines are sterically hindered or inaccessible to maleimide groups on long 20 kDa chains and that covalent bonds are most likely to occur at lysines near the terminal ends of IL-10.

PEG-IL10 released from degrading PEG-IL10 hydrogels should have an analogous structure to the PEG-IL10 tested immediately after PEGylation and, thus, retain its bioactivity after release. Additionally, there is no logical reason why PEG-IL10 incorporated within a hydrogel would be presenting a different motif than PEG-IL10 that has not been crosslinked. Therefore, the mechanism of IL-10 treatment by PEG-IL10 hydrogels is 3-fold:

1) Unincorporated IL-10 is immediately released and diffuses to encapsulated DCs and nearby endogenous cells
2) As hydrogels degrade, PEG-IL10 is released from the mesh network and treats DCs and nearby endogenous cells
3) Incorporated PEG-IL10 is presented to encapsulated DCs and induces tolerogenic signaling

5.4.3 IL-10 Release is Sustained for at Least 4 Days

A key design parameter to these tolerogenic hydrogels is that IL-10 treatment is continued for a significant duration (at least three days) to offset injected-related

inflammation and the elevated inflammation characteristic to subjects with autoimmune disease. Thus, it is essential to design a biomaterial that has controlled release of incorporated IL-10.

To assess the release of PEG-IL10 from hydrogels, fluorophore-tagged IL-10 was thiolated, PEGylated, and hydrogels were synthesized. Hydrogels were loaded with 50 ng of IL-10 so the effect of these hydrogels could be directly compared to DC controls receiving IL-10 (50 ng/10^6 cells) in later phenotypic studies. Hydrogels were degraded hydrolytically or with collagenase I and the fluorescence intensity of supernatants was analyzed over time. Hydrogels with untethered IL-10 and both hydrogel groups in collagenase I released almost all incorporated IL-10 after just 5 hours, suggesting mostly unimpeded release of protein. Alternatively, hydrogels with tethered IL-10 in PBS had an initial burst release of ~30 ng, which likely consists of the unreacted IL-10 represented by the faint band in Lane 3 of the SDS-PAGE gel at 20 kDa (black arrow) in Figure 5.2. Following this burst release, these hydrogels then exhibited controlled release of ~10ng over the next four days. After 96 hours, collagenase I was added to these hydrogels to release any remaining IL-10, which totaled the amount of IL-10 released by hydrogels with untethered protein. At the rate of release for tethered IL-10 in PBS, extrapolation of the release curve predicts that complete release will occur at ~8 days. Based on the mass of IL-10 released immediately, it is estimated that the extent of incorporation into PEG-IL10 hydrogels is between 40-50%. This release study confirms the first two parts of the 3-fold mechanism of IL-10 treatment proposed previously.

5.4.4 IL-10 Functionalization Improves Duration of Viability and Maturation Effects

While the optimized PEG-4MAL hydrogels without IL-10 were capable of maintaining DC viability and immature after 24 hours of encapsulation, DCs will likely persist in the biomaterial longer than 24 hours *in vivo*. Thus, we sought to assess the potential benefit of functionalization with IL-10 at 48 hours post-encapsulation.

Again, hydrogels were synthesized with or without 50 ng of IL-10 to match the IL-10 dose of DC controls for direct comparison. At 24 hours post-encapsulation, there were no differences between DCs in PEG-4MAL and PEG-IL10 hydrogels based on viability and CD86 expression (data not shown). However, at 48 hours post-encapsulation, we observe that DCs in PEG-4MAL hydrogels have increased cell death and increased expression of CD86 while DCs in PEG-IL10 hydrogels remain viable and immature. This cell death and activation may be due to the mechanical stress of processing DCs and hydrogel synthesis or the PEG-4MAL environment itself. This data suggests that PEG-IL10 hydrogels support DC viability and an immature phenotype longer than PEG-4MAL hydrogels without IL-10. Release studies (Figure 5.4) show that unreacted IL-10 would be almost completely released from hydrogels in 6 hours based on the trajectory of the burst release profile. Thus, the prolonged support provided by PEG-IL10 hydrogels can be attributed to incorporated IL-10 presented by the polymer to encapsulated DCs since the untethered IL-10 is no longer present after 6 hours and the differences in viability and phenotype occur between 24 and 48 hours later.

Additionally, the viability of PEG-IL10 hydrogel-encapsulated DCs was evaluated against a control hydrogel containing unmodified IL-10 at the same concentration. Based on calcein AM and EthD-1 staining of DCs within hydrogels, DCs from both PEG-IL10

hydrogels and PEG-4MAL hydrogels loaded with native IL-10 exhibit similar viability 48 hours post-encapsulation. Thus, the benefit of IL-10 on DC viability is not affected by tethering IL-10 to the polymer network, suggesting that IL-10 is bioactive when presented to DCs as PEG-IL10. This evidence validates the final part of the 3-fold mechanism of IL-10 treatment proposed previously.

This benefit of IL-10 translates into improved potency for the proposed cell therapy. In Multiple Sclerosis, promoting viability and phenotypic stability of tolerogenic DCs is a significant challenge in retaining their effectiveness. This study illustrates that PEG-IL10 delivery systems improve the duration of DC viability and an immature phenotype, correlating to an increased capacity for regulatory immunomodulation after delivery.

5.4.5 Both IL-10 and Hydrogel Encapsulation Contribute to DC's Resistance to Inflammation

Multiple Sclerosis patients also have increased levels of inflammatory cytokines and hyper-activated immune systems that can lead to dysregulated cytokine networks and the development of unrelated autoimmune disease[69]. It has been established that PEG-IL10 hydrogels support viability and an immature phenotype in DCs, so we next sought to assess the extent to which these hydrogels could protect encapsulated DCs from inflammation.

To assess the resistance of these DCs to re-stimulation, DCs were treated with IL-10 or encapsulated in PEG-4MAL or PEG-IL10 hydrogels for 24 hours before re-stimulation with either a moderate stimulus (150 ng/mL of TNF-α and 30 ng/mL IFN-γ "STIM 3x") or severe stimulus (2 μg/mL of LPS "LPS 2x"). 48 hours after re-stimulation, DCs in PEG-4MAL and unencapsulated groups had significantly higher proportions of CD86+ DCs in response to STIM treatment, while DCs in PEG-IL10 hydrogels were

protected. In response to the severe stimulus, however, DCs in PEG-IL10 hydrogels were also significantly higher in the frequency of CD86+ DCs, albeit to an amount less than DCs in PEG-4MAL hydrogels with only a moderate stimulus.

In an attempt to decouple the tolerogenic effects of IL-10 and the protective effects of biomaterial encapsulation, we can compare our results to the various control groups. Controls re-stimulated with STIM and LPS stimuli resulted in higher CD86+ frequencies in iDC controls (~65% and ~90%) than DC10 controls (~50% and ~80%), suggesting that treatment with IL-10 conveys some tolerogenic stability. Additionally, the frequency of CD86+ DCs in PEG-4MAL groups were much lower than unencapsulated iDC controls, providing evidence that hydrogel encapsulation also has protective effects against inflammation. This is further supported by the significant differences between PEG-4MAL and PEG-IL10 groups. It is likely that this protection by biomaterial encapsulation is due to a hindrance of inflammatory agent diffusion into the hydrogels resulting in a physical isolation of DCs. The ability for PEG-4MAL hydrogels to inhibit biomolecule diffusion was also illustrated in Figure 4.6, where hydrogels with high polymer densities resulted in DC death by inhibiting the diffusion of biomolecules necessary for DC survival. The contributions to maturation resistance from IL-10 and biomaterial encapsulation combined are sufficient to protect encapsulated DCs from the moderate stimulus, whereas either treatment alone (DC10 & PEG-4MAL groups) does not confer resistance to severe inflammation.

While IL-10 treatment and hydrogel encapsulation do not entirely protect DCs from 2 μg/mL of LPS, these DCs are much less activated than iDC or DC10 controls, suggesting

substantial resistance to re-stimulation. Additionally, LPS is regarded as a very harsh stimulus that is not generally experienced *in vivo*, especially at the tested concentrations.

The designed biomaterial is meant to overcome several significant challenges in tolerogenic cell therapy applications: (1) co-localizing therapeutic cells to the site of activity, (2) promoting viability and phenotypic stability in delivered cells, and (3) preventing changes in cell viability, phenotype, and function post-injection. The PEG-4MAL hydrogel system was chosen because it is highly modular, injectable, gelates *in situ*, and does not inherently activate immune cells. The properties of this hydrogel system enabled the precise delivery of therapeutic cells to any target location reachable with a needle. Hydrogel modularity allowed manipulation of biophysical characteristics to support encapsulated DCs. Lastly, the functionalization of these hydrogels with IL-10 resulted in the reinforcement of DC viability and phenotypic stability, protection from even severe inflammatory stimuli, and a 3-fold mechanism of treatment that extends to nearby endogenous immune cells.

CHAPTER 6. EFFECTIVENESS OF PEG-4MAL DELIVERED DENDRITIC CELLS IN AMELIORATING SYMPTOMS IN MICE WITH EXPERIMENTAL AUTOIMMUNE ENCEPHALOMYELITIS

6.1 Overview

Current treatment strategies for MS have several significant shortcomings, including: (1) only functioning to slow disease progression; (2) variability in patient responsiveness; and (3) dangerous side effects such as a higher risk of opportunistic infection, risk of autoimmunity, depression, and organ damage[4,61,67]. EAE in mice has been shown to be a highly representative model of MS in terms of pathophysiology and expression of symptoms[59,207]. Recently, tolerogenic DC therapy has been highlighted as a promising strategy to treat autoimmune diseases with selective tolerance[6,109,191,194,208]. The objective of this aim is to use a model of EAE to illustrate the effectiveness of hydrogel-delivered DC10s in ameliorating symptoms of MS. The working hypothesis is that antigen-specific DC10s delivered to cervical LNs by PEG-4MAL hydrogels will ameliorate symptoms of EAE by skewing the autoreactive T cell population towards tolerance through an IL-10-dependent mechanism. The rationale for this hypothesis is that tolerogenic DCs are capable of conditioning T cells towards a regulatory phenotype and can even inhibit autoreactive effector T cells[191,209]. The use of biomaterial delivery systems enables localized delivery to disease-relevant sites while supporting encapsulated cells post-delivery, thereby improving the efficacy of cell therapies. Tolerogenic DCs induced by IL-10 treatment primarily function through increased secretion of IL-10[7], but DCs are also capable of promoting

tolerogenic behavior in T cells is through upregulation of PD-L1[210,211]. Completion of this aim is expected to highlight the capacity for this cell-biomaterial treatment to ameliorate symptoms of EAE as a proof-of-concept for the treatment of autoimmunity. Insight into the role of the biomaterial delivery platform and the mechanism by which this cell therapy promotes selective tolerance is also a primary objective.

6.2 Materials and Methods

6.2.1 Animals

All live animal procedures were conducted under the approval of the Institutional Animal Care and Use Committee (IACUC) of the Georgia Institute of Technology. Mice were housed, maintained, and bred in the Physiological Research Laboratory (PRL) Animal Facility of the Georgia Institute of Technology. Animals were 8-to-12-week-old male C57BL/6J mice (Jackson Laboratories, Inc.)

6.2.2 Induction of Experimental Autoimmune Encephalomyelitis

After receipt, age- and sex-matched C57BL/6 mice procured from Jackson Laboratories are given several days to adjust to their new environment. There are two major immunization components to induce EAE: (1) MOG_{35-55} antigen and complete Freund's adjuvant (CFA) are injected subcutaneously into mice on each flank to activate immunity against the myelin-associated self-peptide; and (2) pertussis toxin (PT) is injected intraperitoneally two days later to promote permeability of the blood-brain barrier.

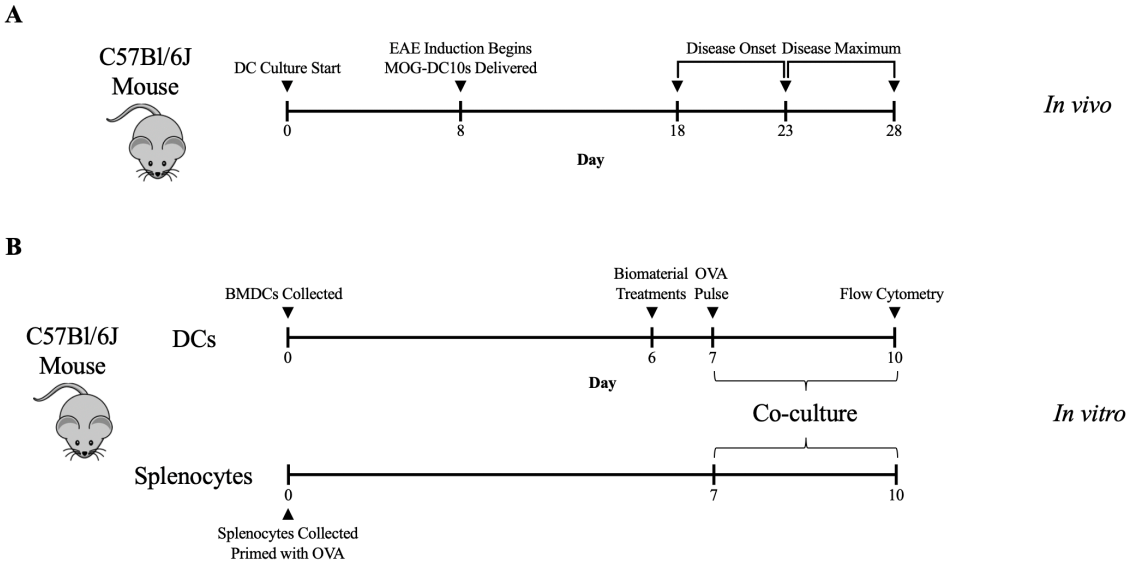

Figure 6.1. Experimental overview for *in vivo* studies with EAE mice and *in vitro* co-culture studies. a) EAE induction and prophylactic treatment timeline and b) autologous co-culture design for recapitulation *in vitro*.

6.2.3 Clinical Scoring

Clinical Scores are given to mice with EAE based on their level of paralysis. These scores are outlined below in Table 6.1. Scoring was done every 24-48 hours in a blinded setting.

Table 6.1. Clinical Scoring Guidelines

Clinical Score	Description
0	No Disease
1	Flaccid Tail
2	Hind Limb Weakness
3	Hind Limb Paralysis
4	Forelimb Weakness
5	Moribund

6.2.4 PEG-4MAL Delivery of DC10s

DCs were cultured from bone marrow as described previously. On Day 8, DC10s were pulsed with MOG_{35-55} peptide for 2-4 hours and then encapsulated in 50 μL PEG-4MAL hydrogels at a concentration of $1x10^6$ DCs/hydrogel. Hydrogel-encapsulated cells were injected subcutaneously into the neck proximal to the cervical lymph nodes in mice with EAE.

6.2.5 Congenic Tracking of Delivered Dendritic Cells

DCs were cultured from bone marrow, as described previously, using congenic mice (CD45.2+). Recipient mice were CD45.1+ such that delivered and endogenous leukocytes could be distinctly identified. The frequency and number of CD45.1 and CD45.2 cells in various tissues were evaluated by flow cytometry.

6.2.6 Organ Explantation and Tissue Processing

EAE-bearing mice were sacrificed and perfused with sterile PBS via the heart. Tissues such as the central nervous system, lymph nodes, spleens, and the hydrogel will be collected and individually homogenized through mechanical disruption. Cells were washed twice with sterile PBS before analysis.

6.2.7 Cell Infiltration into PEG-4MAL Hydrogels in vitro

DCs were cultured from bone marrow as described previously. On Day 6, iDCs were stained with CellTracker Red CMTPX (Life Technologies) according to the manufacturer's protocol. Optimized PEG-4MAL hydrogels were synthesized as described previously with or without iDCs in an 8-chamber imaging slide (Ibidi). Silicone molds

were used to maintain a standard shape and height for each hydrogel. RBC-lysed splenocytes from the same mouse were incubated for 6 days in T25 Flasks with IL-2 (30 U/mL). On Day 6, splenocytes were stained with CellTracker Green CMFDA (Life Technologies) according to the manufacturer's protocol. Stained splenocytes were then seeded on top of hydrogels for 6 hours. The infiltration of splenocytes into hydrogels was evaluated by confocal microscopy, as previously described.

6.2.8 Co-Incubation of Dendritic Cells with Autologous Splenocytes in vitro

DCs were cultured from bone marrow as described previously. RBC-lysed splenocytes from the same mouse were plated at $5x10^6$ cells/mL in 24-well plates (2mL/well) with IL-2 (30 U/mL), ovalbumin $(OVA)_{257-264}$ (5 μg/mL), and $OVA_{323-339}$ (5 μg/mL) for 7 days. On Day 7, treated DCs were pulsed for 2-4 hours with $OVA_{257-264}$ (10 μg/mL), and $OVA_{323-339}$ (10 μg/mL). Treated DCs were then collected and plated in U-bottom 96-well plates with 100 μL of OVA-primed splenocytes ($1x10^6$ cells/mL) for 3 days. Splenocytes were stained with carboxyfluorescein succinimidyl ester (CFSE) prior to being plated with DCs. On Day 10, DCs and splenocytes were collected and processed for flow cytometry.

6.2.9 Flow Cytometry

DCs and splenocytes were washed with 1x PBS and then reconstituted in 100 μL of 1x PBS. Cells were stained with 1 μL/sample of Zombie Violet Fixable Viability Kit (BioLegend) for 20 minutes. Cells were then washed with FACS Buffer (Hank's Buffered Salt Solution, HBSS; 1% bovine serum albumin, BSA; 1 mM Ethylenediaminetetraacetic acid, EDTA). TruStain FcX™ (anti-mouse CD16/32; BioLegend) was added, and cells

were incubated on ice for 10 minutes. Cells were then stained with APC/Fire750-CD3 (17A2; BioLegend), APC-CD4 (GK1.5; BioLegend), PerCP-CD8a (53-6.7; BioLegend), PE/Cy7-CD25 (PC61; BioLegend), PE-CF594-CD279 (J43; BD), for 30 minutes on ice, protected from light. Cells were then fixed and permeabilized using True-Nuclear Transcription Factor Buffer Set (BioLegend) according to the manufacturer's protocol. Cells were stained FoxP3-PE (MF23; BD) for 30 minutes and were then washed twice with Perm Buffer and once with FACS buffer before being analyzed on a flow cytometer (LSRFortessa; BD). Gating strategies are illustrated in Figure A.13.

6.2.10 Confocal Microscopy

Cell viability was visualized by staining with calcein AM and ethidium homodimer-1 (EthD-1) and imaging on a confocal microscope (Nikon Eclipse Ti-E C2+). Media was removed and PEG-4MAL hydrogels encapsulating DCs were washed twice with 1x PBS by gentle pipetting. Samples were then stained with 1 μM calcein AM and 1 μM EthD-1 in media without FBS for 20 minutes. Intact hydrogels were then washed two more times and media without FBS was added for imaging.

6.2.11 Cytokine Multiplexing

Supernatants were collected from samples at the end of culture and stored at -80^{o}C until use. Samples were thawed to room temperature and treated according to the manufacturer's protocol for Bio-Plex Pro Mouse Cytokine 23-plex Assay (Bio-Rad). Samples were then analyzed on a Luminex MAGPIX. A linear range of cytokine concentrations was determined to optimal sample dilution according to cytokines of

interest. Cytokines tested are categorized below in Table 4.1 based on their effects being inflammatory, pleiotropic, tolerogenic, or unrelated to DCs.

6.2.12 Statistical Analysis

Experimental values are reported as mean and standard deviation for all samples. Statistical analysis was determined using one or two-way ANOVA coupled with Sidak's posthoc pairwise tests using GraphPad (Prism Inc.). All datasets were normally distributed. If datasets failed the Brown-Forsythe test (due to significant differences in variances between treatment groups), Welch's correction was applied to account for these differences and Dunnett's posthoc pairwise test was used. For co-culture studies, splenocyte-only groups served as the control for comparison tests. For all other experiments, multiple comparisons were used. p-values <0.05 were considered statistically significant. Error bars represent the standard deviation.

6.3 Results

6.3.1 Dendritic Cells Delivered via PEG-4MAL Hydrogels Delay Onset of Symptoms and Ameliorate Symptom Severity in Mice with EAE

Mice with EAE were treated prophylactically with either blank hydrogels, PEG-4MAL hydrogels encapsulated MOG-DC10s (Hydrogel + MOG-DC10), or MOG-DC10s delivered subcutaneously (SubQ MOG-DC10) at disease onset. Figure 6.2 shows that both Hydrogel + MOG-DC10 and SubQ MOG-DC10 groups delayed the onset of symptoms in mice by several days. However, only mice treated with PEG-4MAL hydrogel-delivered DC10s had a significant difference in symptom severity at the peak of disease (Figure 6.2).

Immunophenotyping studies on CNS tissues of sacrificed mice were conducted to investigate the mechanism of amelioration. Both Hydrogel + MOG-DC10 and SubQ MOG-DC10 groups had significantly fewer CD11b+ cells in the CNS, while the Hydrogel + MOG-DC10 had significantly increased frequency of MOG-specific CD11b+ (MOG+CD11b+) cells in the CNS (Figure 6.2). Additionally, CD3+ T cells in the CNS of EAE mice treated with SubQ MOG-DC10 (which did not have lasting symptom reduction) had significantly lower expression of CD4 compared to treatment with blank hydrogels (Figure 6.2).

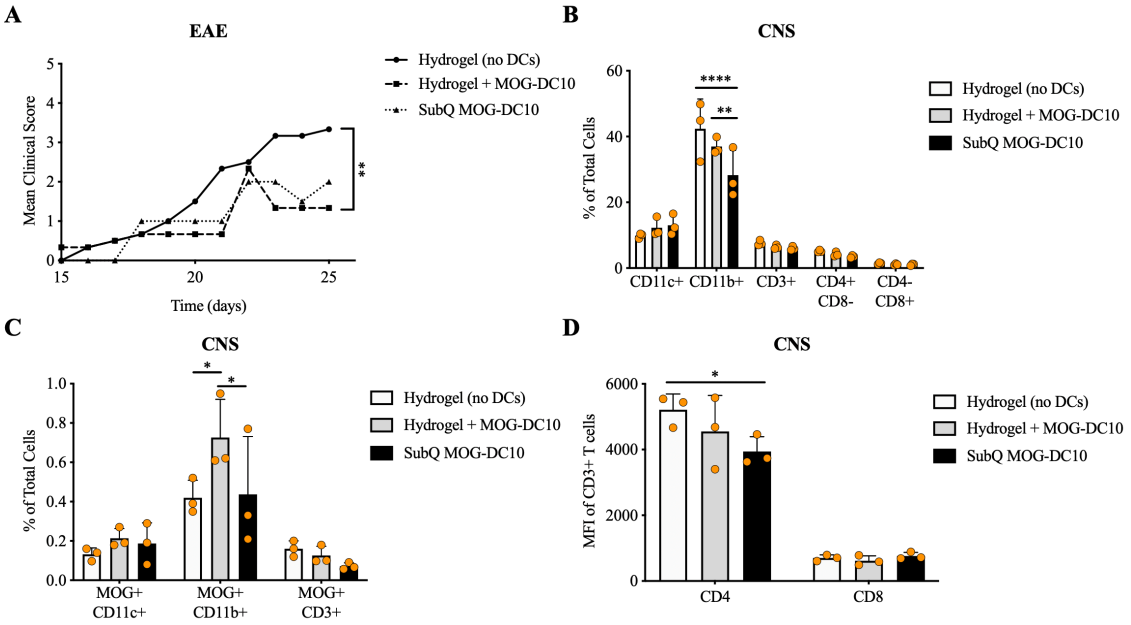

Figure 6.2. Clinical scores of mice with EAE after receiving either blank PEG-4MAL hydrogels, PEG-4MAL hydrogel-delivered DC10s, or DC10s injected subcutaneously. a) Clinical scores of EAE mice. b) Frequency of various cell types, c) MOG-specific cell types, and d) CD4 and CD8 T cell expression in the CNS of EAE mice. ****p<0.0001, **p<0.01, and *p<0.05 via two-way ANOVA and Tukey's multiple comparison test.

This data suggests that DC10s ameliorate symptoms of EAE through tolerance mediated by CD11b+ cells and CD4+ T cells in the CNS.

6.3.2 Dendritic Cells Largely Remain Within the Delivered PEG-4MAL Hydrogel While Endogenous Cells Infiltrate the Hydrogel Environment

Congenic strains of mice were used to distinguish between delivered (CD45.1+) and endogenous (CD45.2+) lymphocytes in EAE mice for tracking and phenotyping purposes. Hydrogels were explanted from EAE mice after 1, 4, 7, or days post-injection. After just 1-day post-injection, delivered DCs constituted only ~25% of the lymphocytes within the hydrogel (Figure 6.3) and by Day 4 nearly 100% of the lymphocytes found in hydrogel explants were CD45.2+ endogenous cells. This data suggests a high degree of endogenous cell infiltration into hydrogels, a significant migration of DCs out of hydrogels, or both.

In evaluating the phenotype of CD45.2+CD11c+ endogenous DCs in the CNS, EAE mice treated with hydrogel-delivered DC10s had significantly lower CD86 expression than EAE mice treated with blank hydrogels (Figure 6.3). Similarly, in mice receiving hydrogel-delivered DCs, CD45.2+CD11c+ endogenous DCs found in hydrogel explants had significantly lower expression of CD86 (Figure 6.3). Additionally, endogenous CD3+ T cells infiltration in hydrogels was observed in blank hydrogel just 1-day post-injection, while hydrogels with DC10s had a higher frequency of CD3+ T cells at 4 days post-injection (Figure 6.3).

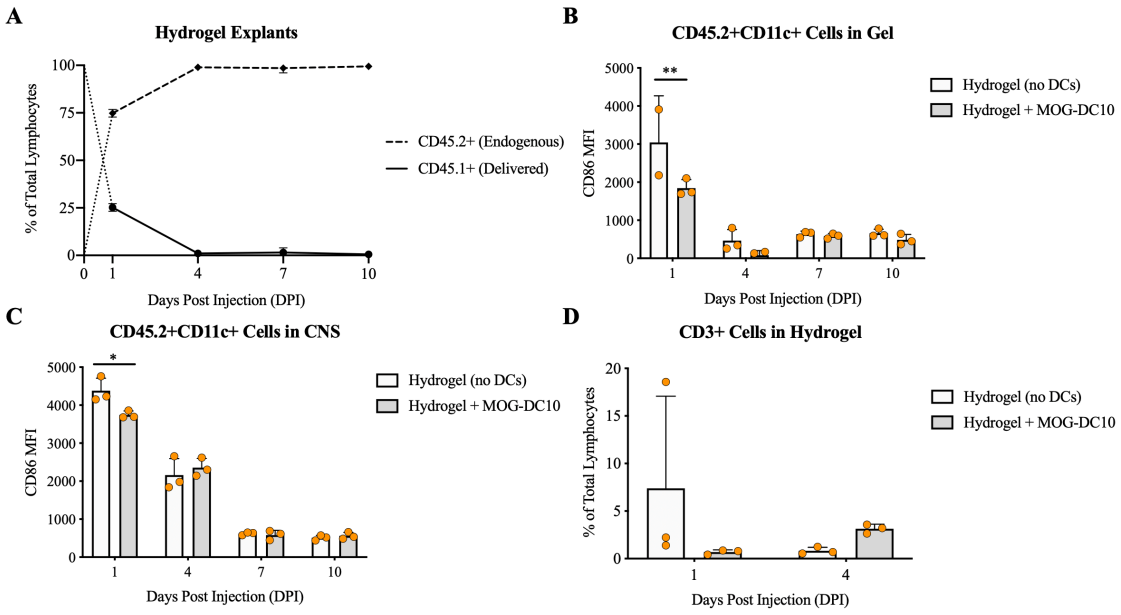

Figure 6.3. Location and phenotypes of hydrogel-delivered DCs at various times post-injection using congenic mouse strains. a) Frequency of CD45.1+ and CD45.2+ cells within hydrogel explants. CD86 expression of endogenous (CD45.2+) CD11c+ DCs in b) within hydrogel explants and c) the CNS. d) Frequency of CD3+ T cells within hydrogel explants as a percentage of total lymphocytes. **p<0.01 and *p<0.05 via two-way ANOVA and Sidak's multiple comparison test.

6.3.3 Immune Cell Infiltration into PEG-4MAL Hydrogels is Recapitulated in vitro

To validate the extent of lymphocyte infiltration into PEG-4MAL hydrogels *in vitro*, PEG-4MAL hydrogels were synthesized with or without iDCs and RBC-lysed splenocytes were seeded on top. After 6 hours, we observed extensive infiltration of splenocytes into hydrogels with iDCs while splenocyte infiltration into blank hydrogels was limited (Figure 6.4). The number of cells infiltrating hydrogels and their depth is quantified in Figure 6.4. This data supports the infiltration of endogenous cells into hydrogels observed *in vivo* in Figure 6.3.

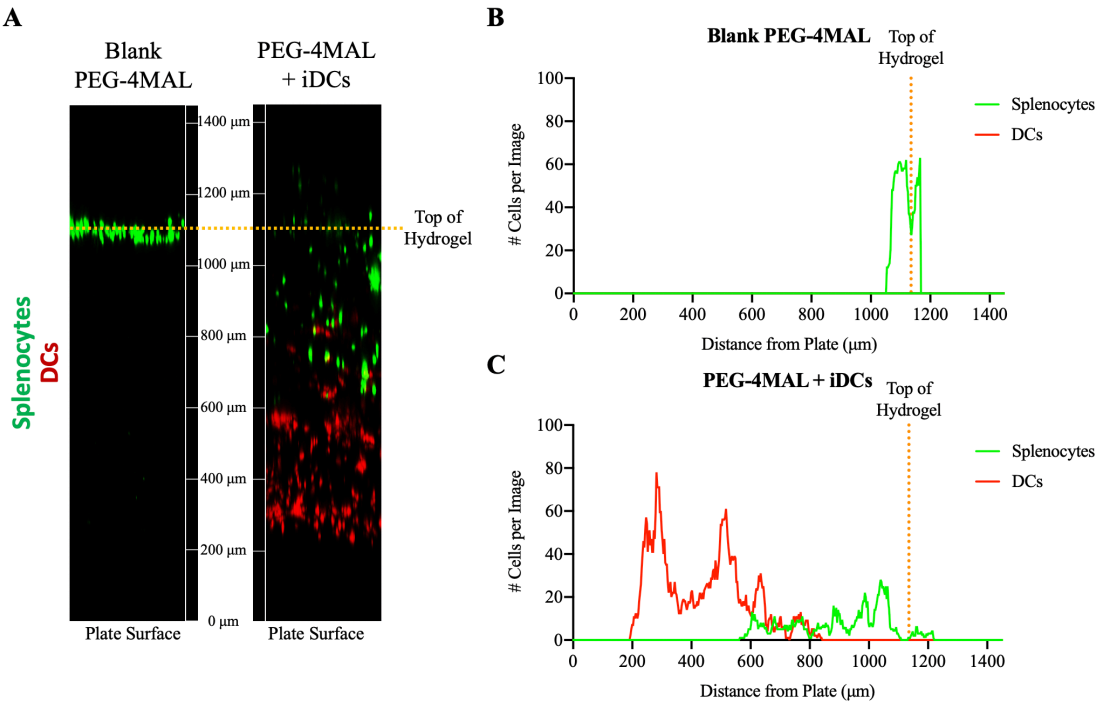

Figure 6.4. RBC-lysed splenocytes stained with CellTracker Green were seeded on top of either blank PEG-4MAL hydrogels or hydrogels encapsulating CD11c+ iDCs stained with CellTracker Red. a) Confocal images illustrating the infiltration of lymphocytes into hydrogels after 6 hours. Quantification of the number of DCs (red) and splenocytes (green) fluorescent cells in each slice for b) blank PEG-4MAL hydrogels and c) PEG-4MAL hydrogels encapsulating iDCs.

6.3.4 Dendritic Cells Treated with IL-10 or PEG-IL10 Encapsulation Inhibit CD8+ T cell Proliferation and Induce FoxP3+ Regulatory T cells in an Antigen-Specific Manner

DCs receiving various treatments were co-incubated with autologous, ovalbumin (OVA)-primed splenocytes for 72 hours to evaluate their effect on T cells *in vitro*. Co-cultures with DCs at ratios of 1:1 and 1:10 (DCs:T cells) had significantly higher viability across all treatment groups except for LPS compared to splenocytes alone (Figure 6.5). This effect was observed across all cells and amongst CD3+ T cells. While the overall frequency of CD3+ T cells was significantly increased with a higher number of DCs, the

frequency of CD4+ T cells was dramatically reduced at higher DC concentrations (Figure 6.5). The expression of CFSE amongst CD4+ T cells was significantly diminished in groups with a ratio of 1:1, suggesting an increase in the amount of CD4+ T cell proliferation in these groups, most notably amongst iDC and DC10 groups (Figure 6.5). This increase in CD4+ T cell proliferation was primarily amongst CD25+FoxP3+ T regulatory cells, as shown by the marked increase in iDC, DC10, PEG-4MAL, and PEG-IL10 groups (Figure 6.6). Figure 6.6 shows a significant increase in the expression of PD-1 on CD4+ T cells, specifically for iDC and DC10 groups at higher DC concentrations (1:1).

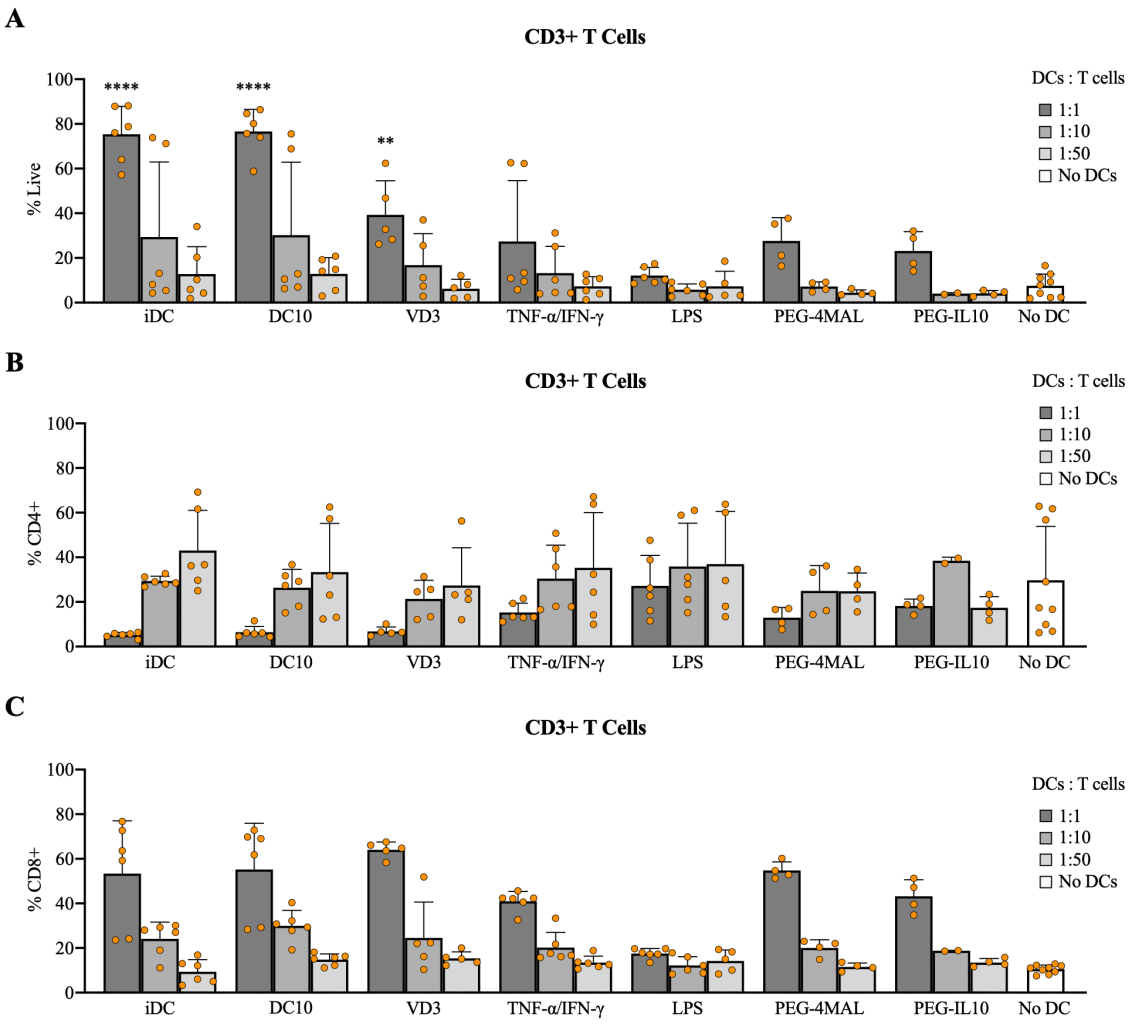

Figure 6.5. Viability and composition of CD3+ T cells after 72 hours of incubation with various DCs at various concentrations. a) Live cells, b) frequency of CD4+ T cells, and c) frequency of CD8+ T cells. Data shown is from 6 replicates across n=3 experiments. Live cells are defined by Zombie Violet negative cells. ****p<0.0001 and **p<0.01 via one-way ANOVA and Dunnett's comparison test.

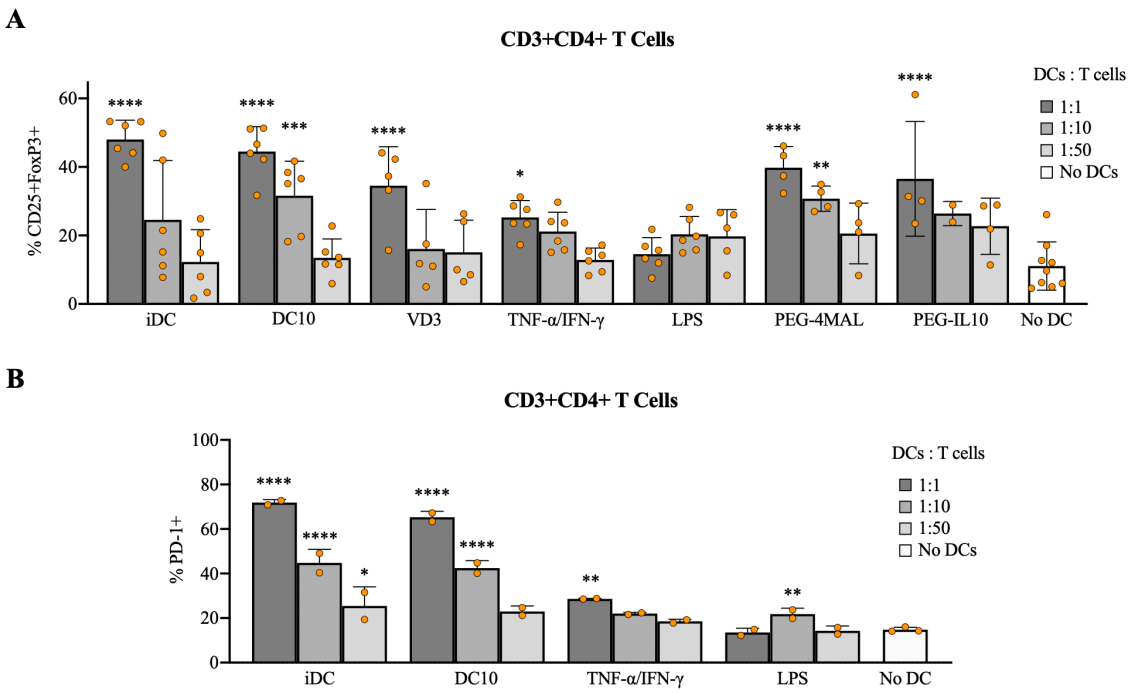

Figure 6.6. Phenotypes of CD4+ T cells after 72 hours of incubation with various DCs at various concentrations. a) CD25+FoxP3+ T regulatory cells and b) PD-1+ T cells assessed by flow cytometry. ****p<0.0001, ***p<0.001, **p<0.01, and *p<0.05 via one-way ANOVA and Dunnett's comparison test.

CFSE expression on CD8+ T cells was also closely correlated to DC concentration across all treatment groups, with significant differences observed at ratios of 1:1 (Figure 6.7). However, PD-1 expression on CD8+ T cells was elevated for iDC and DC10 groups, as was observed in CD4+ T cells (Figure 6.7).

Interestingly, results differ when the co-culture experiment is repeated without the presence of antigen. There are no significant differences between treatments or groups for samples in the absence of OVA. This data suggests that the tolerance mechanism by iDCs and DC10s is an antigen-specific process.

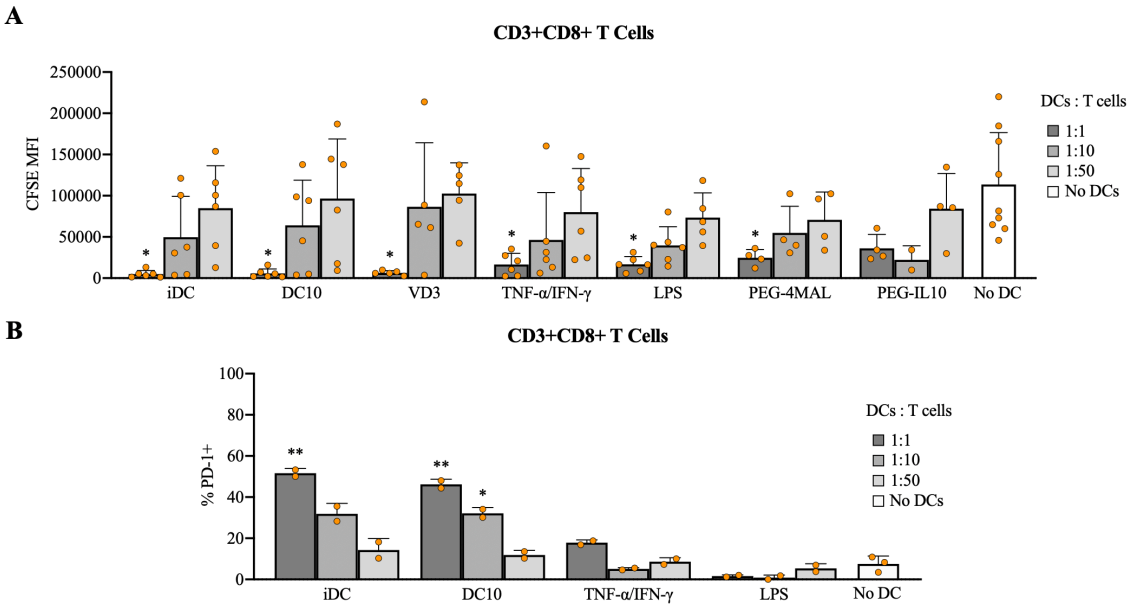

Figure 6.7. Phenotypes of CD8+ T cells after 72 hours of incubation with various DCs at various concentrations. a) MFI of CFSE and b) PD-1+ T cells assessed by flow cytometry. **p<0.01 and *p<0.05 via one-way ANOVA with Welch's correction and Dunnett's comparison test.

6.3.5 Supernatant Profiles from Co-Cultures with Tolerogenic DCs are Characteristic to Regulatory T Cells and T_H2 Cells

Supernatants of co-cultures with various DCs were collected after 72 hours to further assess the phenotype of T cells. Of the cytokines analyzed, those of interest include IL-10 (Tregs), IFN-γ (T_H1 cells), IL-17 (T_H17 cells), and IL-5 (T_H2 cells). Secreted chemokine profiles were also evaluated. Supernatant concentrations of IL-10 were significantly increased for iDC (1:1), DC10 (1:1), VD3 (1:1), LPS (1:1), PEG-4MAL (1:1), and PEG-IL10 (1:1) (Figure 6.8). Concentrations of IFN-γ were significantly increased only in TNF-α/IFN-γ (1:1) co-cultures (Figure 6.8). IL-5 concentrations were significantly increased across all treatment groups at high ratios (1:1), with the exception of PEG-4MAL (Figure 6.8). All treatment groups produced supernatants with increased levels of CCL5, to varying

degrees (Figure 6.8). CCL2 concentrations were notably increased for iDC, DC10, mDC, and PEG-IL10 groups, while only mDC and PEG-IL10 co-cultures exhibited increased levels of CCL3 and CXCL1 (Figure 6.8).

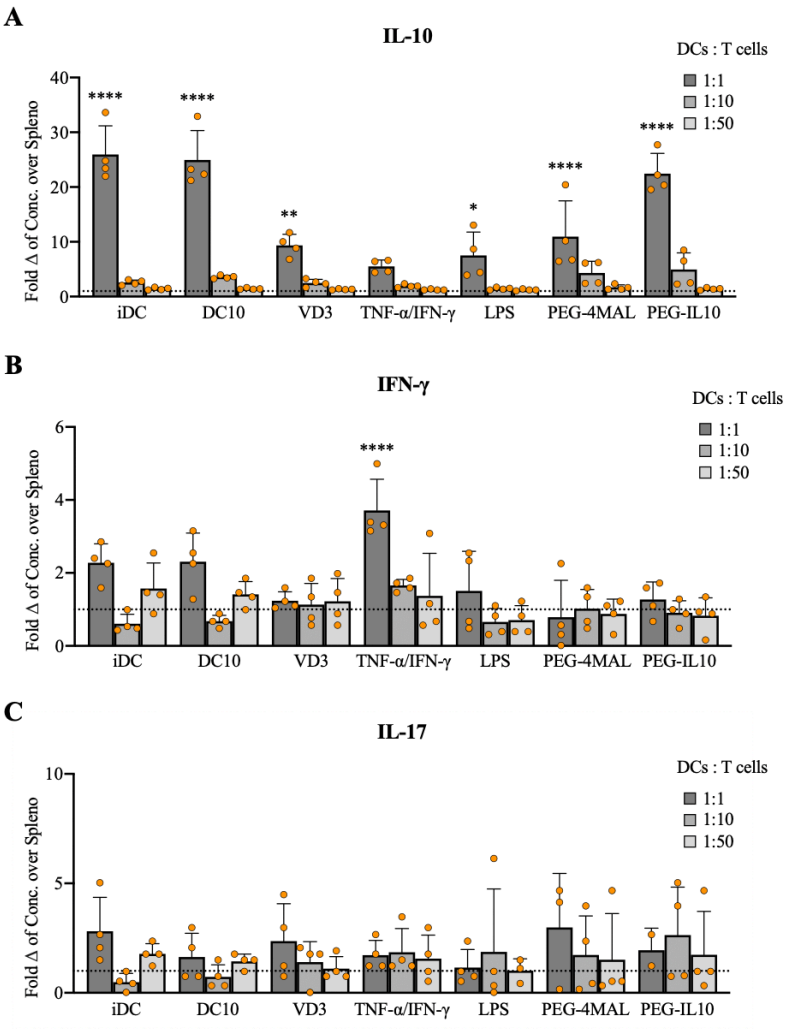

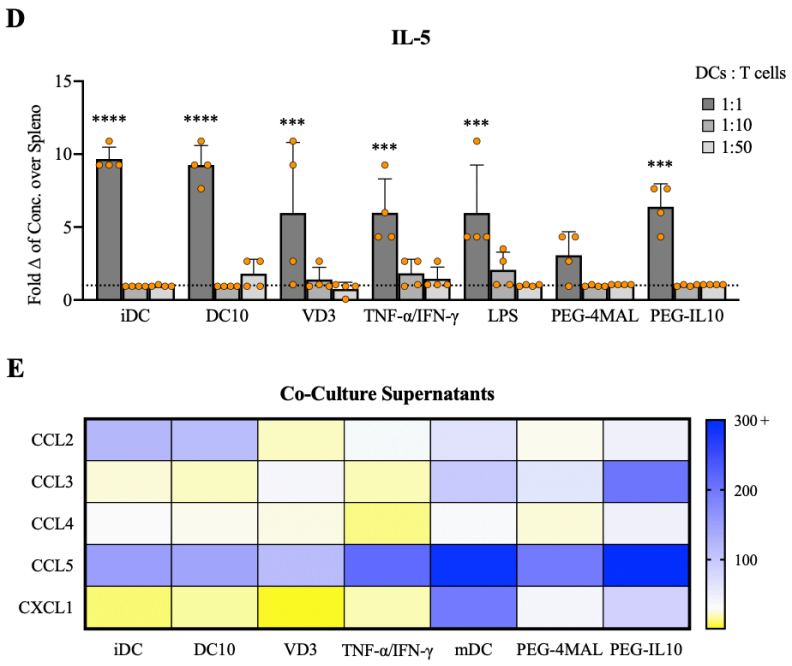

Figure 6.8. Multiplexed analysis of secreted cytokines in co-culture supernatants . Fold changes of a) IL-10 (Tregs), b) IFN-γ (T_H1), c) IL-17 (T_H17), and d) IL-5 (T_H2) for co-culture groups at various treatments ratios. e) Heatmap representing the fold change of selected chemokines for treated groups (1:1) over splenocyte-only controls. Data shown is from 4 replicates across n=2 experiments. ****p<0.0001, ***p<0.001, **p<0.01, and *p<0.05 via one-way ANOVA and Dunnett's comparison test.

6.4 Discussion

Previous work from our lab has shown significant prevention of symptom progression in mice treated with DCs delivered to the neck, but not in mice treated with DCs delivered to the flank. This data confirms that DCs can induce tolerance, but only when co-localized to a site of anatomical relevance, the cervical LNs in the neck. Previous studies have shown the challenges of DC biodistribution and *in vivo* activation associated with traditional delivery methods[104,105]. This motivated the investigation into DC-biomaterial interactions and the development of an immunosuppressive biomaterial delivery system to improve the efficacy of tolerogenic DC therapies. The overarching goal

of Aim 3 was to illustrate the supplemental benefit of a biomaterial delivery system tailored to tolerogenic DCs by utilizing a murine model of MS and elucidating mechanistic properties of immunomodulation with studies both *in vivo* and *in vitro*.

6.4.1 Dendritic Cells Delivered via PEG-4MAL Hydrogels Delay Onset of Symptoms and Ameliorate Symptom Severity in Mice with EAE

To evaluate the effect of biomaterial delivery on the success of DC therapies, mice were induced with EAE and treated prophylactically with subcutaneously delivered MOG-DC10s, PEG-4MAL hydrogel delivered MOG-DC10s, or blank PEG-4MAL hydrogels. The clinical scores of mice were recorded each day to track the progression of symptoms. While it has been previously established that the location of therapeutic cell delivery is highly important to therapeutic effectiveness, this study aimed to highlight the ability of our immunomodulatory biomaterial system in improved the robustness of this therapy by better co-localizing DCs to the target site and by supporting DCs post-injection. The neck of mice was chosen as the delivery site to co-localize DCs to the LNs most relevant to EAE disease pathophysiology, the cervical LNs.

While mice receiving blank hydrogels progressed to average clinical scores >1 by Day 19 and >2 by Day 21, mice treated with hydrogel-delivered MOG-DC10s remained mostly asymptomatic with an average clinical score of <1 on Day 21. By Day 25, mice receiving blank hydrogels had progressed to an average clinical score of >3, whereas only mice treated with hydrogel-delivered MOG-DC10s had a significantly lower average clinical score. Interestingly, both hydrogel-delivered and subcutaneously delivered MOG-DC10 groups demonstrated an apparent delay in the onset of symptoms in EAE mice. However, only mice receiving hydrogel-delivered treatments exhibited a significant

amelioration of symptoms by the end of disease progression. This data suggests that DC therapies are effective in ameliorating symptoms at early timepoints regardless of delivery method, but only hydrogel-delivered DC therapies result in long-term amelioration of symptoms in mice with EAE.

Mice with EAE were sacrificed and their primary tissues were collected and processed to examine their immunophenotype using flow cytometry. Mice receiving blank hydrogels had an increase in the frequency of CD11b+ cells in the CNS, accompanied by a decrease in the frequency of MOG-specific CD11b+ in the same tissue. Oppositely, mice treated with hydrogel-delivered DCs had higher frequencies of CD11b+ cells in the CNS. CD11c+CD11b+ APCs have been implicated in EAE as the cells that regulate immunity through induction of T regulatory cells[212] and depletion of this cell type abrogated these tolerogenic effects[213]. Blank hydrogel groups had a significant increase in the expression of CD4 amongst CD3+ T cells compared to mice receiving DC therapies, while the expression of CD8 remained unchanged. This suggests that immunomodulation by DCs may occur primarily in the CD4 compartment.

6.4.2 Dendritic Cells Largely Remain Within the Delivered PEG-4MAL Hydrogel While Endogenous Cells Infiltrate the Hydrogel Environment

Towards examining whether the long-term effects of biomaterial-delivered DC therapies are due to DCs being more robust in their effects or sustained DC activity for a more extended period, we employed congenic strains of mice to further investigate the immunomodulatory mechanism. DCs from CD45.1+ mice were delivered to CD45.2+ mice to track the delivered DCs and to differentiate between the effects of endogenous and therapeutic cell subsets.

After 1, 4, 7, or 10 days post-injection, mice with EAE were sacrificed and relevant tissues were collected and processed for flow cytometry. In evaluating hydrogel explants, we observed a marked increase in endogenous CD45.2+ just 1-day post-injection and nearly all of the cells in these hydrogel explants were CD45.2+ cells by 4 days post-injection. This suggests a high level of endogenous cell infiltration into PEG-4MAL hydrogels after injection. It is likely that basal chemokine secretions by encapsulated DCs recruit endogenous lymphocytes to the established biomaterial niche. This evidence is in contrast to our original hypothesis that delivered DCs would migrate to nearby LNs to carry out effector functions.

Endogenous DCs infiltrating delivered hydrogels with DC10s had significantly lower expression of CD86 than DCs that infiltrated blank hydrogels. Additionally, endogenous CD45.2+ DCs in the CNS had significantly lower expression of CD86 than endogenous DCs in the CNS of mice receiving blank hydrogels. Lastly, CD3+ cells infiltrated blank hydrogels quickly (Day 1) while hydrogels encapsulating DCs were infiltrated by T cells later (Day 4+). Combined, this data provides evidence contrary to our original proposed mechanism of action. Based on this series of experiments, it is much more likely that endogenous DCs and other lymphocytes infiltrate the highly degradable PEG-4MAL hydrogel, are modulated by the delivered DC10s, and then migrate out to carry out downstream functions in the CNS and elsewhere.

6.4.3 Immune Cell Infiltration into PEG-4MAL Hydrogels is Recapitulated in vitro

Due to these differences in the characteristics of infiltration, we sought to recapitulate the observed infiltration *in vitro*. PEG-4MAL hydrogels with or without DCs were synthesized and autologous splenocytes were then seeded on top of the biomaterial

constructs. Several hours later, hydrogels were imaged to assess the depth of infiltration by splenocytes. Splenocytes (green) infiltration into hydrogels encapsulating DCs was evident at depths of up 550 μm after just 6 hours of incubation, whereas splenocytes seeded on blank hydrogels showed little evidence of infiltration at this early time point. This suggests that the encapsulated DCs are more prevalent than the hydrogel architecture in promoting endogenous cell infiltration early on.

Taken with data from the previous section, it is possible that delivered DCs recruit endogenous DCs and other APCs, which then recruit T cells and other effector lymphocytes. The biomaterial delivery construct may function as an immunomodulatory node, where endogenous cells are recruited to, treated by delivered DCs, and then migrate to sites of therapeutic importance such as LNs and the CNS.

6.4.4 Dendritic Cells Treated with IL-10 or PEG-IL10 Encapsulation Induce FoxP3+ Regulatory T cells and Suppress CD8+ T cells in an Antigen-Dependent Manner

To gain insight into the immunomodulatory process by which DC10s ameliorate symptoms of EAE *in vivo*, we investigated the effects of these DCs on T cells in a co-culture. Autologous splenocytes were chosen to establish a more biomimetic environment of signaling compared to a co-culture with T cells alone. Splenocytes were primed with $OVA_{257-264}$ and $OVA_{323-339}$ (5 μg/mL each) for 7 days prior to co-incubation with DCs based on a protocol previously established in the Babensee Lab[214]. DCs receiving various treatments or biomaterial encapsulations were pulsed with $OVA_{257-264}$ and $OVA_{323-339}$ (10 μg/mL each) for 3-5 hours prior to co-incubation with splenocytes for 3 days. DCs were mixed with splenocytes at ratios of 1:1, 1:10, and 1:50 (DCs:splenocytes). The phenotype of splenocytes prior to incubation with DCs on Day 7 was not directly measured, but we

expect that T cells were viable, had expanded in response to OVA antigen priming, and maintained survival signaling processes, which the Babensee Lab has previously demonstrated in the work by Thomas et al[214].

CD3+ T cell viability appeared to be improved at higher concentrations of DCs, including significant increases in iDC, DC10, and VD3 groups. Higher concentrations of DCs also resulted in a lower frequency of CD4+ T cells and a higher frequency of CD8+ T cells across all groups (excluding LPS). Additionally, higher DC concentrations were correlated with lower fluorescence of CFSE in CD4+ T cells and CD8+ T cells, suggesting substantial proliferation across both T cell subsets. In focusing specifically on CD4+ T cells, we observed a significant increase in CD25+FoxP3+ T regulatory cells for iDCs (1:1), DC10s (1:1, 1:10), VD3 (1:1), PEG-4MAL (1:1, 1:10), and PEG-IL10 (1:1). CD4+ T cells from co-cultures with iDCs and DC10s at higher DC concentrations (1:1 and 1:10) also had a significant increase in the percentage of PD-1+ CD4+ T cells. Similarly, CD8+ T cells mixed with iDCs (1:1) and DC10s (1:1 and 1:10) had a significant increase in PD-1+ CD8+ T cells.

It is not surprising that co-cultures with more DCs have increased T cell viability, as DCs are known to induce maintenance and survival signaling in cognate T cells[74]. In contrast, co-cultures in the absence of antigen had poor viability regardless of treatment group, suggesting that the presence of antigen plays a role in the survival T cells, which has been previously reported[215]. Only a small fraction of T cells survived after 7 days of culture without antigen. There were over 3 times the number of T cells after 7 days of culture with OVA priming, which is likely due to survival signaling and T cell expansion in response to antigen. OVA-primed T cells primarily responded to antigen-pulsed DCs,

while there were no significant changes in viability or phenotype of T cells without antigen present. It is expected that this is due to either a reduction in T cell activity in the absence of antigen or less robust conditioning by DCs in the absence of presented antigen. While the frequency of CD4+ T cells decreased in iDC and DC10 groups, decreasing CFSE fluorescence suggests that CD4+ T cells were still proliferating. Comparing CFSE expression in CD4+ versus CD8+ T cells, CD8+ T cells exhibited dramatically lower CFSE fluorescence, meaning that CD8+ T cell proliferation simply outpaced CD4+ T cell proliferation for these groups, resulting in the observed frequencies.

The marked increase in the percentage of CD25+FoxP3+ Tregs for iDCs, DC10s, PEG-4MAL, and PEG-IL10 groups highlights the primary mechanism of immunomodulation. This likely occurs one of two ways *in vivo*: (1) directly, where tolerogenic DCs interact with endogenous T cells and induce a regulatory phenotype, or (2) indirectly, where tolerogenic DCs modulate endogenous DCs and other APCs, which then induce Tregs. This increase in Tregs is accompanied by an increase in PD-1 for the same groups, suggesting that PD-1 is involved in downstream tolerance. In the CD8+ T cell compartment, the marked increase in PD-1 combined with dramatic proliferation indicates that these cells are approaching a state of immunosuppression where they will no longer be capable of detrimental autoreactive processes. While we have evidence of PD-1 expression for the control groups, time constraints prohibited studies of PD-1 expression in hydrogel groups, but we can infer that the mechanism of iDC and DC10 tolerogenic function does not change due to encapsulation.

When applied to the previous data observed *in vivo*, we can confirm that immunomodulation of the CD4+ T cell compartment is the most likely mechanism of

tolerance induced by therapeutic DCs. Both iDCs and DC10s have been shown to be potent inducers of Tregs previously[7,8], and these experiments illustrate that DCs tolerized via PEG-IL10 hydrogels are just as effective at inducing Tregs. Despite immunosuppression of CD8+ T cells *in vitro*, it is unclear whether they become benign or retain their cytotoxic profile *in vivo*, and further studies are needed. Additionally, decreased CD86 expression in endogenous DCs in the hydrogel and CNS signifies that immunomodulation is not limited to T cells, supporting the indirect mechanism of tolerance.

However, antigen matters not only to viability and cell survival but to DC-T cell interactions and the downstream signaling that results in Treg induction and increased expression of PD-1. CFSE fluorescence, PD-1 expression, and Treg frequency remained largely unchanged across all groups when antigen was omitted from co-cultures. The antigen-dependence illustrated by these experiments also confirms that although the MHC-II expression of DC10s is lower than mDCs, it is still sufficient to present antigen to T cells. Since cell contact between APCs and T cells is necessary to condition antigen-specific cellular immunity, it is expected that these DCs induce tolerance through direct interactions with endogenous lymphocytes. This is supported by the lack of differences in T cell viability and phenotype in the absence of antigen. In co-cultures without OVA, it is likely that no response was observed due to only a small fraction of the T cell population being OVA-specific (without OVA-induced T cell expansion), lower T cell yields and poor activity (without OVA-induced signaling), inhibited conditioning by DCs (without OVA presentation), or a combination of these reasons. Thus, the dependence on antigen for immunomodulation in an antigen-specific autoimmune disease implies that delivered DCs

also act directly and that the downstream effects observed *in vivo* are likely a mix of direct and indirect mechanisms.

It should be noted that while both iDCs and DC10s effectively induce Tregs, iDCs have a less stable phenotype and are sensitive to inflammation, putting them at risk of losing their therapeutic capacity due to maturation. However, DC10s are phenotypically stable, resistant to moderate levels of inflammation, and contribute to other anti-inflammatory processes and tolerance mechanisms. In treating a patient with rampant inflammation, these properties of DC10s are necessary for effective treatment. It is possible that the digestion of hydrogels with collagenase diminishes the function of encapsulated DCs, but trends between biomaterial groups and their unencapsulated counterparts are very similar. The effect of collagenase treatment on DC function needs to be better understood.

Taken together, this data has changed our understanding of the immunomodulation taking place *in vivo*. Our revised mechanism proposes that hydrogel delivered DCs recruit endogenous APCs and T cells to the biomaterial niche. It is at this immunomodulatory node that DCs induce Tregs and suppress CD8+ T cells, either directly, or indirectly through endogenous APCs, in an antigen-specific manner. Afterward, tolerized endogenous lymphocytes migrate to the cervical LNs and CNS where autoreactive immunity is inhibited, ameliorating symptoms of paralysis. Further studies are needed to validate this mechanism and identify any potential benefit provided by IL-10 modulated hydrogels.

6.4.5 Supernatant Profiles from Co-Cultures with Tolerogenic DCs are Characteristic to Regulatory T Cells and T_H2 Cells

The supernatants of co-culture samples were multiplexed to characterize the secretory profiles splenocytes treated with various DCs to further evaluate the phenotype of the T cells present. The values of cytokines are represented as the fold change in concentration compared to splenocytes without DC-treatment to highlight any changes in cytokine secretions. T_H1 and T_H17 cells are regularly implicated in the pathophysiology of EAE mice[82,216] and MS patients[57], whereas Tregs[15,180] and T_H2 cells[217,218] have widely been shown to play a role in immune tolerance and the resolution of autoimmune symptoms. Thus, these studies aimed to further identify the T cell subtype induced by treatment with various DCs.

DCs receiving various treatments resulted in a significant increase in supernatant IL-10 concentrations, most notably for iDC (1:1), DC10 (1:1), PEG-4MAL (1:1), and PEG-IL10 (1:1) groups. If DCs alone were responsible for the observed increase in IL-10 secretion, we would expect the levels of IL-10 to correlate with the concentration of DCs. While we cannot directly decouple the cell source of IL-10 in these studies, it is apparent that IL-10 levels in samples with a ratio of 1:1 are markedly higher than samples with 1:10 and 1:50 ratios (which are very similar). This data suggests that CD25+FoxP3+ Tregs contribute to the increased levels of IL-10 in these supernatants, which further supports the induction of Tregs discussed previously. Regardless of whether increased IL-10 levels are primarily due to DCs or Tregs, these results further implicate IL-10 as a mechanism of tolerance by this DC therapy.

As expected, TNF-α/IFN-γ-treated DCs (1:1) induced IFN-γ secretion amongst T cells in co-cultures, which is a hallmark of T_H1 cells. No other DCs were capable of conditioning T cells towards T_H1 cells based on the secretion of IFN-γ in these co-cultures. Similarly, the concentrations of IL-17 in co-culture supernatants remained largely unchanged across all of the tested treatment groups.

High ratios of DC treatment (1:1) induced significantly higher levels of IL-5 secretion across all treatments, with the exception of PEG-4MAL-treated DCs. Each of these treatments resulted in similar concentrations of IL-5, between 5-10 times higher than IL-5 produced by splenocytes alone. This data suggests that these DCs may have an inherent capacity to induce T_H2 cells, regardless of treatment. Further investigation is needed to determine whether these T cells are, in fact, T_H2 cells (based on the expression of GATA-binding protein 3, GATA3) and if these cells play a role in the amelioration of symptoms in EAE mice after treatment with DCs. The presence of these cells in co-cultures may explain the increased levels of IL-10 in VD3 (1:1) and LPS (1:1) groups, as T_H2 cells also secrete IL-10.

The chemokines CCL2, CCL3, CCL4, CCL5, and CXCL1 are predominantly secreted by DCs[219] and, thus, the fold change in chemokine expression is notably high (100-300x) when compared to the splenocyte-only control group. Interestingly, CCL2 and CCL5 were the chemokines with the largest increase in supernatants from iDC and DC10 groups, whereas CCL3 and CCL5 exhibited the biggest increase in PEG-4MAL samples. These effects appeared to compound for PEG-IL10 supernatants, where all chemokines were significantly increased, and CCL5 was increased higher than every other group. CXCL1, which has been shown to inhibit oligodendrocyte migration[220] and correlate to

decreased symptom severity in EAE[221], was also significantly increased in PEG-IL10 co-cultures. The chemokines addressed in this study attract monocytes (CCL2, CCL3, CCL4), macrophages (CCL3, CCL4), DCs (CCL2), T cells (CCL2, CCL4, CCL5), neutrophils (CCL3, CXCL1) and other leukocytes, most commonly in response to inflammation or tissue repair[219]. The high level of chemokines expressed by these DCs supports the phenomenon of endogenous cell infiltration demonstrated in Figure 6.4. In total, these results suggest that immunomodulation occurs within the DC-laden hydrogel after chemokine-mediated recruitment of endogenous immune cells *in vivo*.

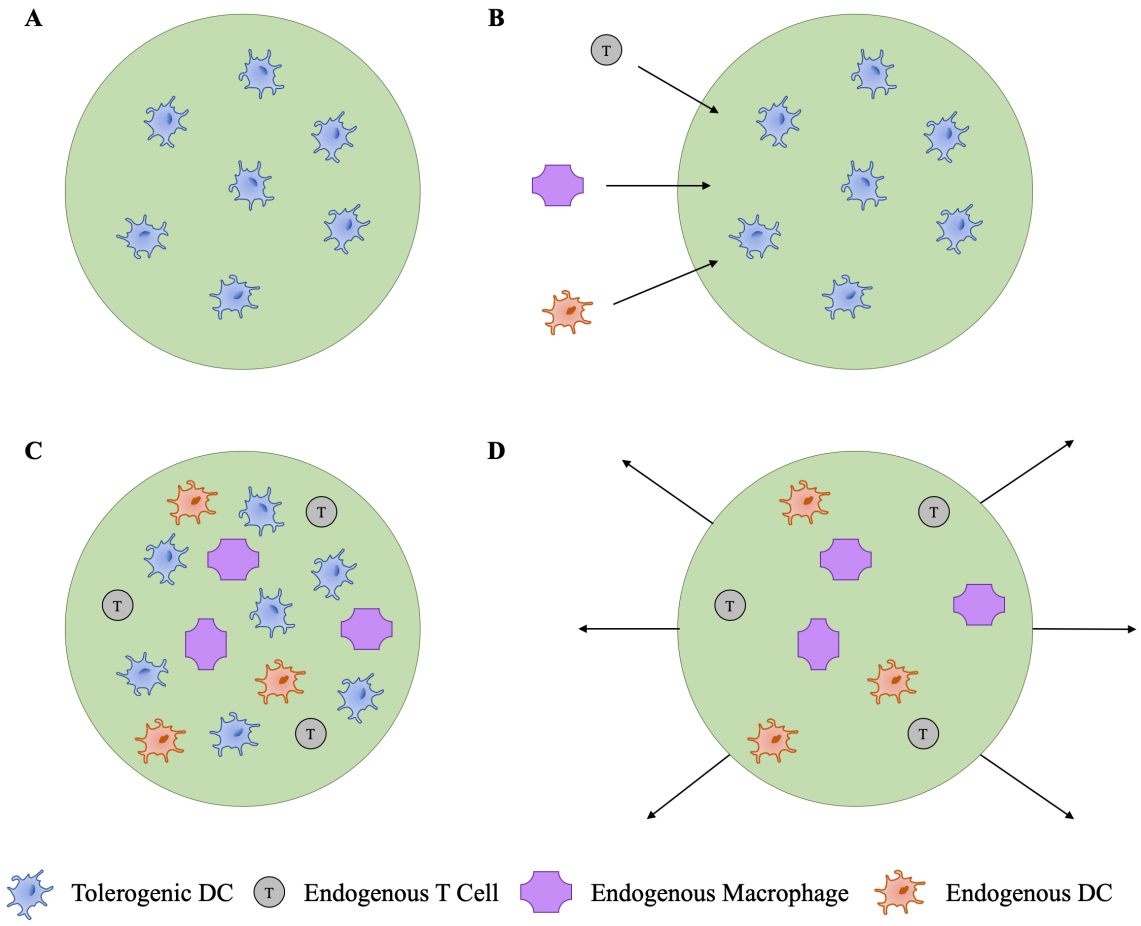

Figure 6.9. Schematic representing the proposed mechanism of amelioration in vivo after injection of PEG-IL10 hydrogels carrying DCs. a) DC-laden hydrogels are injected into mice and synthesize *in vivo*. b) DCs recruit endogenous lymphocytes to the immunosuppressive biomaterial niche. c) Endogenous lymphocytes infiltrate the hydrogel and are tolerized by MOG-specific DC10s, biomaterial-released IL-10, and protection from inflammation. d) Tolerized endogenous cells migrate out of the biomaterial and carry out downstream processes, eventually reaching the CNS.

CHAPTER 7. CONCLUSIONS AND FUTURE DIRECTIONS

7.1 Conclusions

DCs are potent mediators of immunity and have shown effectiveness as a cell therapy, but significant limitations limit their robustness. The research study described herein elucidates the governing factors in the development of a tolerogenic biomaterial delivery system for DC therapies in the treatment of pathologies with over-activated immune systems. This work has shown the parameters most relevant to the support of DCs in a tolerogenic context by characterizing the relationship between three-dimensional biomaterial properties and the viability and maturation of DCs. Based on these findings, PEG-4MAL hydrogels were tuned specifically to promote DC effectiveness in treating mice with EAE, an animal model of MS. PEG-4MAL hydrogels were further functionalized with tolerogenic cytokine IL-10, which was shown to prolong the benefits of encapsulation, protect DCs from inflammation, and exhibit controlled release of IL-10 through multiple mechanisms. Experiments herein demonstrated that PEG-4MAL hydrogel-delivered DC10s significantly ameliorated symptoms of EAE at peak disease compared to DCs delivered subcutaneously. Through a series of *in vivo* and *in vitro* experiments, Treg induction and PD-1 mediated immunosuppression was identified as the primary responses to treatment with hydrogel-delivered DCs. These studies validated significant infiltration of endogenous lymphocytes into our immunosuppressive biomaterial niche and verified that downstream effects are realized in the CNS, the anatomically relevant site of disease.

In Chapter 4, PEG-4MAL hydrogel stiffness, mesh size, degradability, and adhesive properties were modulated through manipulation of polymer density, macromer size, crosslinker type, and adhesive peptides, respectively. Hydrogel stiffness was shown to significantly impact the viability and morphology of encapsulated DCs, and scaffolds with a storage modulus of ~200 Pa were found to best support DCs. Parameters such as macromer size, crosslinker type, and adhesive peptide concentration did not significantly alter the viability or phenotype of DCs at the broad range of values tested. This flexibility enabled a selection of parameters (Table 4.2) specifically tuned for an autoimmunity proof-of-concept application and provided the opportunity for PEG-4MAL hydrogels to be manipulated for other non-adjuvanting applications. This set of studies provides a framework for the development of PEG-4MAL based delivery systems for any DC therapy where activation is detrimental to the treatment, such as transplantation, autoimmune disease, and chronic inflammatory diseases.

In Chapter 5, optimized PEG-4MAL hydrogels were further functionalized with the tolerogenic cytokine IL-10, which induces tolerance in DCs, T cells, and other lymphocytes. Three-dimensional analysis of murine IL-10 crystal structures indicated only minor overlap between residues involved in ligation of IL-10R and lysine residues, the target for thiolation. IL-10 thiolation resulted in ~13 thiolated lysine residues, which enabled subsequent binding of IL-10 to PEG-4MAL through covalent bonds. Bioactivity experiments demonstrated that PEG-IL10 retained its bioactivity, with EC_{50} values almost identical to that of native IL-10. PEG-IL10 hydrogels exhibited a 3-fold mechanism of IL-10 treatment through (1) an initial burst release of unreacted IL-10, (2) controlled release of PEG-IL10 as the hydrogel degrades, and (3) direct presentation of polymer-bound IL-

10 to encapsulated DCs. These hydrogels protected DCs from severe inflammation in the media due to both hydrogel encapsulation and treatment with IL-10. These combined effects were shown to extend the duration of DC support to at least 48 hours.

Lastly, Chapter 6 focused on applying the developed treatment *in vivo* using a murine model of MS. Mice receiving DC10s exhibited a delayed onset of symptoms regardless of the delivery method. However, mice treated with hydrogel-encapsulated DC10s had significantly lower clinical scores compared to subcutaneously-delivered DC groups at the peak of disease. Significant differences were identified in the number of MOG-specific CD11b+ cells in the CNS. The maturation marker CD86 was significantly lower in CD11c+ DCs in both the hydrogel environment and the CNS. A set of *in vitro* and *in vivo* experiments illustrated marked infiltration of lymphocytes into the hydrogel environment indicated that the site of immunomodulation is likely within the immunosuppressive biomaterial niche. Autologous co-culture experiments established a promising mechanism of tolerance by which hydrogel-delivered DC10s ameliorate symptoms of autoimmunity. iDCs, DC10s, and DCs from PEG-4MAL or PEG-IL10 hydrogels stimulated proliferation of CD4+ T cells and induced CD25+FoxP3+ T regulatory cells. CD8+ T cell proliferation outpaced that of CD4+ T cells, but both groups presented higher PD-1 expression, signifying immunosuppression. Co-culture studies also identified the presence of antigen as a necessary component, as the reported effects were not observed in the absence of antigen.

Taken together, these experiments elucidate the DC-biomaterial interactions relevant to the development of a non-activated biomaterial, the regulatory benefits of

functionalizing PEG-4MAL with IL-10, and the improved efficacy of DC therapies in treated symptoms of EAE with accompanying mechanistic insights.

7.2 Significance of Findings

The work described here has contributed the scientific research community by elucidating the effects of biophysical and biochemical properties of biomaterials on DCs, developing a biomaterial delivery system capable of directly inducing tolerance, demonstrating the bioactivity of PEG-IL10, providing a proof-of-concept example of biomaterials improving the efficacy of DC therapies, and identifying a biomaterial framework for establishing and immunosuppressive niche or other delivery applications. The potential for DC-based cell therapies to treat autoimmune disease is substantial and limited only by inadequacies in cell delivery and functional support post-injection. Tolerogenic DCs have limited migratory capabilities and have been shown to disperse after injection into mice[104,105]. Additionally, rampant inflammation in subjects with over-activated immune systems can render DCs useless by activating DCs. Much effort has been dedicated to studying materials that act as adjuvants to DCs (including past work from this lab), but little has been done to further develop biomaterial delivery systems for DCs functioning in the opposite context, immunosuppression. Biomaterial epitopes that mimic PAMPs and DAMPs have long been the focus of immune cell-biomaterial interactions. However, the research covered in this thesis has characterized the relationship between biophysical and biochemical properties, both microscopic and macroscopic, and DC viability and phenotype. Additionally, materials that have no effect on immune cells have been discovered and were previously considered “bioinert,” but the research herein

transforms a polymer-based biomaterial into a material that is capable of directly inducing tolerance while also achieving targeted cell delivery.

The bioactivity experiments described here also concretely validate the bioactivity of PEG-4MAL-bound IL-10. Studies in Chapter 5 and Chapter 6 proved that encapsulation in biomaterial not only maintains an immature DC phenotype but tolerizes DCs to an extent similar to IL-10 treatment. Studies in EAE mice added to the evidence that biomaterial delivery systems can improve the downstream effects of cell therapies through targeted delivery and post-delivery functional support. Moreover, these studies showed that improvements in treatment efficacy are also achievable in a tolerogenic application. This hydrogel-delivered DC therapy represents a promising strategy for the treatment of autoimmune disease. The versatility in PEG-4MAL hydrogel design illustrated here enables biomaterial design for a breadth of tolerogenic applications and points to the possibility of using this platform as an immunosuppressive niche for applications outside of autoimmune disease. These findings collectively broaden the range of possibilities for DC therapies and will hopefully push clinical translation of DC therapies forward.

7.3 Future Directions

The results of this thesis verify that biomaterial delivery systems tailored to a particular type of cell therapy can improve their efficacy and clinical outcomes in mice. This work provides a foundation for understanding the cellular and molecular basis of tolerance induction by hydrogel-delivered DC10s, but there are many promising next steps to this project. A more thorough set of immunoprofiling experiments is needed to further clarify the mechanism of regulating immunity that occurs in EAE mice. With more detailed insights, iteration of PEG-4MAL hydrogel design to fit the needs of the system is expected

to provide an added benefit to treatment efficacy. PEG-IL10 hydrogel development was still in progress when logistical constraints prevented access to the EAE animal model, so a critical next step is to test the efficacy of PEG-IL10-delivered DC10s both prophylactically (as in Chapter 6) and therapeutically. Literature support and observational evidence of tissue remodeling and vascularization of hydrogel constructs post-injection suggest that this system can be utilized as a tertiary lymphoid organoid (TLO) therapeutically. Lastly, reproducing the phenomena characterized herein using human PBMC-derived DCs from healthy patients and MS patients will be necessary to explore the translatability of this strategy to the clinic.

Murine BMDCs cultured with similar differentiation protocols are used widely across academic labs. However, BMDCs from different labs are reported to have varying phenotypes and functional identities, and BMDCs do not generally conform to any of the well-characterized DC subtypes identified *in vivo*[178,179]. Unfortunately, this characterization work is outside the scope of this lab, but a better understanding of DCs development, behavior, plasticity, migration, antigen processing, secretory profile, and genetic profile would greatly help DCs users engineer their systems to develop better treatment regimens.

7.3.1 Immunoprofiling EAE Mice Receiving Treatment with PEG-4MAL Delivered DC10s

The experiments discussed in Chapter 6 provide some evidence surrounding the mechanism of tolerance *in vivo*, but there are still unresolved questions about the exact nature of immune regulation. Congenic studies showed that almost all delivered DCs had disappeared from the hydrogel environment by 4 days post-injection, but it is still unknown

whether this is due to migration of DCs or cell death. To address this, future studies could employ Green Fluorescent Protein (GFP) DCs and *in vivo* imaging systems (IVIS) to track the movement of fluorescence. Increasing fluorescence in tissues of immunological or pathological interest, such as the spleen, LNs, and CNS would indicate migration of delivered DCs. In contrast, a random distribution or dissipation of fluorescence would indicate DC death.

Another important aspect of this therapeutic mechanism is which endogenous cellular compartment is the primary driver of downstream effects initiated by the delivered DCs. The immunoprofiling study covered in Chapter 6 shows a reduction in maturation markers amongst endogenous CD11b+ and CD11c+ cells, and studies described here and elsewhere[212,213] have shown that these DCs are capable of inducing T regulatory cells and inhibiting CD8+ T cells. Future experiments could use flow cytometry to better characterize the cellular composition of lymphocytes in the hydrogel environment and CNS. To identify the driving mechanism of tolerance induction, the number and functional capacity of various T cell subtypes across various immune and neurological tissues (LNs, spleen, CNS) should be identified by flow cytometry and analysis of secreted cytokines.Tissue samples from treated mice can be counted and phenotyped by using counting beads and intracellular antibodies for T-bet (T_H1 cells), ROR-γt (T_H17 cells), and FoxP3 (Treg cells). T cell activity should be measured by correlating cell number to the amount of IFN-γ and TNF-α (T_H1 cells), IL-17 (T_H17 cells), and IL-10 and TGF-β (Treg cells) in tissue lysates. Any observed changes in T cell number or activity should be validated with co-culture experiments *in vitro*, along with the identification of tolerance-inducing molecules known to be expressed by DCs (IDO, PD-L1, IL-10).

Immunohistochemical and histological sections from the CNS could be stained with hematoxylin and eosin (H&E) or for CD3+ (T cells), CD19+ (B cells), CD11c+ (DCs) to identify any changes in the cellular composition near the site of injury. Separate CNS tissue slices could also be stained with Luxol fast blue (LFB), which stains myelin, to illustrate differences in the demyelination of neural tissues in EAE mice. Multiplexing relevant cytokines (such as those tested in Chapter 4) from CNS lysates may provide additional evidence of the state of immunity within the CNS for treated and untreated EAE mice.

Lastly, two additional controls should be included in full-scale EAE follow up experiments: (1) hydrogel-delivered DCs pulsed with OVA antigen instead of MOG to test antigen specificity and (2) DCs injected intravenously as an additional control of a well-characterized delivery method. The studies in this section may elucidate the primary cell type driving amelioration, the path and process of migration for DCs and endogenous cells, the extent of co-localization of DCs and downstream effectors to lesions in the CNS, and the role of antigen-specificity in this treatment. Once a more complete understanding of the mechanism of amelioration is reached, PEG-4MAL hydrogel delivery systems could be iterated to further improve DC efficacy.

7.3.2 Iteration of PEG-IL10 Biomaterial Design and its Efficacy as a Therapeutic Treatment

A greater understanding of how the employed DC therapy works on a cellular level could identify potential adjustments to the PEG-4MAL hydrogel design that would further contribute to the robustness of delivered DCs against EAE. Insights into drivers of endogenous cell recruitment and effector cell migration to the CNS can be leveraged to

iterate PEG-IL10 hydrogel design to conform to the identified *in vivo* mechanisms of tolerance.

Due to constraints in access to the EAE model, hydrogels assessed *in vivo* for this project were not functionalized with IL-10. While hydrogel encapsulation was shown to provide some protection against inflammation, an important next step is to determine the added benefit of IL-10 to this system. Experiments in Chapter 5 illustrated that IL-10 functionalization grants improved protection against inflammation and more durable support to DCs than PEG-4MAL hydrogels. Between this and the ability of IL-10 to tolerize nearby endogenous cells as they begin to infiltrate hydrogels, functionalized PEG-IL10 hydrogels are expected to synergize with encapsulated DC10s and improve therapeutic outcomes.

Lastly, the capacity for this hydrogel-delivered DC therapy to be effective therapeutically is of great interest to the medical community. The immune system is highly dynamic and T cells[222], DCs[223], and innate immune cells[224] have all been shown to be plastic, suggesting that even after disease onset, the proper cell therapy delivered to the right location should be capable of reversing immune-related pathologies. Depending on the duration of tolerogenic DC persistence *in vivo*, as shown by mechanistic studies in the previous section, administrating multiple doses of PEG-IL10-delivered DCs should be considered. Future work should include hydrogel-delivered DC treatment at a therapeutic time point in the previously discussed EAE experiments.

7.3.3 Therapeutic Generation of Artificial Lymph Nodes

Interestingly, while explanting hydrogels from EAE during the congenic studies in Chapter 6, a noticeable difference in hydrogel size and presence was recognized

macroscopically. When explanting blank hydrogels, the biomaterial constructs were difficult to locate due to their small size, and at later time points (Day 7-10), one or both of the hydrogels were unable to be recovered. PEG-4MAL hydrogel-delivered DC10s appeared to be integrated, vascularized, and retained their original volume after 10 days post-injection. While purely observational, this data suggests that the presence of DC10s in the hydrogels is correlated with remodeling and vascularization processes *in vivo*. As illustrated by subsequent functional studies, the hydrogel environment acts as an immunosuppressive biomaterial niche or node where endogenous cells are modulated by DCs. This remodeled, vascularized, node-like structure may potentially resemble a TLO or ectopic lymph node-like tissue growth.

Upon investigation of the literature, several of the conditions characteristic in LN development during embryogenesis[225] are recapitulated in the system developed herein. Beyond RGD-assisted infiltration, vascularization, and rapid degradation to facilitate ECM remodeling, several other factors align with physiological LN development. Ectopic TLO formation has been shown to occur at the onset of various autoimmune diseases[226,227] and is initiated by lymphotoxins and CXCL13[228], which are likely a result of the heightened inflammation that occurs in autoimmune disease[59]. In fact, antibodies against various lymphotoxins have been produced to treat autoimmunity through inhibition of inflammation and exacerbating TLOs[216]. Data from Chapter 6 highlights T cell infiltration into PEG-4MAL hydrogels *in vivo*, and lymphotoxin-α (LTα) has been shown to be predominantly expressed by T_H1 and T_H17 cells in mice with autoimmune disease[216]. After initiation, TLO development is primarily driven by interactions between a subset of DCs and fibroblastic reticular cells (FRCs)[229], and DCs are already present within our

biomaterial construct. A recent study also delivered hydrogels encapsulating lymphotoxins and chemokines to recruit DCs, T cells, and B cells to the hydrogel, promoting the formation of TLOs with well-defined architecture that were capable of mounting adaptive immunes responses[230]. The overall goal of driving TLO formation within a hydrogel seeded with tolerogenic DCs is to create a LN-like center of immunomodulation that drives tolerance rather than exacerbates inflammation. In this case, PEG-4MAL hydrogels may produce better outcomes than PEG-IL10 hydrogels, as IL-10 may counteract the inflammation-based tissue growth.

Future studies should inject hydrogel-delivered DCs into EAE mice and, following an incubation period, explant and section hydrogel constructs for immunohistochemical staining to examine the organization of CD3 (T cells), CD19 (B cells), CD11c (DCs), GP38 (FRCs), and MECA-79 (high endothelial venules, HEVs) to be compared to LN architecture. The presence of organized MECA-79+ HEVs would signify the existence of LN-relevant cardiac structures and validate the vascularization observed macroscopically. To determine if the remodeled hydrogel structures are lymphatically connected, future experiments should employ tail vein injections of Indian Ink. This easily recognizable dye that is known to drain through lymphatic vessels and stain lymphatically connected LNs[231]. If this research identifies LN-like architecture, vascularization, or lymphatic connectivity, a partial re-design of the hydrogel-delivered DC system to promote therapeutic artificial LN (aLN) development has the potential to be highly impactful. Therapeutic aLNs could provide a permanent node of immunomodulation that results in the persistent and durable treatment of autoimmunity, although genetic kill switches or other methods of control might need to be included for safety purposes.

7.3.4 Therapy Effectiveness on Human MS-Patient PBMCs in vitro

Towards the ultimate goal of curing autoimmune disease in human patients, a series of *in vitro* experiments validating the murine results discussed here would be a significant step toward pushing DC therapies to clinical trials. After establishing treatment protocols and control phenotypes, the DC-biomaterial interactions characterized in Chapter 4 should be confirmed with human PBMC-derived DCs. Most importantly, the necessity for antigen and the mechanism of tolerance induction by DC10s should be determined in an experiment similar to the co-culture in Chapter 6.

This future work should first be established using PBMCs from healthy patients, but the next step would be to reproduce the experiments described in this section using PBMCs from age-matched and sex-matched MS patients. Due to stark differences in inflammation between healthy patients and MS patients, the ability of inherently-activated PBMCs from MS patients' blood to reach a functional and tolerogenic DC phenotype would need to be validated. A final investigation into the efficacy and tolerance mechanism of hydrogel-delivered DC10s derived from human PBMCs on humanized mice with EAE would result in the most clinically-relevant support for DC therapies as promising, translatable options for healthcare in the near future.

APPENDIX A.

A.1 Supplemental to Chapter 4

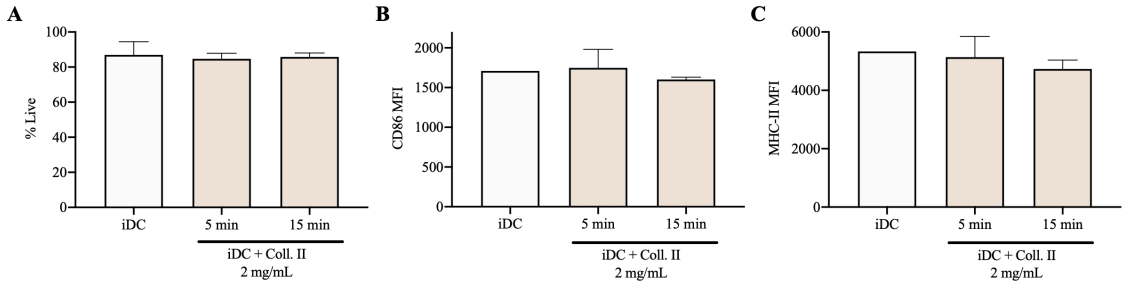

Figure A. 1. Cell surface expression of DCs after collagenase II treatment at various concentrations for various durations. a) Propidium iodide negative cells, b) CD86 expression, and c) MHC-II expression analyzed by flow cytometry.

Day 6 iDCs were treated with collagenase II (2 mg/mL) for 5 or 15 minutes. Cells in collagenase solution were added to media with 25% FBS to cease collagenase II activity and subsequently reconstituted in complete media. Phenotypes of treated DCs were compared to untreated iDCs based on CD86 and MHC-II expression analyzed by flow cytometry. Collagenase II treatment did not significantly affect the viability or phenotype of iDCs (Figure A.1).

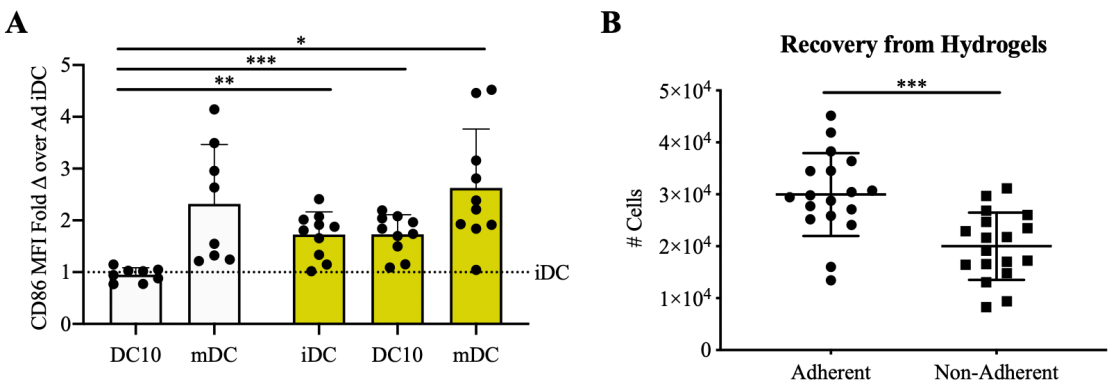

Figure A. 2. Comparison of adherent and non-adherent fractions of DCs. a) CD86 expression of adherent and non-adherent DCs after various treatments. b) Recovery of cells from hydrogels after collagenase II digestion. ***p<0.001, **p<0.01, and *p<0.05 via one-way ANOVA with Welch's correction and Dunnett's comparison test for a). ***p<0.001 via parametric unpaired t-test for b).

iDCs, DC10s, and mDCs across various experiments were produced using adherent and non-adherent cell fractions from DC cultures, separated on Day 6 of differentiation. The expression of CD11c was not significantly different between adherent and non-adherent DCs, but CD86 expression was significantly increased in all non-adherent controls compared to adherent DC10s (Figure A.2). Adherent cells were recovered from PEG-4MAL hydrogels in significantly higher numbers than non-adherent, suggesting that adherent DCs may be more stable and better suited for encapsulation (Figure A.2). Adherent DCs likely fare better within hydrogels due to enhanced binding to RGD, which can promote maintenance and survival signaling in some cell types[128,158]. Lower expression of co-stimulatory molecules is desired for immunosuppressive applications, implicating adherent DCs as the fraction of interest for DC10-based tolerogenic studies.

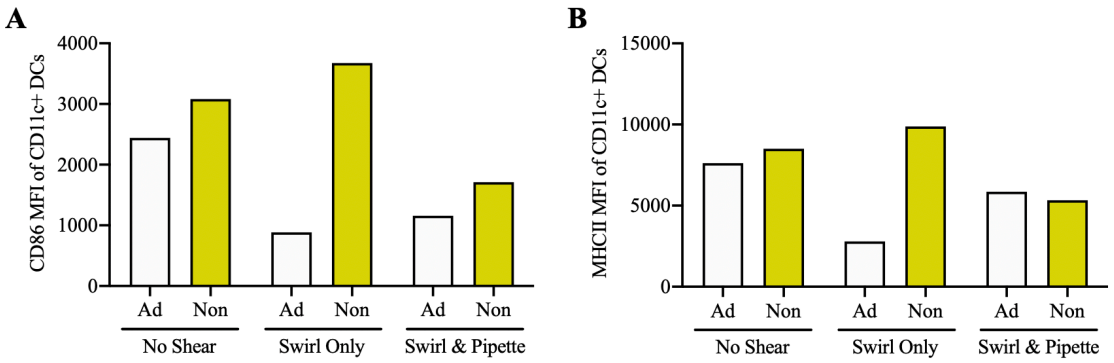

Figure A. 3. Comparison of Day 6 iDCs collected from plates with different techniques. Phenotypic differences in a) CD86 expression and b) MHC-II expression analyzed by flow cytometry.

Variations in CD86 expression amongst immature DC controls in early cultures prompted the investigation into the method of DC collection. Based on the differential CD86 expression between adherent and non-adherent DC fractions, it was hypothesized that incomplete collection of non-adherent cells could increase the mean fluorescence intensity (MFI) of CD86 by "contaminating" the adherent fraction. When collecting DCs without any prior perturbations, the CD86 and MHC-II expression of both fractions were nearly identical (Figure A.3). However, gently swirling media in the plates before collection led to a distinct separation between adherent and non-adherent fractions with no adverse effects (Figure A.3). Oppositely, if gentle swirling and pipetting of the plate surface were both employed, the expression of CD86 and MHC-II decreased in the non-adherent fraction, suggesting that some adherent cells had lifted from the plate (Figure A.3). This experiment validated the uncertainty in collection methods, and DC fractions were separated only by plate swirling for subsequent studies.

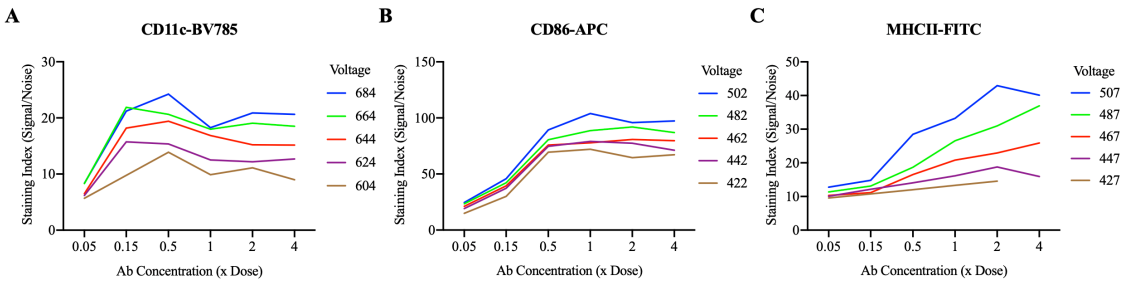

Figure A. 4. Titration of antibody concentrations and flow cytometer voltages to optimize staining index (signal to noise ratio). a) CD11c-BV785, b) CD86-APC, and c) MHCII-FITC for DC flow cytometry panel.

Towards the proper design of flow cytometry experiments, the staining index (SI) was determined for various concentrations of antibodies and cytometer voltages based on the manufacturer's recommended dosages and expected fluorophore brightness, respectively. iDCs were pooled and then stained with a single antibody at various concentrations, and fluorescence data was collected at different voltages (Figure A.4). The SI was calculated using the formula below:

$$SI = \frac{MFI_{Pos} - MFI_{Neg}}{2\sigma_{Neg}}$$

Where SI = staining index

MFI_{Pos} = MFI of positive population

MFI_{Neg} = MFI of negative population

And σ_{Neg} = standard deviation of negative population.

The combination of antibody concentration and voltage that produced the best SI for each antibody was selected for subsequent flow cytometry experiments.

For the T cell panel utilized in co-culture experiments in Chapter 6, antibody concentrations and voltages were adopted from a collaborator with an established panel.

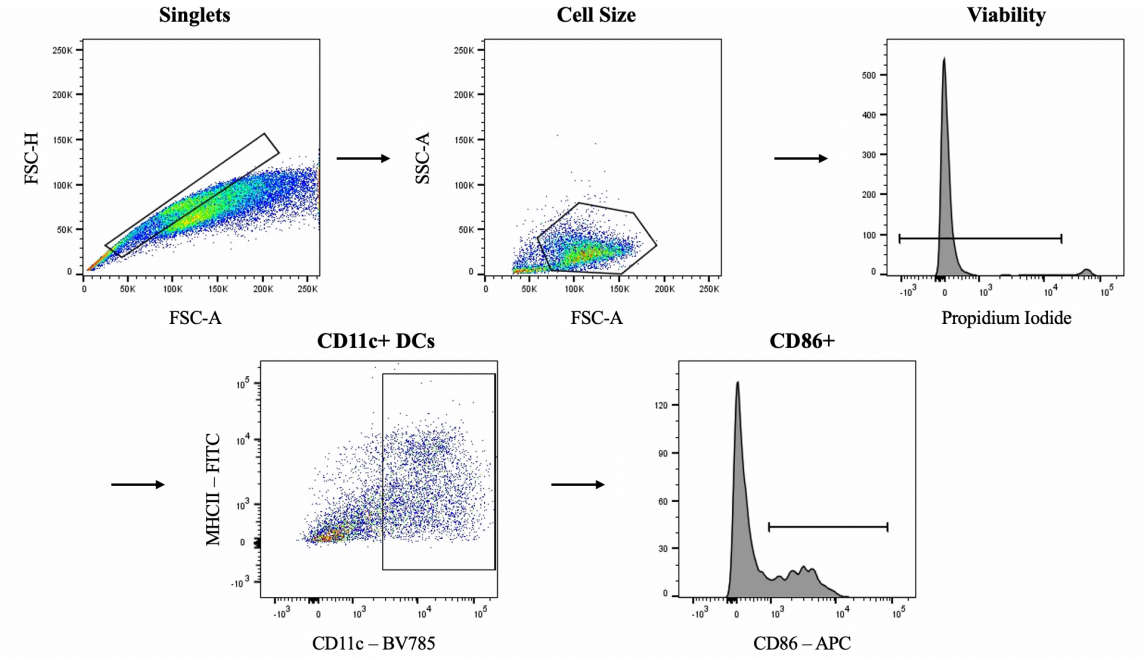

Figure A. 5. Series of gates used to identify relevant populations of dendritic cells.

Figure A.5 represents the gating strategy used for DCs analyzed by flow cytometry. Singlets were first identified to exclude cell clusters, followed by the selection of a cell population based on size (forward scatter, FSC) and granularity (side scatter, SSC) (Figure A.5). Cells positively stained by propidium iodide, signifying a compromised cellular membrane, were excluded as dead cells. Next, CD11c+ DCs were selected based on a gate set by fluorescence minus one (FMO) controls, which is considered to be the most stringent technique in determining positive cell populations. FMO controls were also used to identify positive populations of CD86+ DCs.

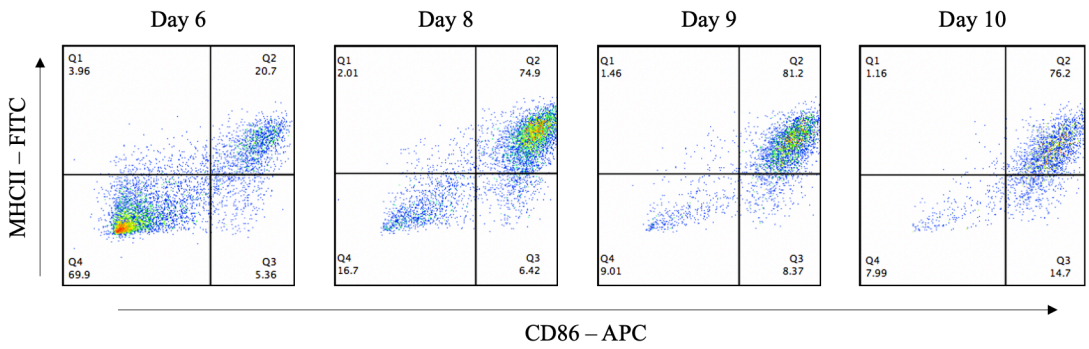

Figure A. 6. Phenotypic progression of iDCs based on the expression of CD86 and MHC-II from 6 to 10 days in cultures.

DCs were maintained in culture for up to 10 days, with replenishing of media occurring every 2 days after Day 6. Pseudocolor dot plots of CD86 and MHC-II expression in iDCs from Day 6 to Day 10 is shown in Figure A.6. A transition of immature DCs from primarily $CD86^{LO}MHC\text{-}II^{LO}$ cells (69.9%) at Day 6 to $CD86^{HI}MHC\text{-}II^{HI}$ cells (81.2%) at Day 9 illustrates the maturation that inherently occurs in extended cultures (Figure A.6). Additionally, a reduction in the number of viable cells is observed due to PI exclusion of dead cells leading to fewer dots plotted (Figure A.6). Previous studies have shown that prolonged culture of DCs can lead to maturation as DC clustering increases and DC-DC interactions induce activated signaling[232,233]. These results suggest that, unless treated with IL-10, only Day 6 DCs should be utilized for immunosuppressive applications where activated DCs would be detrimental.

A.2 Supplemental to Chapter 5

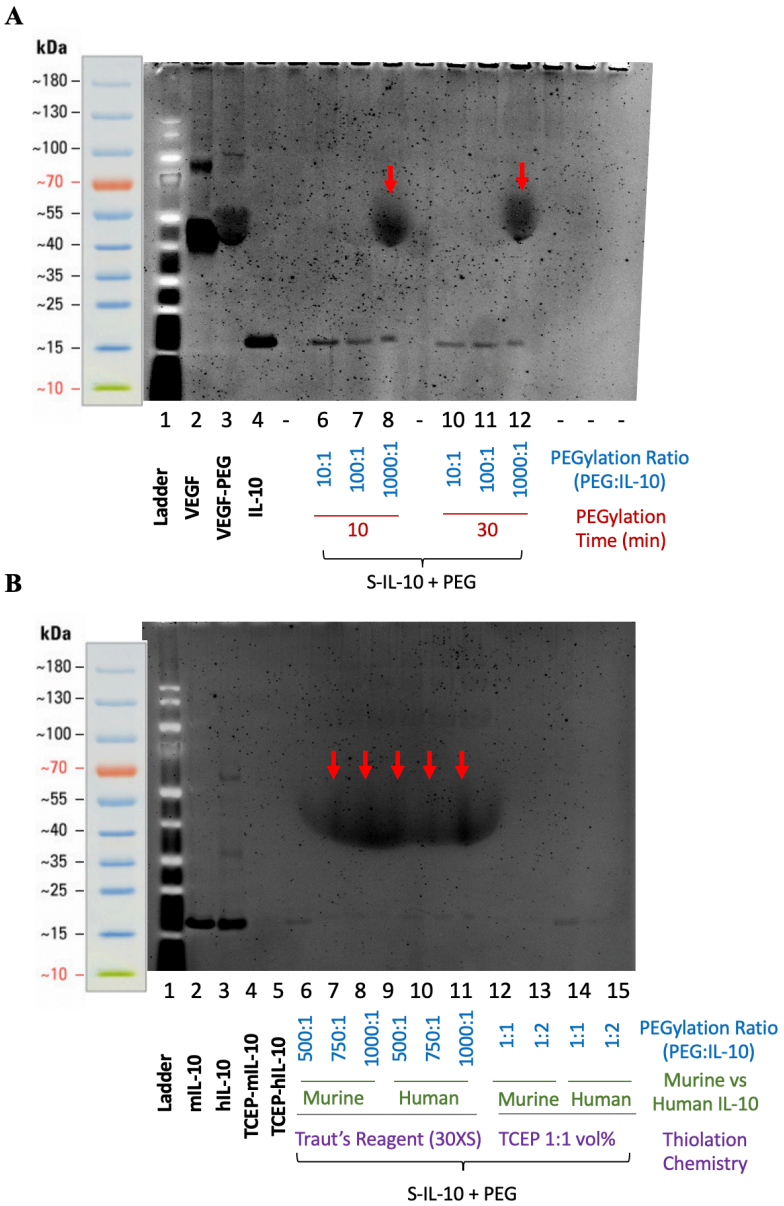

Figure A. 7. Optimization of parameters for PEGylating IL-10. a) SDS-PAGE gel showing the effect of PEGylation ratio and PEGylation time on thiolated IL-10. Red arrows point to PEGylated IL-10. b) SDS-PAGE gel showing the effect of PEGylation ratio, IL-10 species, and thiolation chemistry on thiolated IL-10. Red arrows point to PEGylated IL-10.

Many factors were tested in the PEGylation process of thiolated IL-10, including the ratio of PEG-4MAL to IL-10, the incubation time, thiolation reagents, and human versus murine IL-10. PEGylation at ratios of 10:1 (Lane 6, 10) and 100:1 (Lane 7, 11) resulted in no observable band at 40 kDa after both 10 and 30 minutes of incubation (Figure A.7A). However, a ratio of 1000:1 (Lane 8, 12) produced substantial mono-PEGylated IL-10 at both durations (Figure A.7A). In subsequent studies, ratios of 500:1 (Lane 6, 9) and 750:1 (Lane 7, 10) both resulted in observable bands at 40 kDa, but faint bands at 20 kDa were still present, suggesting less PEGylation of IL-10 compared to 1000:1 (Lane 8, 11) (Figure A.7B). No differences in PEGylation between murine and human IL-10 were observed, which was expected considering the homologs are 73% analogous[203]. Thiolation of IL-10 with tris(2-carboxyethyl)phosphine (TCEP) (Lanes 12-15) did not produce any bands at 40 kDa, although lower ratios were applied due to volume constraints (Figure A.7B). Based on these results, a PEGylation protocol of Traut's-based thiolation, a ratio of 1000:1 (PEG-4MAL:IL-10), and 15 minutes of incubation was selected for modification of murine IL-10. Based on the dosages of IL-10 being incorporated into PEG-4MAL hydrogels, the upper limit of PEGylation for IL-10 is ~44,000:1. An incubation time of 15 minutes was chosen to simplify the hydrogel synthesis process, as the incubation time for adhesive peptide RGD is also 15 minutes.

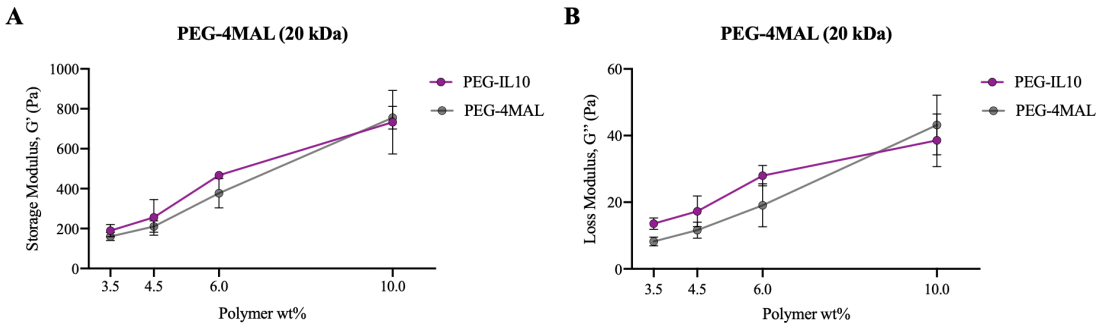

Figure A. 8. Comparison of rheological parameters for PEG-4MAL and PEG-IL10 hydrogels. a) Storage modulus and b) loss modulus of PEG-4MAL and PEG-IL10 hydrogels assessed on an Anton Paar rheometer.

The molar ratios of components in PEG-4MAL hydrogels are paramount to achieve complete and homogeneous crosslinking, which can affect the mechanical properties of hydrogels. For PEG-IL10 hydrogels, the molarity of VPM was reduced to account for the maleimide groups now occupied by IL-10. Investigation of changes to hydrogel mechanical properties due to IL-10 incorporation was necessary to determine if the polymer density of optimized hydrogels needed to be modified to conform to the ~200 Pa storage modulus previously defined as optimal. Storage modulus and loss modulus were not significantly affected by the incorporation of IL-10 at any of the tested polymer densities, likely due to the relatively small amount of IL-10 compared to maleimide groups in hydrogels (Figure A.8).

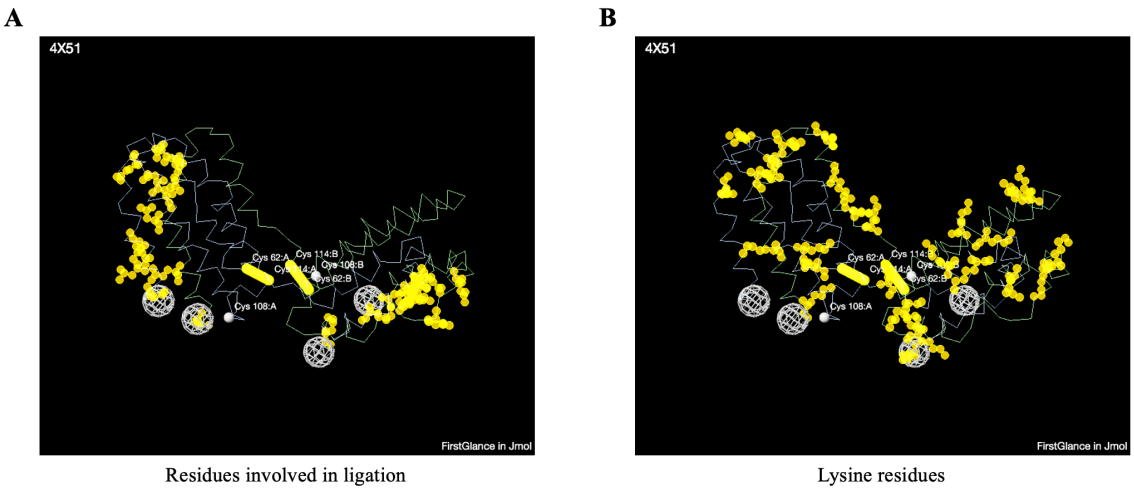

Figure A. 9. Crystal structure (4X51) of murine IL-10 dimers. a) residues involved in ligation of IL-10R and b) lysine residues. Each chain of highlighted circles represents one lysine residue, for a total of 13 (26 per dimer).

Murine IL-10 crystal structures[234] were modeled in FirstGlance (Jmol) to identify any potential overlap in lysine residues and residues involved in ligation of IL-10R[200-203] (Figure A.9). Each IL-10 contains 13 lysine residues (26 per dimer), most of which were shown to be thiolated using Traut's reagent (Figure 5.2). Lysines were determined to be a favorable target for thiolation due to the limited (~4) residues in proximity to IL-10R-binding residues. Experiments in Chapter 5 demonstrated no reduction in bioactivity upon PEGylation, indicating that the IL-10R-binding epitope was not changed in any impactful way due to the thiolation and PEGylation processes. It is expected that PEG-4MAL polymer chains primarily react with lysines near end chains and that other lysine residues are inaccessible as a result of steric hindrance.

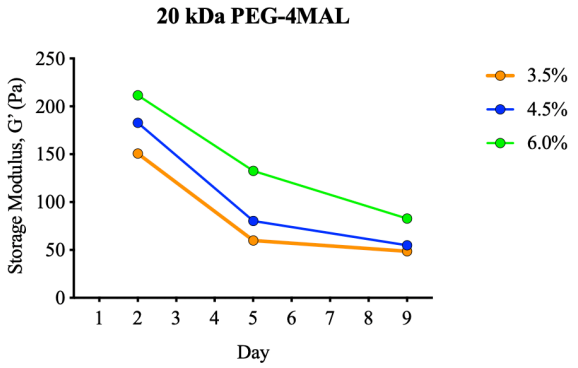

Figure A. 10. The degradation rate of PEG-4MAL hydrogels with various polymer densities over time based on hydrogel stiffness.

Previous experiments in this thesis show that PEG-4MAL hydrogels are sufficiently digested by collagenase II. However, the degradation of scaffolds due to hydrolysis is also relevant to processes occurring *in vivo*. PEG-4MAL hydrogels with various polymer densities were synthesized and incubated in PBS (pH 7.4) for 9 days with daily pH adjustments. The rate of degradation, expressed as decreases in hydrogel stiffness, is plotted in Figure A.10.

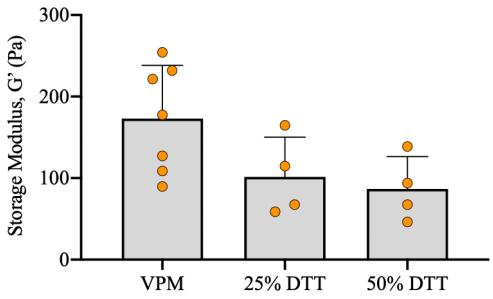

Figure A. 11. The storage modulus of hydrogels synthesized with various ratios of VPM and DTT crosslinkers.

PEG-4MAL hydrogels were synthesized with various ratios of crosslinkers and their stiffnesses were measured using rheological methods. Hydrogels with the same polymer density, but different amounts of DTT seemed to produce hydrogels with differing stiffnesses, although not significantly different (Figure A.11). Later troubleshooting revealed crosslinker stability during hydrogel preparation to be the reason for this artefact.

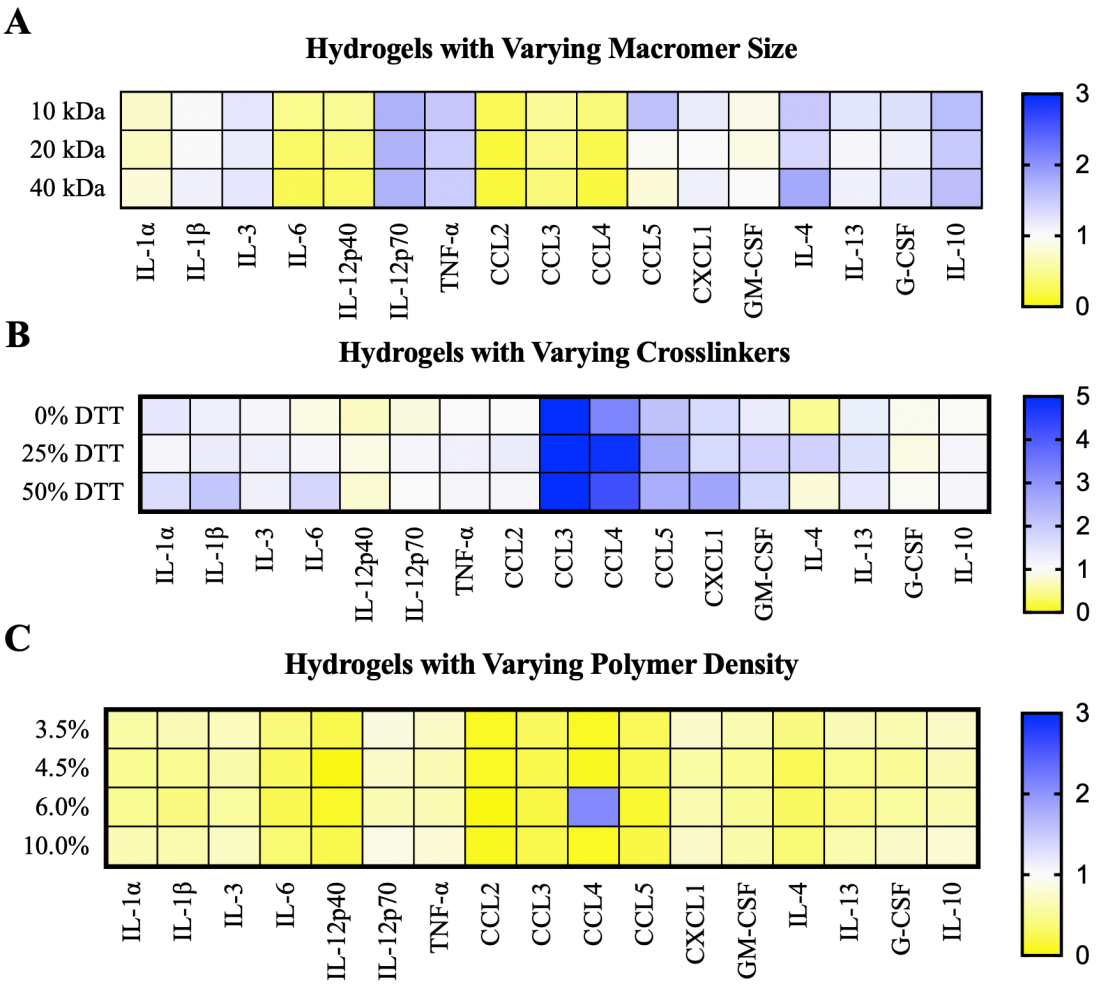

Figure A. 12. Heatmaps illustrating the concentrations of relevant cytokines in supernatants of various PEG-4MAL hydrogels. a) varying macromer size, b) varying crosslinkers, and c) varying polymer density.

Supernatants from PEG-4MAL hydrogels with various formulations were analyzed to quantify the concentration of relevant cytokines, similarly to control samples in Figure 4.4. Although significant differences could not be assessed due to low sample size (n=2), cytokine concentration values are shown here for reference (Figure A.12).

A.3 Supplemental to Chapter 6

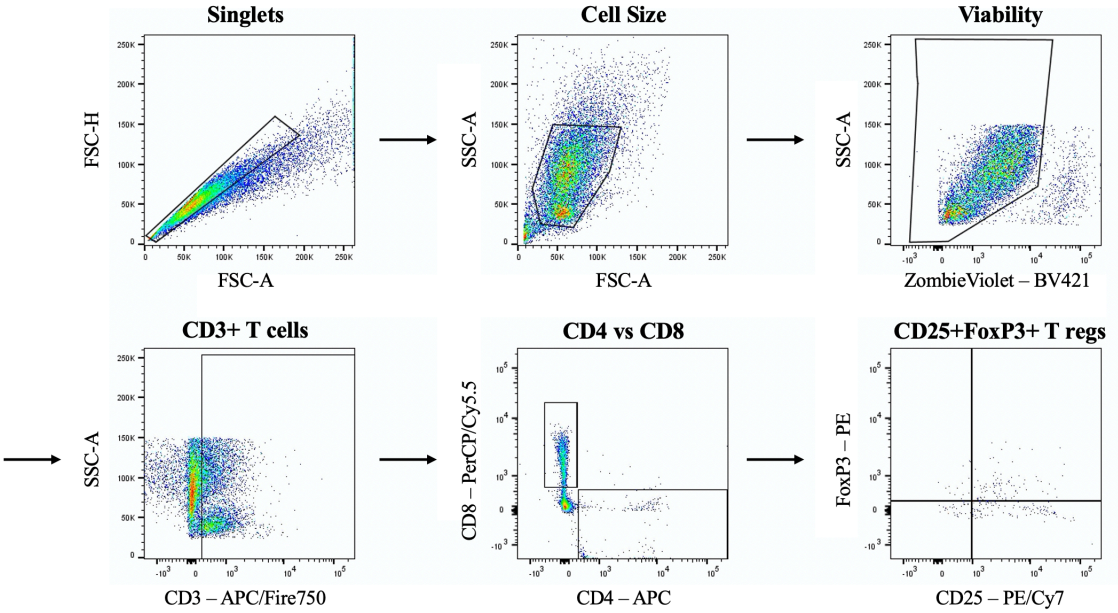

Figure A. 13. Series of gates used to identify relevant populations of T cells.

Figure A.13 represents the gating strategy used for splenocytes analyzed by flow cytometry. Similar to the gating strategy in Figure A.5, cell clusters were excluded, and the remaining cells were selected based on cell size and granularity for the population of interest. Zombie Violet, a fixable viability dye, was used to exclude dead cells based both on fluorescence and SSC.

A.4 Additional Studies

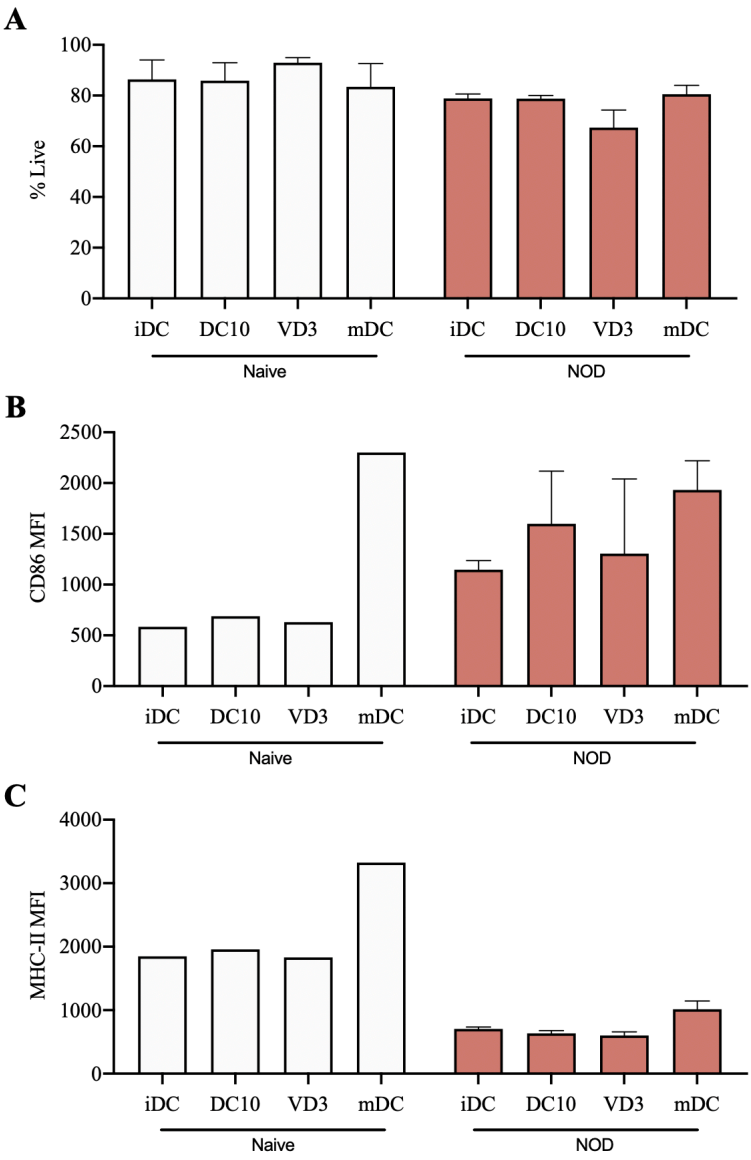

Figure A. 14. Viability and phenotypic data for DCs from naïve C57Bl/6J mice (white bars) and non-obese diabetic (NOD) mice (red bars). a) Propidium iodide negative cells, b) CD86 expression, and c) MHC-II expression analyzed by flow cytometry.

In support of translating our tolerogenic DC therapy to the clinic, it was essential to determine the ability of DCs from autoimmune subjects to become tolerized. BMDCs from naïve C57Bl/6J mice or non-obese diabetic (NOD) mice were differentiated into DCs and treated with IL-10, VD3, or LPS. Although significance cannot be evaluated due to

low sample size (n=2), CD86 expression in DCs from NOD mice is observably increased in immature controls compared to DCs from naïve mice (Figure A.14). Interestingly, MHC-II expression appeared to be lower in NOD-DCs across all treatment types (Figure A.14). Previous studies have illustrated that PBMCs from patients with SLE[20] and MS[21] can be effectively tolerized. We expect that a tolerogenic phenotype in NOD-DCs could be achieved with a higher dose of tolerogenic treatment.

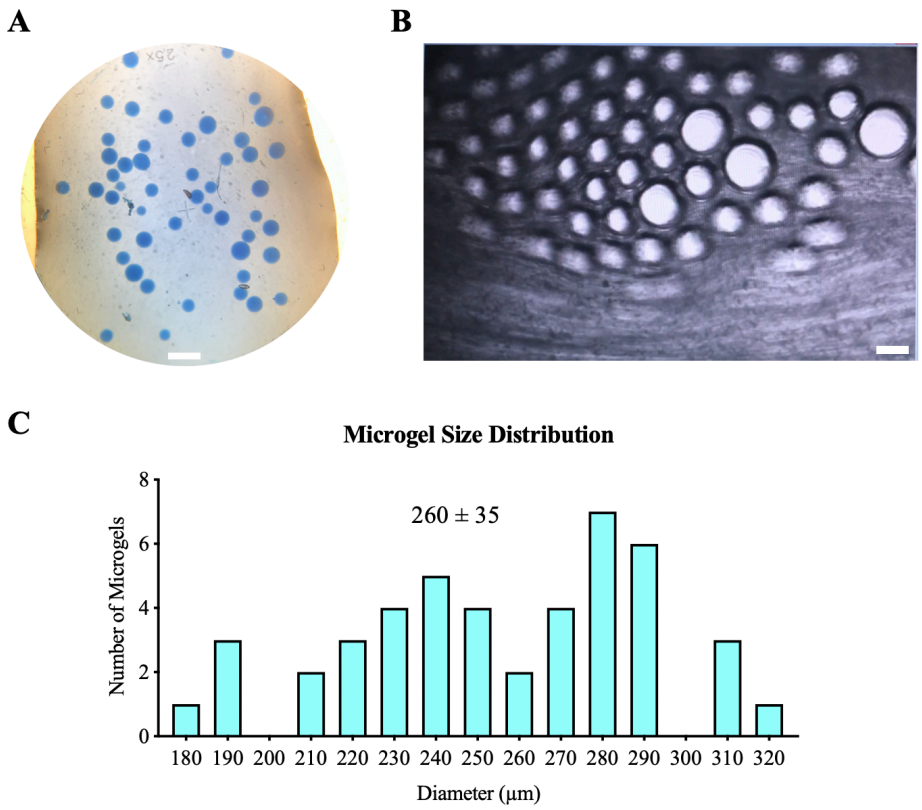

Figure A. 15. Characterization of 20 kDa PEG-4MAL microgels as an alternative controlled release strategy for IL-10. a) macroscopic image of PEG-4MAL microgels (scale bar = 500 µm). b) Image of PEG-4MAL microgels exiting PDMS microfluidic device (scale bar = 200 µm). c) Size distribution of microgels synthesized using PDMS device, analyzed by FIJI.

As an alternative method for the controlled release of IL-10, PEG-4MAL microgels were synthesized using a polydimethylsiloxane (PDMS) microfluidic chip. This strategy aimed to restrict diffusion of IL-10 by entrapping protein within microgels with relatively tight mesh sizes. Microgels were effectively synthesized with diameters of 260 ± 35 µm and were stable in solution for weeks (Figure A.15). Successful thiolation and PEGylation of IL-10, as illustrated in Chapter 5, was selected as the method of controlled release based on (1) the bioavailability of PEG-IL10 within hydrogel scaffolds, (2) better control over release characteristics, and (3) reagent constraints associated with microgel synthesis.

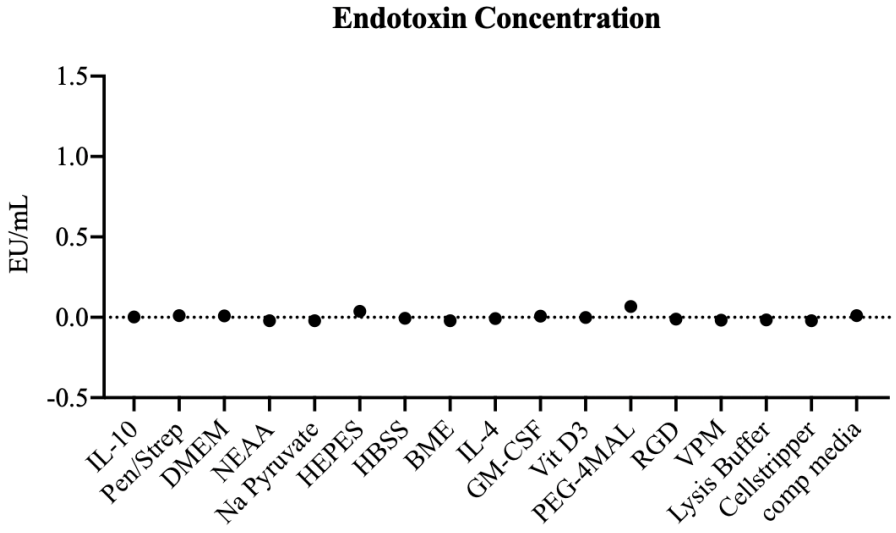

Figure A. 16. Presence of endotoxins in media components and other reagents as evaluated by Pierce Chromogenic Endotoxin Quant Kit.

Validating the absence of endotoxin in biological reagents is paramount, especially in experiments involving immune cell types, as endotoxin can be an immunological stimulus that confounds the results of an experiment[235]. Reagents used in every part of cell culture, treatment, and hydrogel synthesis were tested and endotoxin levels were found to be <0.1 EU/mL for all reagents (Figure A.16).

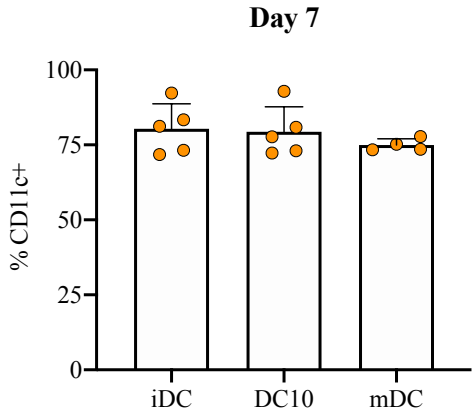

Figure A. 17. Purity of CD11c+ cells produced by Day 7 of bone marrow-derived DC differentiation.

Differentiation of murine BMDCs using the culture protocol provided by Pulendran et al. [177,178] results in cell populations that are ~80% CD11c+ DCs by Day 7. The purity of CD11c+ DCs is consistent across the treatments tested here. Thus, the cell populations utilized herein are primarily CD11c+ DCs.

REFERENCES

1. Compston, A. & Coles, A. Multiple sclerosis. *The Lancet* **372,** 1502–1517 (2008).
2. Dooley, M. A. & Hogan, S. L. Environmental epidemiology and risk factors for autoimmune disease. *Current Opinion in Rheumatology* **15,** 99–103 (2003).
3. Hauser, S. L. & Oksenberg, J. R. The neurobiology of multiple sclerosis: genes, inflammation, and neurodegeneration. *Neuron* **52,** 61–76 (2006).
4. Feinstein, A., Freeman, J., The Lancet Neurology, Lo, A. C.2015. Treatment of progressive multiple sclerosis: what works, what does not, and what is needed. *Elsevier*
5. Torkildsen, Ø., Myhr, K. M. & Bø, L. Disease-modifying treatments for multiple sclerosis - a review of approved medications. *Eur. J. Neurol.* **23 Suppl 1,** 18–27 (2016).
6. Comabella, M., Montalban, X., Münz, C. & Lünemann, J. D. Targeting dendritic cells to treat multiple sclerosis. *Nature Publishing Group* **6,** 499–507 (2010).
7. Boks, M. A. *et al.* IL-10-generated tolerogenic dendritic cells are optimal for functional regulatory T cell induction--a comparative study of human clinical-applicable DC. *Clin. Immunol.* **142,** 332–342 (2012).
8. Müller, G. *et al.* Interleukin-10-Treated Dendritic Cells Modulate Immune Responses of Naive and Sensitized T Cells In Vivo. *Journal of Investigative Dermatology* **119,** 836–841 (2002).
9. Amodio, G. & Gregori, S. Human tolerogenic DC-10: perspectives for clinical applications. *Transplant Res* **1,** 14 (2012).
10. Lucca, L. E. *et al.* Myelin oligodendrocyte glycoprotein induces incomplete tolerance of CD4+ T cells specific for both a myelin and a neuronal self-antigen in mice. *Eur. J. Immunol.* **46,** 2247–2259 (2016).
11. Gholamzad, M., Ebtekar, M. & Shafiee Ardestani, M. Intravenous Injection of Myelin Oligodendrocyte Glycoprotein-coated PLGA Microparticles Have Tolerogenic Effects in Experimental Autoimmune Encephalomyelitis. *Iran J Allergy Asthma Immunol* **16,** 271–281 (2017).
12. Cho, J. J. *et al.* An antigen-specific semi-therapeutic treatment with local delivery of tolerogenic factors through a dual-sized microparticle system blocks experimental autoimmune encephalomyelitis. **143,** 79–92 (2017).
13. Zheng, P. *et al.* Antigen-oriented T cell migration contributes to myelin peptide induced-EAE and immune tolerance. *Clin. Immunol.* **169,** 36–46 (2016).
14. De Laere, M., Berneman, Z. N. & Cools, N. To the Brain and Back: Migratory Paths of Dendritic Cells in Multiple Sclerosis. *J. Neuropathol. Exp. Neurol.* **77,** 178–192 (2018).
15. Huang, Y.-H. *et al.* Specific central nervous system recruitment of HLA-G(+) regulatory T cells in multiple sclerosis. *Ann. Neurol.* **66,** 171–183 (2009).

16. Collison, L. W., Pillai, M. R., Chaturvedi, V. & Vignali, D. A. A. Regulatory T cell suppression is potentiated by target T cells in a cell contact, IL-35- and IL-10-dependent manner. *J. Immunol.* **182,** 6121–6128 (2009).
17. Chaudhry, A. *et al.* Interleukin-10 signaling in regulatory T cells is required for suppression of Th17 cell-mediated inflammation. *Immunity* **34,** 566–578 (2011).
18. LeMaoult, J. *et al.* Immune regulation by pretenders: cell-to-cell transfers of HLA-G make effector T cells act as regulatory cells. *Blood* **109,** 2040–2048 (2007).
19. Gregori, S. *et al.* Differentiation of type 1 T regulatory cells (Tr1) by tolerogenic DC-10 requires the IL-10-dependent ILT4/HLA-G pathway. *Blood* **116,** 935–944 (2010).
20. Obreque, J. *et al.* Autologous tolerogenic dendritic cells derived from monocytes of systemic lupus erythematosus patients and healthy donors show a stable and immunosuppressive phenotype. *Immunology* **152,** 648–659 (2017).
21. Raïch-Regué, D. *et al.* Stable antigen-specific T-cell hyporesponsiveness induced by tolerogenic dendritic cells from multiple sclerosis patients. *Eur. J. Immunol.* **42,** 771–782 (2012).
22. Getts, D. R. *et al.* Tolerance Induced by Apoptotic Antigen-Coupled Leukocytes Is Induced by PD-L1+ and IL-10-Producing Splenic Macrophages and Maintained by T Regulatory Cells. *The Journal of Immunology* **187,** 2405–2417 (2011).
23. Lake, J., Weller, R. O., Phillips, M. J. & Needham, M. Lymphocyte targeting of the brain in adoptive transfer cryolesion-EAE. *J. Pathol.* **187,** 259–265 (1999).
24. van Zwam, M. *et al.* Brain antigens in functionally distinct antigen-presenting cell populations in cervical lymph nodes in MS and EAE. *J. Mol. Med.* **87,** 273–286 (2009).
25. Sun, B.-L. *et al.* Lymphatic drainage system of the brain: A novel target for intervention of neurological diseases. *Prog. Neurobiol.* **163-164,** 118–143 (2018).
26. Louveau, A. *et al.* Structural and functional features of central nervous system lymphatic vessels. *Nature* **523,** 337–341 (2015).
27. van Zwam, M. *et al.* Surgical excision of CNS-draining lymph nodes reduces relapse severity in chronic-relapsing experimental autoimmune encephalomyelitis. *J. Pathol.* **217,** 543–551 (2009).
28. Phelps, E. A., Landazuri, N., Thule, P. M., Taylor, W. R. & Garcia, A. J. Bioartificial matrices for therapeutic vascularization. *Proceedings of the National Academy of Sciences* **107,** 3323–3328 (2010).
29. Weaver, J. D. *et al.* Vasculogenic hydrogel enhances islet survival, engraftment, and function in leading extrahepatic sites. *Sci Adv* **3,** e1700184 (2017).
30. Han, W. M. *et al.* Synthetic matrix enhances transplanted satellite cell engraftment in dystrophic and aged skeletal muscle with comorbid trauma. *Sci Adv* **4,** eaar4008 (2018).

31. Cruz-Acuña, R. *et al.* Synthetic hydrogels for human intestinal organoid generation and colonic wound repair. *Nat. Cell Biol.* **19,** 1326–1335 (2017).
32. Steinman, R. M. & Cohn, Z. A. Identification of a novel cell type in peripheral lymphoid organs of mice. I. Morphology, quantitation, tissue distribution. *J. Exp. Med.* **137,** 1142–1162 (1973).
33. Chaplin, D. D. Overview of the immune response. *J. Allergy Clin. Immunol.* **125,** S3–23 (2010).
34. Murphy, K. *Janeway's Immunobiology*. (Garland Science, 2016). doi:10.1201/9781315533247
35. Merad, M., Sathe, P., Helft, J., Miller, J. & Mortha, A. The Dendritic Cell Lineage: Ontogeny and Function of Dendritic Cells and Their Subsets in the Steady State and the Inflamed Setting. *Annu. Rev. Immunol.* **31,** 563–604 (2013).
36. BANCHEREAU, J. *et al.* Immunobiology of dendritic cells. *Annu. Rev. Immunol.* **18,** 767–811 (2000).
37. Kamath, A. T., Henri, S., Battye, F., Tough, D. F. & Shortman, K. Developmental kinetics and lifespan of dendritic cells in mouse lymphoid organs. *Blood* **100,** 1734–1741 (2002).
38. Kawai, T. & Akira, S. The roles of TLRs, RLRs and NLRs in pathogen recognition. *International Immunology* **21,** 317–337 (2009).
39. Lanzavecchia, A. Mechanisms of antigen uptake for presentation. *Curr. Opin. Immunol.* **8,** 348–354 (1996).
40. Kamphorst, A. O., Guermonprez, P., Dudziak, D. & Nussenzweig, M. C. Route of antigen uptake differentially impacts presentation by dendritic cells and activated monocytes. *J. Immunol.* **185,** 3426–3435 (2010).
41. Mantegazza, A. R., Magalhaes, J. G., Amigorena, S. & Marks, M. S. Presentation of phagocytosed antigens by MHC class I and II. *Traffic* **14,** 135–152 (2013).
42. Saeki, H., Moore, A. M., Brown, M. J. & Hwang, S. T. Cutting edge: secondary lymphoid-tissue chemokine (SLC) and CC chemokine receptor 7 (CCR7) participate in the emigration pathway of mature dendritic cells from the skin to regional lymph nodes. *The Journal of Immunology* **162,** 2472–2475 (1999).
43. Sittig, S. P. *et al.* A Comparative Study of the T Cell Stimulatory and Polarizing Capacity of Human Primary Blood Dendritic Cell Subsets. *Mediators Inflamm.* **2016,** 3605643–11 (2016).
44. Eisenbarth, S. C. Dendritic cell subsets in T cell programming: location dictates function. *Nat Rev Immunol* **19,** 89–103 (2018).
45. Kapsenberg, M. L. Dendritic-cell control of pathogen-driven T-cell polarization. *Nat Rev Immunol* **3,** 984–993 (2003).
46. Weiner, H. L., da Cunha, A. P., Quintana, F. & Wu, H. Oral tolerance. *Immunol. Rev.* **241,** 241–259 (2011).
47. Sigmundsdottir, H. *et al.* DCs metabolize sunlight-induced vitamin D3 to 'program' T cell attraction to the epidermal chemokine CCL27. *Nat Immunol* **8,** 285–293 (2007).

48. Mikhak, Z., Strassner, J. P. & Luster, A. D. Lung dendritic cells imprint T cell lung homing and promote lung immunity through the chemokine receptor CCR4. *J. Exp. Med.* **210,** 1855–1869 (2013).
49. Pejoski, D. *et al.* Site-Specific DC Surface Signatures Influence CD4+ T Cell Co-stimulation and Lung-Homing. *Front Immunol* **10,** 1650 (2019).
50. Song, H. *et al.* Injectable polypeptide hydrogel for dual-delivery of antigen and TLR3 agonist to modulate dendritic cells in vivo and enhance potent cytotoxic T-lymphocyte response against melanoma. **159,** 119–129 (2018).
51. Jadidi-Niaragh, F. *et al.* CD73 specific siRNA loaded chitosan lactate nanoparticles potentiate the antitumor effect of a dendritic cell vaccine in 4T1 breast cancer bearing mice. *J Control Release* **246,** 46–59 (2017).
52. Moreau, A., Alliot-Licht, B., Cuturi, M.-C. & Blancho, G. Tolerogenic dendritic cell therapy in organ transplantation. *Transpl Int* **30,** 754–764 (2017).
53. Beaudoin, L. *et al.* Plasmacytoid dendritic cells license regulatory T cells, upon iNKT-cell stimulation, to prevent autoimmune diabetes. *Eur. J. Immunol.* **44,** 1454–1466 (2014).
54. Cauwels, A. *et al.* Targeting interferon activity to dendritic cells enables in vivo tolerization and protection against EAE in mice. *J. Autoimmun.* (2018). doi:10.1016/j.jaut.2018.10.010
55. Beecham, A. H. *et al.* Analysis of immune-related loci identifies 48 new susceptibility variants for multiple sclerosis. *Nat. Genet.* **45,** 1353–1362 (2013).
56. Belbasis, L., Bellou, V., Evangelou, E., Ioannidis, J. P. A. & Tzoulaki, I. Environmental risk factors and multiple sclerosis: an umbrella review of systematic reviews and meta-analyses. *The Lancet Neurology* **14,** 263–273 (2015).
57. Ammitzbøll, C. *et al.* GPR15+ T cells are Th17 like, increased in smokers and associated with multiple sclerosis. *J. Autoimmun.* (2018). doi:10.1016/j.jaut.2018.09.005
58. Stadinski, B. D. & Huseby, E. S. Identifying environmental antigens that activate myelin-specific T cells. *Trends in Immunology* **35,** 231–232 (2014).
59. Dendrou, C. A., Fugger, L. & Friese, M. A. Immunopathology of multiple sclerosis. *Nat Rev Immunol* **15,** 545–558 (2015).
60. Hemmer, B., Kieseier, B., Cepok, S. & Hartung, H.-P. New immunopathologic insights into multiple sclerosis. *Curr Neurol Neurosci Rep* **3,** 246–255 (2003).
61. Rubin, S. M. Management of multiple sclerosis: an overview. *Dis Mon* **59,** 253–260 (2013).
62. 't Hart, B. A., Hintzen, R. Q. & Laman, J. D. Multiple sclerosis - a response-to-damage model. *Trends Mol Med* **15,** 235–244 (2009).
63. El-behi, M., Rostami, A. & Ciric, B. Current views on the roles of Th1 and Th17 cells in experimental autoimmune encephalomyelitis. *J Neuroimmune Pharmacol* **5,** 189–197 (2010).
64. Cheng, Y. *et al.* Diversity of immune cell types in multiple sclerosis and its animal model: Pathological and therapeutic implications. *J. Neurosci. Res.* **95,** 1973–1983 (2017).

65. Fritzsching, B. *et al.* Intracerebral human regulatory T cells: analysis of CD4+ CD25+ FOXP3+ T cells in brain lesions and cerebrospinal fluid of multiple sclerosis patients. *PLoS ONE* **6,** e17988 (2011).
66. Amodio, G. & Gregori, S. Dendritic cells a double-edge sword in autoimmune responses. *Front Immunol* **3,** 233 (2012).
67. Miller, D. H. *et al.* A controlled trial of natalizumab for relapsing multiple sclerosis. *N. Engl. J. Med.* **348,** 15–23 (2003).
68. Karussis, D. Immunotherapy of multiple sclerosis: the state of the art. *BioDrugs* **27,** 113–148 (2013).
69. Becher, B., Spath, S. & Goverman, J. Cytokine networks in neuroinflammation. *Nature Publishing Group* (2016). doi:10.1038/nri.2016.123
70. Blanco, P., Palucka, A. K., Pascual, V. & Banchereau, J. Dendritic cells and cytokines in human inflammatory and autoimmune diseases. *Cytokine Growth Factor Rev* **19,** 41–52 (2008).
71. Owen, D. L. *et al.* Thymic regulatory T cells arise via two distinct developmental programs. *Nat Immunol* **20,** 195–205 (2019).
72. Ohkura, N., Kitagawa, Y. & Sakaguchi, S. Development and Maintenance of Regulatory T cells. *Immunity* **38,** 414–423 (2013).
73. Richards, D. M., Kyewski, B. & Feuerer, M. Re-examining the Nature and Function of Self-Reactive T cells. *Trends in Immunology* **37,** 114–125 (2016).
74. Dustin, M. L., Tseng, S.-Y., Varma, R. & Campi, G. T cell-dendritic cell immunological synapses. *Curr. Opin. Immunol.* **18,** 512–516 (2006).
75. Torres-Aguilar, H. *et al.* Tolerogenic Dendritic Cells Generated with Different Immunosuppressive Cytokines Induce Antigen-Specific Anergy and Regulatory Properties in Memory CD4+ T Cells. *The Journal of Immunology* **184,** 1765–1775 (2010).
76. Vignali, D. A. A., Collison, L. W. & Workman, C. J. How regulatory T cells work. *Nature Publishing Group* **8,** 523–532 (2008).
77. Kingsley, C. I., Karim, M., Bushell, A. R. & Wood, K. J. CD25+CD4+ regulatory T cells prevent graft rejection: CTLA-4- and IL-10-dependent immunoregulation of alloresponses. *The Journal of Immunology* **168,** 1080–1086 (2002).
78. Akkaya, B. *et al.* Regulatory T cells mediate specific suppression by depleting peptide-MHC class II from dendritic cells. *Nat Immunol* **20,** 218–231 (2019).
79. Sharma, M. D. *et al.* Plasmacytoid dendritic cells from mouse tumor-draining lymph nodes directly activate mature Tregs via indoleamine 2,3-dioxygenase. *J Clin Invest* **117,** 2570–2582 (2007).
80. Gondek, D. C., Lu, L.-F., Quezada, S. A., Sakaguchi, S. & Noelle, R. J. Cutting edge: contact-mediated suppression by CD4+CD25+ regulatory cells involves a granzyme B-dependent, perforin-independent mechanism. *The Journal of Immunology* **174,** 1783–1786 (2005).
81. Pandiyan, P., Zheng, L., Ishihara, S., Reed, J. & Lenardo, M. J. CD4+CD25+Foxp3+ regulatory T cells induce cytokine deprivation-mediated apoptosis of effector CD4+ T cells. *Nat Immunol* **8,** 1353–1362 (2007).

82. Bailey, S. L., Schreiner, B., McMahon, E. J. & Miller, S. D. CNS myeloid DCs presenting endogenous myelin peptides 'preferentially' polarize CD4+ T(H)-17 cells in relapsing EAE. *Nat Immunol* **8,** 172–180 (2007).
83. Deshpande, P., King, I. L. & Segal, B. M. Cutting edge: CNS CD11c+ cells from mice with encephalomyelitis polarize Th17 cells and support CD25+CD4+ T cell-mediated immunosuppression, suggesting dual roles in the disease process. *The Journal of Immunology* **178,** 6695–6699 (2007).
84. Wood, K. J. & Sakaguchi, S. Regulatory T cells in transplantation tolerance. *Nat Rev Immunol* **3,** 199–210 (2003).
85. Jones, A. & Hawiger, D. Peripherally Induced Regulatory T Cells: Recruited Protectors of the Central Nervous System against Autoimmune Neuroinflammation. *Front Immunol* **8,** 532 (2017).
86. Shi, Y. *et al.* Immethridine, histamine H3-receptor (H3R) agonist, alleviated experimental autoimmune encephalomyelitis via inhibiting the function of dendritic cells. *Oncotarget* **8,** 75038–75049 (2017).
87. Ano, Y., Ikado, K., Shindo, K., Koizumi, H. & Fujiwara, D. Identification of 14-dehydroergosterol as a novel anti-inflammatory compound inducing tolerogenic dendritic cells. *Sci Rep* **7,** 13903 (2017).
88. Lutterotti, A. *et al.* Antigen-Specific Tolerance by Autologous Myelin Peptide-Coupled Cells: A Phase 1 Trial in Multiple Sclerosis. *Science Translational Medicine* **5,** 188ra75–188ra75 (2013).
89. Xie, Z. *et al.* 1,25-dihydroxyvitamin D_3 -induced dendritic cells suppress experimental autoimmune encephalomyelitis by increasing proportions of the regulatory lymphocytes and reducing T helper type 1 and type 17 cells. *Immunology* **152,** 414–424 (2017).
90. Besusso, D. *et al.* 1,25-dihydroxyvitamin D_3-conditioned CD11c+ dendritic cells are effective initiators of CNS autoimmune disease. *Front Immunol* **6,** 575 (2015).
91. Yamamoto, E. & Jørgensen, T. N. Immunological effects of vitamin D and their relations to autoimmunity. *J. Autoimmun.* **100,** 7–16 (2019).
92. Kryczanowsky, F. IL-10?Modulated Human Dendritic Cells for Clinical Use: Identification of a Stable and Migratory Subset with Improved Tolerogenic Activity. *The Journal of Immunology* **197,** 3607–3617 (2016).
93. Benkhoucha, M. *et al.* Hepatocyte growth factor limits autoimmune neuroinflammation via glucocorticoid-induced leucine zipper expression in dendritic cells. *J. Immunol.* **193,** 2743–2752 (2014).
94. Benkhoucha, M. *et al.* Hepatocyte growth factor inhibits CNS autoimmunity by inducing tolerogenic dendritic cells and CD25+Foxp3+ regulatory T cells. *Proc. Natl. Acad. Sci. U.S.A.* **107,** 6424–6429 (2010).
95. Zhou, Y. *et al.* Tolerogenic dendritic cells induced by BD750 ameliorate proinflammatory T cell responses and experimental autoimmune encephalitis in mice. *Mol. Med.* **23,** 204–214 (2017).
96. Doñas, C. *et al.* The histone demethylase inhibitor GSK-J4 limits inflammation through the induction of a tolerogenic phenotype on DCs. *J. Autoimmun.* **75,** 105–117 (2016).

97. Wei, H.-J., Pareek, T. K., Liu, Q. & Letterio, J. J. A unique tolerizing dendritic cell phenotype induced by the synthetic triterpenoid CDDO-DFPA (RTA-408) is protective against EAE. *Sci Rep* **7,** 9886 (2017).
98. Zhou, Y. *et al.* Tolerogenic Dendritic Cells Generated with Tofacitinib Ameliorate Experimental Autoimmune Encephalomyelitis through Modulation of Th17/Treg Balance. *J Immunol Res* **2016,** 5021537 (2016).
99. Zhou, F., Ciric, B., Zhang, G. X. & Rostami, A. Immunotherapy using lipopolysaccharide-stimulated bone marrow-derived dendritic cells to treat experimental autoimmune encephalomyelitis. *Clinical & Experimental Immunology* **178,** 447–458 (2014).
100. Zhou, F., Zhang, G.-X. & Rostami, A. Apoptotic cell-treated dendritic cells induce immune tolerance by specifically inhibiting development of CD4 + effector memory T cells. *Immunologic Research* **64,** 73–81 (2016).
101. Zhou, F. *et al.* Intravenous transfer of apoptotic cell-treated dendritic cells leads to immune tolerance by blocking Th17 cell activity. *Immunobiology* **218,** 1069–1076 (2013).
102. Kalantari, T. *et al.* Tolerogenic dendritic cells produced by lentiviral-mediated CD40- and interleukin-23p19-specific shRNA can ameliorate experimental autoimmune encephalomyelitis by suppressing T helper type 17 cells. *Clinical & Experimental Immunology* **176,** 180–189 (2014).
103. De Laere, M. *et al.* Shuttling tolerogenic dendritic cells across the blood-brain barrier in vitro via the introduction of de Novo C-C chemokine receptor 5 expression using messenger RNA electroporation. *Front Immunol* **8,** 1964 (2018).
104. Mansilla, M. J. *et al.* Beneficial effect of tolerogenic dendritic cells pulsed with MOG autoantigen in experimental autoimmune encephalomyelitis. *CNS Neurosci Ther* **21,** 222–230 (2015).
105. Verdijk, P. *et al.* Limited amounts of dendritic cells migrate into the T-cell area of lymph nodes but have high immune activating potential in melanoma patients. *Clin. Cancer Res.* **15,** 2531–2540 (2009).
106. Zozulya, A. L. *et al.* Intracerebral dendritic cells critically modulate encephalitogenic versus regulatory immune responses in the CNS. *J. Neurosci.* **29,** 140–152 (2009).
107. Isaacs, J. & Hilkens, C. *Tolerogenic Antigen-Presenting Cells – Modulating Unwanted Immune Response at Their Core*. (Frontiers Media SA, 2019). doi:10.1016/j.autrev.2013.09.008
108. Mansilla, M. J. *et al.* Cryopreserved vitamin D3-tolerogenic dendritic cells pulsed with autoantigens as a potential therapy for multiple sclerosis patients. *J Neuroinflammation* **13,** 113 (2016).
109. Willekens, B. *et al.* Tolerogenic dendritic cell-based treatment for multiple sclerosis (MS): A harmonised study protocol for two phase i clinical trials comparing intradermal and intranodal cell administration. *BMJ Open* **9,** e030309 (2019).
110. Phillips, B. E., Garciafigueroa, Y., Trucco, M. & Giannoukakis, N. Clinical tolerogenic dendritic cells: Exploring therapeutic impact on human autoimmune disease. *Front Immunol* **8,** 1279 (2017).

111. Willekens, B. & Cools, N. Beyond the Magic Bullet: Current Progress of Therapeutic Vaccination in Multiple Sclerosis. *CNS Drugs* **32,** 401–410 (2018).
112. Mohammad, M. G. *et al.* Immune cell trafficking from the brain maintains CNS immune tolerance. *Journal of Clinical Investigation* **124,** 1228–1241 (2014).
113. De Vries, I. J. M. *et al.* Effective migration of antigen-pulsed dendritic cells to lymph nodes in melanoma patients is determined by their maturation state. *Cancer Research* **63,** 12–17 (2003).
114. Ridolfi, R. *et al.* Evaluation of in vivo labelled dendritic cell migration in cancer patients. *J Transl Med* **2,** 27 (2004).
115. Babensee, J. E. Interaction of dendritic cells with biomaterials. *Seminars in Immunology* **20,** 101–108 (2008).
116. Kou, P. M. & Babensee, J. E. Macrophage and dendritic cell phenotypic diversity in the context of biomaterials. *J. Biomed. Mater. Res.* **96,** 239–260 (2011).
117. Park, J. & Babensee, J. E. Differential functional effects of biomaterials on dendritic cell maturation. *Acta Biomaterialia* **8,** 3606–3617 (2012).
118. Hotaling, N. A., Ratner, D. M., Cummings, R. D. & Babensee, J. E. Presentation modality of glycoconjugates modulates dendritic cell phenotype. *Biomater. Sci.* **2,** 1426–1439 (2014).
119. Hotaling, N. A., Cummings, R. D., Ratner, D. M. & Babensee, J. E. Molecular factors in dendritic cell responses to adsorbed glycoconjugates. **35,** 5862–5874 (2014).
120. Bennewitz, N. L. & Babensee, J. E. The effect of the physical form of poly(lactic-co-glycolic acid) carriers on the humoral immune response to co-delivered antigen. **26,** 2991–2999 (2005).
121. Hotaling, N. A., Tang, L., Irvine, D. J. & Babensee, J. E. Biomaterial Strategies for Immunomodulation. *Annu. Rev. Biomed. Eng.* **17,** 317–349 (2015).
122. Maldonado, R. A. *et al.* Polymeric synthetic nanoparticles for the induction of antigen-specific immunological tolerance. *Proceedings of the National Academy of Sciences* **112,** E156–E165 (2015).
123. Kim, J. *et al.* Injectable, spontaneously assembling, inorganic scaffolds modulate immune cells in vivo and increase vaccine efficacy. *Nat Biotechnol* **33,** 64–72 (2014).
124. Li, A. W. *et al.* A facile approach to enhance antigen response for personalized cancer vaccination. *Nat Mater* **125,** 1–7 (2018).
125. Vlahos, A. E., Cober, N. & Sefton, M. V. Modular tissue engineering for the vascularization of subcutaneously transplanted pancreatic islets. *Proc. Natl. Acad. Sci. U.S.A.* **114,** 9337–9342 (2017).
126. Verma, V. *et al.* Activated dendritic cells delivered in tissue compatible biomatrices induce in-situ anti-tumor CTL responses leading to tumor regression. *Oncotarget* **7,** 39894–39906 (2016).
127. Stark, R. J. *et al.* Endothelial cell tolerance to lipopolysaccharide challenge is induced by monophosphoryl lipid A. *Clin. Sci.* **130,** 451–461 (2016).
128. Stabenfeldt, S. E., Munglani, G., Garcia, A. J. & LaPlaca, M. C. Biomimetic microenvironment modulates neural stem cell survival, migration, and differentiation. *Tissue Engineering Part A* **16,** 3747–3758 (2010).

129. Mamidi, A. *et al.* Mechanosignalling via integrins directs fate decisions of pancreatic progenitors. *Nature* (2018). doi:10.1038/s41586-018-0762-2
130. Haugh, M. G. *et al.* Investigating the interplay between substrate stiffness and ligand chemistry in directing mesenchymal stem cell differentiation within 3D macro-porous substrates. **171,** 23–33 (2018).
131. Enemchukwu, N. O. *et al.* Synthetic matrices reveal contributions of ECM biophysical and biochemical properties to epithelial morphogenesis. *J. Cell Biol.* **212,** 113–124 (2016).
132. Huebsch, N. *et al.* Harnessing traction-mediated manipulation of the cell/matrix interface to control stem-cell fate. *Nat Mater* **9,** 518–526 (2010).
133. Acharya, A. P. *et al.* The modulation of dendritic cell integrin binding and activation by RGD-peptide density gradient substrates. **31,** 7444–7454 (2010).
134. Discher, D. E., Janmey, P. & Wang, Y.-L. Tissue cells feel and respond to the stiffness of their substrate. *Science* **310,** 1139–1143 (2005).
135. Keselowsky, B. G., Collard, D. M. & Garcia, A. J. Surface chemistry modulates fibronectin conformation and directs integrin binding and specificity to control cell adhesion. *J. Biomed. Mater. Res.* **66A,** 247–259 (2003).
136. Duval, K. *et al.* Modeling Physiological Events in 2D vs. 3D Cell Culture. *Physiology (Bethesda)* **32,** 266–277 (2017).
137. Lewis, J. S. *et al.* The effect of cyclic mechanical strain on activation of dendritic cells cultured on adhesive substrates. **34,** 9063–9070 (2013).
138. Chen, R., Ma, H., Zhang, L. & Bryers, J. D. Precision-porous templated scaffolds of varying pore size drive dendritic cell activation. *Biotechnol. Bioeng.* **115,** 1086–1095 (2018).
139. Danhier, F. *et al.* PLGA-based nanoparticles: An overview of biomedical applications. *Journal of Controlled Release* **161,** 505–522 (2012).
140. Zhang, Y., Chan, H. F. & Leong, K. W. Advanced materials and processing for drug delivery: The past and the future. *Advanced Drug Delivery Reviews* **65,** 104–120 (2013).
141. Yoo, J.-W., Irvine, D. J., Discher, D. E. & Mitragotri, S. Bio-inspired, bioengineered and biomimetic drug delivery carriers. *Nat Rev Drug Discov* **10,** 521–535 (2011).
142. De Koker, S. *et al.* Engineering Polymer Hydrogel Nanoparticles for Lymph Node-Targeted Delivery. *Angewandte Chemie International Edition* **55,** 1334–1339 (2016).
143. Toy, R. & Roy, K. Engineering nanoparticles to overcome barriers to immunotherapy. *Bioengineering & Translational Medicine* **1,** 47–62 (2016).
144. KIM, S. W., BAE, Y. H. & OKANO, T. Hydrogels - Swelling, Drug Loading, and Release. *Pharm. Res.* **9,** 283–290 (1992).
145. Hoare, T. R. & Kohane, D. S. Hydrogels in drug delivery: Progress and challenges. *Polymer* **49,** 1993–2007 (2008).
146. Bertz, A. *et al.* Encapsulation of proteins in hydrogel carrier systems for controlled drug delivery: influence of network structure and drug size on release rate. *Journal of Biotechnology* **163,** 243–249 (2013).
147. Schipper, M. L. *et al.* Particle size, surface coating, and PEGylation influence the biodistribution of quantum dots in living mice. *Small* **5,** 126–134 (2009).

148. Zustiak, S. P. & Leach, J. B. Hydrolytically Degradable Poly(Ethylene Glycol) Hydrogel Scaffolds with Tunable Degradation and Mechanical Properties. *Biomacromolecules* **11,** 1348–1357 (2010).
149. Foster, G. A. *et al.* Protease-degradable microgels for protein delivery for vascularization. **113,** 170–175 (2017).
150. Gutowski, S. M. *et al.* Protease-degradable PEG-maleimide coating with on-demand release of IL-1Ra to improve tissue response to neural electrodes. **44,** 55–70 (2015).
151. Lee, T. T. *et al.* Light-triggered in vivo activation of adhesive peptides regulates cell adhesion, inflammation and vascularization of biomaterials. *Nat Mater* **14,** 352–360 (2014).
152. Rizwan, M. *et al.* pH Sensitive Hydrogels in Drug Delivery: Brief History, Properties, Swelling, and Release Mechanism, Material Selection and Applications. *Polymers* **9,** 137 (2017).
153. Badeau, B. A., Comerford, M. P., Arakawa, C. K., Shadish, J. A. & DeForest, C. A. Engineered modular biomaterial logic gates for environmentally triggered therapeutic delivery. *Nat Chem* **10,** 251–258 (2018).
154. Pashuck, E. T. & Stevens, M. M. Designing Regenerative Biomaterial Therapies for the Clinic. *Science Translational Medicine* **4,** 160sr4–160sr4 (2012).
155. Singh, A. Biomaterials innovation for next generation ex vivo immune tissue engineering. **130,** 104–110 (2017).
156. Garcia, J. R., Clark, A. Y. & Garcia, A. J. Integrin-specific hydrogels functionalized with VEGF for vascularization and bone regeneration of critical-size bone defects. *J. Biomed. Mater. Res.* **104,** 889–900 (2016).
157. Apoorva, F. N. U. *et al.* Lymph node stiffness-mimicking hydrogels regulate human B-cell lymphoma growth and cell surface receptor expression in a molecular subtype-specific manner. *J. Biomed. Mater. Res.* **105,** 1833–1844 (2017).
158. Bott, K. *et al.* The effect of matrix characteristics on fibroblast proliferation in 3D gels. **31,** 8454–8464 (2010).
159. Phelps, E. A. *et al.* Maleimide Cross-Linked Bioactive PEG Hydrogel Exhibits Improved Reaction Kinetics and Cross-Linking for Cell Encapsulation and In Situ Delivery. *Adv. Mater.* **24,** 64–70 (2011).
160. Corradetti, B. *et al.* Chondroitin Sulfate Immobilized on a Biomimetic Scaffold Modulates Inflammation While Driving Chondrogenesis. *STEM CELLS Translational Medicine* **5,** 670–682 (2016).
161. Bartneck, M. *et al.* Inducing healing-like human primary macrophage phenotypes by 3D hydrogel coated nanofibres. **33,** 4136–4146 (2012).
162. Raïch-Regué, D., Glancy, M. & Thomson, A. W. Regulatory dendritic cell therapy: from rodents to clinical application. *Immunol. Lett.* **161,** 216–221 (2014).
163. Voigtländer, C. *et al.* Dendritic cells matured with TNF can be further activated in vitro and after subcutaneous injection in vivo which converts their tolerogenicity into immunogenicity. *J. Immunother.* **29,** 407–415 (2006).

164. Weaver, J. D. *et al. Design of a Vascularized Synthetic Poly(ethylene Glycol) Macroencapsulation Device for Islet Transplantation*. *Biomaterials* **172,** 54–65 (2018).
165. Bhutani, S. *et al.* Evaluation of Hydrogels Presenting Extracellular Matrix-Derived Adhesion Peptides and Encapsulating Cardiac Progenitor Cells for Cardiac Repair. *ACS Biomater. Sci. Eng.* **4,** 200–210 (2018).
166. Han, W. M., Jang, Y. C. & Garcia, A. J. Engineered matrices for skeletal muscle satellite cell engraftment and function. *Matrix Biol.* **60-61,** 96–109 (2017).
167. Cruz-Acuña, R. & Garcia, A. J. Synthetic hydrogels mimicking basement membrane matrices to promote cell-matrix interactions. *Matrix Biol.* (2016). doi:10.1016/j.matbio.2016.06.002
168. Dellacherie, M. O., Seo, B. R. & Mooney, D. J. Macroscale biomaterials strategies for local immunomodulation. *Nat Rev Mater* **4,** 379–397 (2019).
169. Shekaran, A. *et al.* Bone regeneration using an alpha 2 beta 1 integrin-specific hydrogel as a BMP-2 delivery vehicle. **35,** 5453–5461 (2014).
170. Darling, N. J., Hung, Y.-S., Sharma, S. & Segura, T. Controlling the kinetics of thiol-maleimide Michael-type addition gelation kinetics for the generation of homogenous poly(ethylene glycol) hydrogels. **101,** 199–206 (2016).
171. Chen, J., Alexander, J. S. & Orr, A. W. Integrins and their extracellular matrix ligands in lymphangiogenesis and lymph node metastasis. *Int J Cell Biol* **2012,** 853703–853703 (2012).
172. Tilghman, R. W. *et al.* Matrix rigidity regulates cancer cell growth and cellular phenotype. *PLoS ONE* **5,** e12905 (2010).
173. Majedi, F. S. *et al.* T-cell activation is modulated by the 3D mechanical microenvironment. **252,** 120058 (2020).
174. Rachev, A. Design and Fabrication of a Mechanically Matched Vascular Graft. *J Biomech Eng* **133,** 091004–8 (2011).
175. Rubinstein, M. & Colby, R. H. *Polymer Physics*. (OUP Oxford, 2003).
176. Welzel, P. B. *et al.* Modulating Biofunctional starPEG Heparin Hydrogels by Varying Size and Ratio of the Constituents. *Polymers* **3,** 602–620 (2011).
177. Pulendran, B. *et al.* Distinct dendritic cell subsets differentially regulate the class of immune response in vivo. *Proceedings of the National Academy of Sciences* **96,** 1036–1041 (1999).
178. Xu, Y., Zhan, Y., Lew, A. M., Naik, S. H. & Kershaw, M. H. Differential development of murine dendritic cells by GM-CSF versus Flt3 ligand has implications for inflammation and trafficking. *J. Immunol.* **179,** 7577–7584 (2007).
179. Efron, P. A. *et al.* Differential maturation of murine bone-marrow derived dendritic cells with lipopolysaccharide and tumor necrosis factor-alpha. *J. Endotoxin Res.* **11,** 145–160 (2005).
180. Zhou, F., Zhang, G.-X. & Rostami, A. LPS-treated bone marrow-derived dendritic cells induce immune tolerance through modulating differentiation of CD4 + regulatory T cell subpopulations mediated by 3G11 and CD127. *Immunologic Research* **65,** 630–638 (2017).

181. Hirsch, S. *et al.* MR elastography of the liver and the spleen using a piezoelectric driver, single-shot wave-field acquisition, and multifrequency dual parameter reconstruction. *Magn Reson Med* **71,** 267–277 (2014).
182. Rohner, N. A. *et al.* Lymph node biophysical remodeling is associated with melanoma lymphatic drainage. *FASEB J.* **29,** 4512–4522 (2015).
183. Parada, G. A., Yuk, H., Liu, X., Hsieh, A. J. & Zhao, X. Impermeable Robust Hydrogels via Hybrid Lamination. *Adv. Healthcare Mater.* **6,** (2017).
184. O'Sullivan, E. S., Vegas, A., Anderson, D. G. & Weir, G. C. Islets transplanted in immunoisolation devices: a review of the progress and the challenges that remain. *Endocr. Rev.* **32,** 827–844 (2011).
185. Petrie, T. A., Capadona, J. R., Reyes, C. D. & Garcia, A. J. Integrin specificity and enhanced cellular activities associated with surfaces presenting a recombinant fibronectin fragment compared to RGD supports. **27,** 5459–5470 (2006).
186. Khetan, S. *et al.* Degradation-mediated cellular traction directs stem cell fate in covalently crosslinked three-dimensional hydrogels. *Nat Mater* **12,** 458–465 (2013).
187. Kouwenhoven, M. *et al.* Monocyte-derived dendritic cells express and secrete matrix-degrading metalloproteinases and their inhibitors and are imbalanced in multiple sclerosis. *J. Neuroimmunol.* **126,** 161–171 (2002).
188. Phelps, E. A., Headen, D. M., Taylor, W. R., Thulé, P. M. & Garcia, A. J. Vasculogenic bio-synthetic hydrogel for enhancement of pancreatic islet engraftment and function in type 1 diabetes. **34,** 4602–4611 (2013).
189. Patterson, J. & Hubbell, J. A. Enhanced proteolytic degradation of molecularly engineered PEG hydrogels in response to MMP-1 and MMP-2. **31,** 7836–7845 (2010).
190. Turk, B. E., Huang, L. L., Piro, E. T. & Cantley, L. C. Determination of protease cleavage site motifs using mixture-based oriented peptide libraries. *Nat Biotechnol* **19,** 661–667 (2001).
191. Manicassamy, S. & Pulendran, B. Dendritic cell control of tolerogenic responses. *Immunol. Rev.* **241,** 206–227 (2011).
192. Hubo, M. *et al.* Costimulatory molecules on immunogenic versus tolerogenic human dendritic cells. *Front Immunol* **4,** (2013).
193. Paterka, M. *et al.* Dendritic cells tip the balance towards induction of regulatory T cells upon priming in experimental autoimmune encephalomyelitis. *J. Autoimmun.* (2016). doi:10.1016/j.jaut.2016.09.008
194. Gordon, J. R., Ma, Y., Churchman, L., Gordon, S. A. & Dawicki, W. Regulatory dendritic cells for immunotherapy in immunologic diseases. *Front Immunol* **5,** (2014).
195. Leifer, C. A. Dendritic cells in host response to biologic scaffolds. *Seminars in Immunology* **29,** 41–48 (2017).
196. Oft, M. IL-10: master switch from tumor-promoting inflammation to antitumor immunity. *Cancer Immunol Res* **2,** 194–199 (2014).
197. Mumm, J. B., Emmerich, J. & Oft, M. Killing from within. *Oncoimmunology* **1,** 1598–1600 (2012).

198. Soderquist, R. G. *et al.* PEGylation of interleukin-10 for the mitigation of enhanced pain states. *J. Biomed. Mater. Res.* **93,** 1169–1179 (2010).
199. Baker, N., Sok, M., McClain, C., Open, H. L. S. G.2020. SPADE Analysis Reveals The Recruitment Of Rare Immune Cell Subtypes To Site Of Injury Following Treatment With Immunomodulatory Hydrogels. *journals.lww.com*
200. Walter, M. R. *The molecular basis of IL-10 function: From receptor structure to the onset of signaling*. *Current Topics in Microbiology and Immunology* **380,** 191–212 (2014).
201. Shouval, D. S. *et al.* Interleukin 10 receptor signaling: master regulator of intestinal mucosal homeostasis in mice and humans. *Adv. Immunol.* **122,** 177–210 (2014).
202. Zdanov, A. Structural features of the interleukin-10 family of cytokines. *Curr. Pharm. Des.* **10,** 3873–3884 (2004).
203. Windsor, W. T. *et al.* Disulfide bond assignments and secondary structure analysis of human and murine interleukin 10. *Biochemistry* **32,** 8807–8815 (1993).
204. Thompson-Snipes, L. *et al.* Interleukin 10: A novel stimulatory factor for mast cells and their progenitors. *Journal of Experimental Medicine* **173,** 507–510 (1991).
205. Klompus, S., Solomon, G. & Gertler, A. A simple novel method for the preparation of noncovalent homodimeric, biologically active human interleukin 10 in Escherichia coli-enhancing protein expression by degenerate PCR of 5' DNA in the open reading frame. *Protein Expr. Purif.* **62,** 199–205 (2008).
206. Yang, F. *et al.* Expression and purification of rhIL-10-RGD from Escherichia coli as a potential wound healing agent. *J. Microbiol. Methods* **127,** 62–67 (2016).
207. Constantinescu, C. S., Farooqi, N., O'Brien, K. & Gran, B. Experimental autoimmune encephalomyelitis (EAE) as a model for multiple sclerosis (MS). *British Journal of Pharmacology* **164,** 1079–1106 (2011).
208. Yoo, S. & Ha, S.-J. Generation of tolerogenic dendritic cells and their therapeutic applications. *Immune Netw* **16,** 52–60 (2016).
209. Liu, J. & Cao, X. Regulatory dendritic cells in autoimmunity: A comprehensive review. *J. Autoimmun.* **63,** 1–12 (2015).
210. Unger, W. W. J., Laban, S., Kleijwegt, F. S., van der Slik, A. R. & Roep, B. O. Induction of Treg by monocyte-derived DC modulated by vitamin D3 or dexamethasone: differential role for PD-L1. *Eur. J. Immunol.* **39,** 3147–3159 (2009).
211. Fan, Z. *et al.* A new class of biological materials: Cell membrane-derived hydrogel scaffolds. **197,** 244–254 (2019).
212. Kaushansky, N., Kaminitz, A., Allouche-Arnon, H. & Ben-Nun, A. Modulation of MS-like disease by a multi epitope protein is mediated by induction of CD11c+CD11b+Gr1+ myeloid-derived dendritic cells. *J. Neuroimmunol.* **333,** 476953 (2019).
213. Wang, L. *et al.* Selective depletion of CD11c+ CD11b+ dendritic cells partially abrogates tolerogenic effects of intravenous MOG in murine EAE. *Eur. J. Immunol.* **46,** 2454–2466 (2016).

214. Thomas, A. M. *et al.* Brief exposure to hyperglycemia activates dendritic cells in vitro and in vivo. *J. Cell. Physiol.* **31,** 7444 (2019).
215. Geginat, J., Lanzavecchia, A. & Sallusto, F. Proliferation and differentiation potential of human CD8+ memory T-cell subsets in response to antigen or homeostatic cytokines. *Blood* **101,** 4260–4266 (2003).
216. Chiang, E. Y. *et al.* Targeted depletion of lymphotoxin-alpha-expressing TH1 and TH17 cells inhibits autoimmune disease. *Nat Med* **15,** 766–773 (2009).
217. Araki, M. *et al.* Th2 bias of CD4+ NKT cells derived from multiple sclerosis in remission. *International Immunology* **15,** 279–288 (2003).
218. Clerici, M. *et al.* Single-cell analysis of cytokine production shows different immune profiles in multiple sclerosis patients with active or quiescent disease. *J. Neuroimmunol.* **121,** 88–101 (2001).
219. Xie, Z.-X. *et al.* Role of the Immunogenic and Tolerogenic Subsets of Dendritic Cells in Multiple Sclerosis. *Mediators Inflamm.* **2015,** 513295 (2015).
220. Tsai, H.-H. *et al.* The chemokine receptor CXCR2 controls positioning of oligodendrocyte precursors in developing spinal cord by arresting their migration. *Cell* **110,** 373–383 (2002).
221. Omari, K. M., Lutz, S. E., Santambrogio, L., Lira, S. A. & Raine, C. S. Neuroprotection and remyelination after autoimmune demyelination in mice that inducibly overexpress CXCL1. *Am. J. Pathol.* **174,** 164–176 (2009).
222. DuPage, M. & Bluestone, J. A. Harnessing the plasticity of CD4(+) T cells to treat immune-mediated disease. *Nat Rev Immunol* **16,** 149–163 (2016).
223. Liu, Y. J., Kanzler, H., Soumelis, V. & Gilliet, M. Dendritic cell lineage, plasticity and cross-regulation. *Nat Immunol* **2,** 585–589 (2001).
224. Galli, S. J., Borregaard, N. & Wynn, T. A. Phenotypic and functional plasticity of cells of innate immunity: macrophages, mast cells and neutrophils. *Nat Immunol* **12,** 1035–1044 (2011).
225. Mebius, R. E. Organogenesis of lymphoid tissues. *Nat Rev Immunol* **3,** 292–303 (2003).
226. Corsiero, E., Nerviani, A., Bombardieri, M. & Pitzalis, C. Ectopic Lymphoid Structures: Powerhouse of Autoimmunity. *Front Immunol* **7,** 430 (2016).
227. Neyt, K., Perros, F., GeurtsvanKessel, C. H., Hammad, H. & Lambrecht, B. N. Tertiary lymphoid organs in infection and autoimmunity. *Trends in Immunology* **33,** 297–305 (2012).
228. Fütterer, A., Mink, K., Luz, A., Kosco-Vilbois, M. H. & Pfeffer, K. The Lymphotoxin β Receptor Controls Organogenesis and Affinity Maturation in Peripheral Lymphoid Tissues. *Immunity* **9,** 59–70 (1998).
229. Buettner, M., Pabst, R. & Bode, U. Stromal cell heterogeneity in lymphoid organs. *Trends in Immunology* **31,** 80–86 (2010).
230. Kobayashi, Y. & Watanabe, T. Gel-Trapped Lymphorganogenic Chemokines Trigger Artificial Tertiary Lymphoid Organs and Mount Adaptive Immune Responses In Vivo. *Front Immunol* **7,** 316 (2016).
231. Frumovitz, M. *et al.* 'Triple injection' lymphatic mapping technique to determine if parametrial nodes are the true sentinel lymph nodes in women with cervical cancer. *Gynecol. Oncol.* **127,** 467–471 (2012).

232. Sauter, A., Yi, D. H., Li, Y., Roersma, S. & Appel, S. The Culture Dish Surface Influences the Phenotype and Cytokine Production of Human Monocyte-Derived Dendritic Cells. *Front Immunol* **10,** 419 (2019).
233. Vremec, D. *et al.* Factors determining the spontaneous activation of splenic dendritic cells in culture. *Innate Immun* **17,** 338–352 (2011).
234. Berman, H., Henrick, K. & Nakamura, H. Announcing the worldwide Protein Data Bank. *Nat. Struct. Biol.* **10,** 980–980 (2003).
235. Larsson, R., Rocksén, D., Lilliehöök, B., Jonsson, A. & Bucht, A. Dose-dependent activation of lymphocytes in endotoxin-induced airway inflammation. *Infect. Immun.* **68,** 6962–6969 (2000).